People's Democratic Republic of Algeria
Ministry of Higher Education and Scientific Research

Batna 2 University – Mostefa Ben Boulaïd
Faculty of Technology
Department of Mechanical Engineering

Thesis

Prepared within the
(Laboratory of Structural Mechanics and Materials (LaMSM))

Presented for the degree of:
LMD Doctor in Mechanical Engineering
Option: Materials engineering

Theme:

Numerical modeling and study of the behavior of metallic foams under impact

Defended by:

BENSALEM Ilyas

Before the Jury composed of :

Mr OUTTAS Toufik	Professor	University of Batna2	President
Mr BENHIZIA Abdennour	MCA	University of Batna2	Supervisor
Mr MADANI Salah	Professor	University of Batna2	Examiner
Mr HECINI Mabrouk	Professor	University of Biskra	Examiner
Mr CHEBBAH Mohamed-Saïd	Professor	University of Biskra	Examiner

16/03/2023

DEDICATION

To my Mother

For her everlasting love,

To my deceased father

May God have mercy on him

And

To my brother and sister, Oussama and Roumayssa for their love, affection, and unwavering support, for believing in my capability more than me, and for encouraging, motivating, and inspiring me every day.

ACKNOWLEDGEMENTS

I would like to thank my supervisor **Dr. Abdennour BENHIZIA** for his unconditional support, guidance, and encouragement throughout my Ph.D. research. He was my mentor, friend, and guide in the true sense. I have learned a lot from him and consider myself lucky to have been his student. I am thankful to him for introducing me to the world of metal foams and credit him for all the work I did in my Ph.D. research. Without his help, I couldn't have done it.

This work was carried out within the laboratory of Mechanics of Structures and Materials, for this, I would like to address my deep gratitude as well as my sincere thanks to the director and to all the members of the laboratory for their professionalism and for all the facilities and the advice they were kind enough to provide me.

I thank my family for encouraging me to register for the doctorate. They have been my strength and inspiration throughout. It wouldn't have been possible without them.

My gratitude is also extended to the honorable members of the jury, **Pr. OUTTAS Toufik**, **Pr. MADANI Salah**, **Pr. HECINI Mabrouk**, and **Pr. CHEBBAH Mohamed-Saïd** for devoting time and patience to read and examine this humble research work.

I thank my colleagues at URME for all the encouragement and help in order to pursue my Ph.D. career.

TABLE OF CONTENTS

LIST OF FIGURES

List of tables

GENERAL INTRODUCTION

Due to their significant and excellent characteristics, closed-cell foams are widely used in various engineering applications [1-6], and it becomes an important subject of modern research. Therefore many published experimental and numerical studies focused on the mechanical performances of the closed-cell foam material, including its effective elastic modulus [7-10], yield behaviors [7, 11, 12, 13, 14], and energy absorption capacity [2, 15, 16, 17, 18, 19, 20].

These mechanical performances have been studied experimentally under various mechanical loadings, essentially under quasi-static, dynamic uniaxial compression [2, 14, 15, 21-28] and three-point bending [29-31]. It was found that the mechanical properties of these foams are strongly influenced by the microstructural parameters such as relative density, cell size, and cell morphology [22, 25, 26, and 32].

In its turn, the microstructure of closed-cell foam is strongly affected by the selected manufacturing method. The most common techniques are powder metallurgy and melting techniques [33]. The effect of production parameters on the mechanical properties of foam has been studied by several researchers, see for example [33-36].

The main drawback of experimental studies is the difficulty to study the influence of each morphological parameter separately due to the complexity, and the high cost of manufacturing methods and experimental tests [37], which restrict the experimental methods and suggest adopting an alternative approach.

Recently, additive manufacturing (AM) or 3D printing has become an alternative method for producing cellular structures. It has great advantages compared to the traditional methods regarding flexibility and design opportunities. However, the current studies of 3D printed cellular structures are mainly restrained to regular foams [38; 39] or periodic lattice structures [40; 41]. The deformation mechanism of these structures occurs in the form of bending [42]. In contrast, the suitable deformation mechanism for energy absorption and crashworthiness applications is the collapse and stretching of cell walls of closed-cell foams [42]. Unfortunately, the high degree of randomness in the real closed-cell foams geometry restricts the studies of these structures using the Additive Manufacturing (AM) methods.

Numerical modeling is another efficient technique to describe the mechanical behavior of foams, it allows to investigate easily each parameter separately. In numerical modeling, two groups of models can be distinguished: image-based models and tessellation-based models [43, 44-46].

The reconstruction of real foam geometry using X-ray tomography is the most accurate method to give it a quantitative description [47; 48]. Furthermore, the final geometrical body is meshed as a solid element. Although it provides valuable results, such studies encountered the same kind of problems as in experimental ones like cost and time of sample preparation, time of scanning, and data post-processing, which limit the study in terms of samples number, and also it requires high geometric discretization to capture accurately the small features existing in the original body, which demands much computational time. That's why in some studies only 5% of compression strain is calculated, and the densification regime is not addressed, see [13].

Tessellation-based models are generated using algorithms such as Random Sequential Addition (RSA) and Random Close Packing (RCP). The principle of the algorithms is inspired from the foam formation process, where bubbles are inflated until each one meets its neighbors with a uniform rate (Voronoi) or a non-uniform rate (Laguerre) [44].

These models has been lately introduced by researchers to analyze the effect of the cell shape irregularity [14], cell wall thickness variation [49], and relative density [26; 50] on the deformation mode and energy absorption of foams.

Compared to real foams, the main disadvantage of the Tessellation models based on shell formulation is the lack of some important features such as cell wall irregularities and thickness variation which limits the functionality of these models, especially in medium-density foams. These imperfections led to the demand for a proper method to generate realistic RVE models, which can capture the real foams geometry more precisely.

In this study, solid models of closed-cell foam are constructed taking into account more precisely the relevant geometrical features in real foams, such as the irregular cell shapes, non-uniform cell wall thickness, and unequally geometric distribution.

The modeling approach is based on the natural foam formation process. It allows control of the foam geometry and gives the exact desired relative density. The efficiency of the finite element (FE) models for predicting the compressive performance of closed-cell foam was assessed by comparing its results to the existing formula from the literature.

This thesis is composed of 4 chapters and is organized as follows:

- Chapter 1 provides an overview of the classification, production, and industrial applications of metal foams. The most relevant manufacturing routes and methods are presented. Then a summary of the most relevant applications with a large number of concrete examples is presented.

- Chapter 2 presents detailed information on the methodology of experimental investigations of metallic foams and the main microstructural parameters affecting the mechanical behavior of closed-cell foams.
- Chapter 3 reviews the methodology devoted to generating 3D solid models of closed-cell foams and its validation through comparison with available experimental data from literature and by 3D printing tests.
- Chapter 4 presents the numerical simulations based on FEM used to control relative density and to estimate the quasi-static crushing behavior of the 3D-designed solid closed-cell foam.

Finally, a general conclusion summarises the main findings and recommendations and gives a strategy for future studies.

CHAPTER I Metal foams – classification, production, and applications

I.1. Introduction

Metal foam is a porous material having a cellular structure comprising metal and gas bubbles [51]. The special combination of lightweight, high thermal stability, air and water permeability, exceptional acoustic properties, energy absorption, and good environmental and corrosion characteristics make it suitable for a wide range of applications [52-54]. However, their applications are still limited, due to the high cost of manufacturing metal foams.

Several methods have been developed to produce porous metals since they were discovered, which result in foams with different features [55]. The foam microstructure depends on how it is manufactured, for example, the density and cell size can be controlled by selecting certain manufacturing parameters, such as gas injection or nozzle vibration [56].

In this chapter, the definition, classification, and manufacturing of metal foams using various production processes are detailed. Finally, several industrial areas that have used them are presented.

I.2. Definition

A metal foam is a cellular structure made up of a void and a metal matrix. There are two types of metal foams: closed-cell foams and open-cell foams (see Figure I.1). The main distinction between these two kinds of porous materials is that, in open pores, the fluid and the solid move relative to one another, whereas, in closed pores, the fluid is contained within the solid matrix. High porosity is the defining characteristic of metal foams; typically, the base material makes up only 5-25% of the volume.

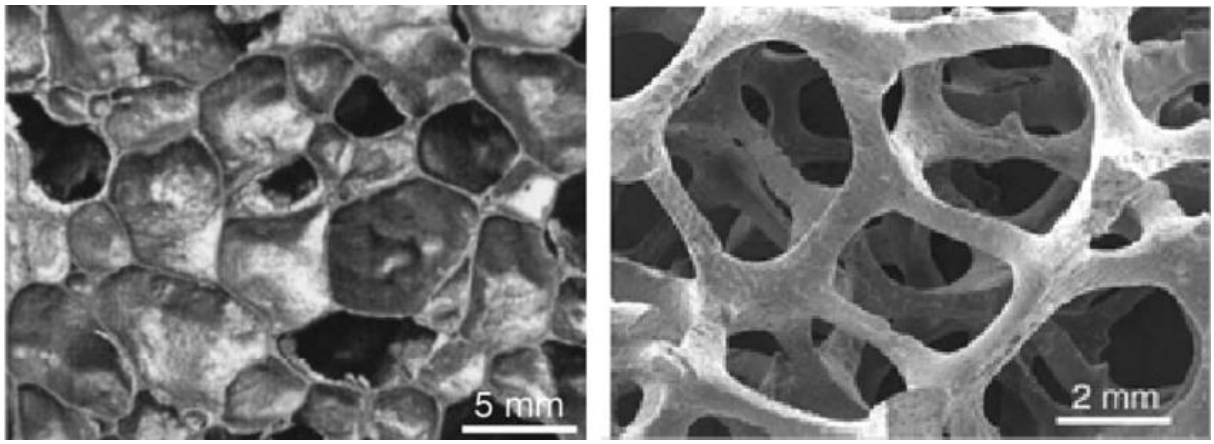

Figure I.1: Micrographs of (left) a closed cell foam and (right) an open cell foam [57].

I.3. Classification

Metal foams can be categorized based on several factors, but the two most crucial are the pore architecture (stochastic or regular) and the type of pore (open or closed).

I.3.1. According to the pore type

a) Open cell foams

Figure I.2 depicts the morphology of typical open-cell foam. The three primary parts of the foam structure are the cell window, strut, and strut joint.

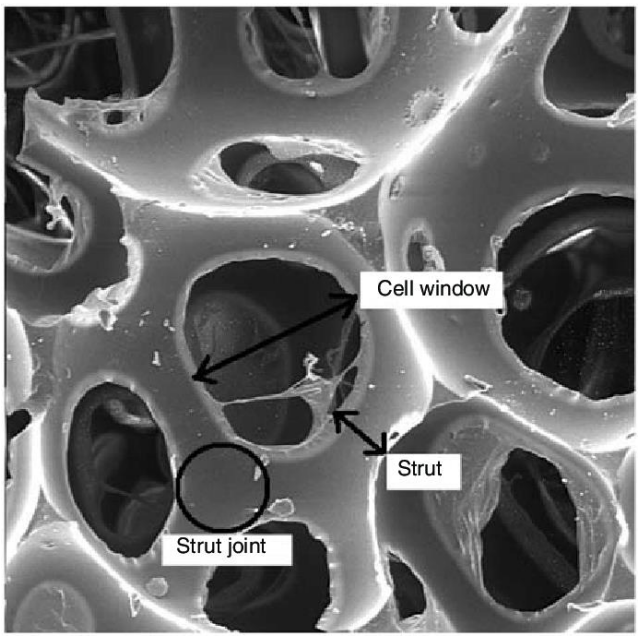

Figure I.2: Morphology of typical open-cell foam [58]

b) Closed cell foams

Unlike open-cell foams, closed-cell foams consist of unconnected spherical cells, which are separated by irregular walls, as shown in Figure I.3.

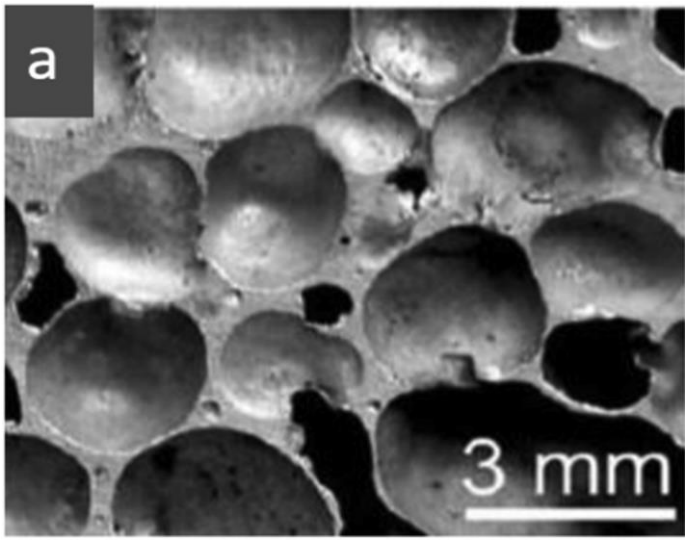

Figure I.3: Morphology of typical Closed-cell foam [59].

I.3.2. According to the pore architecture

a) Stochastic foam

The foam is referred to as stochastic if the porosity distribution is random and contains a wide range of bubble sizes (Figure I.4).

Figure I.4: Example of stochastic foam with spherical and interconnected cavities [60].

b) Regular foam

The foam is referred to as regular when the structure is well-organized (Figure I.5). This type of foam can be produced using direct molding or additive techniques, such as selective laser melting (SLM).

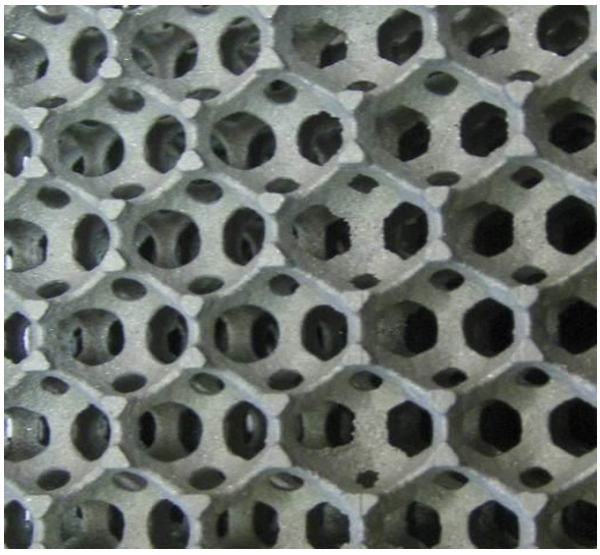

Figure I.5 Regular foam produced by the process developed by TCFI [61].

I.4. Production Methods for Metallic Foams

Metallic foams can be produced using a wide range of techniques. Each method produces foams with typical morphology and density range and is effective for a particular spectrum of metals or alloys. In this section, the most common techniques for creating metal foams are presented.

I.4.1. Manufacturing techniques of closed-cell foams

a) Foaming of molten metal by gas injection

The first technique for producing metal foams was created by the Norwegian company Hydro Aluminum and distributed by the Canadian company Cymat Aluminum. Figure 1.6 illustrates this manufacturing process [53].

The gas injection is usually done using a rotating impeller which generates gas bubbles and distributes them uniformly (Figure 4). The bubbles thus formed, float to the surface of the melt and drain after which the melt begins to solidify into foam. Usually silicon carbide, aluminum oxide or magnesium oxide particles are used to enhance the viscosity of the melt. These particles are added into the melt using sophisticated mixing techniques to ensure a uniform distribution.

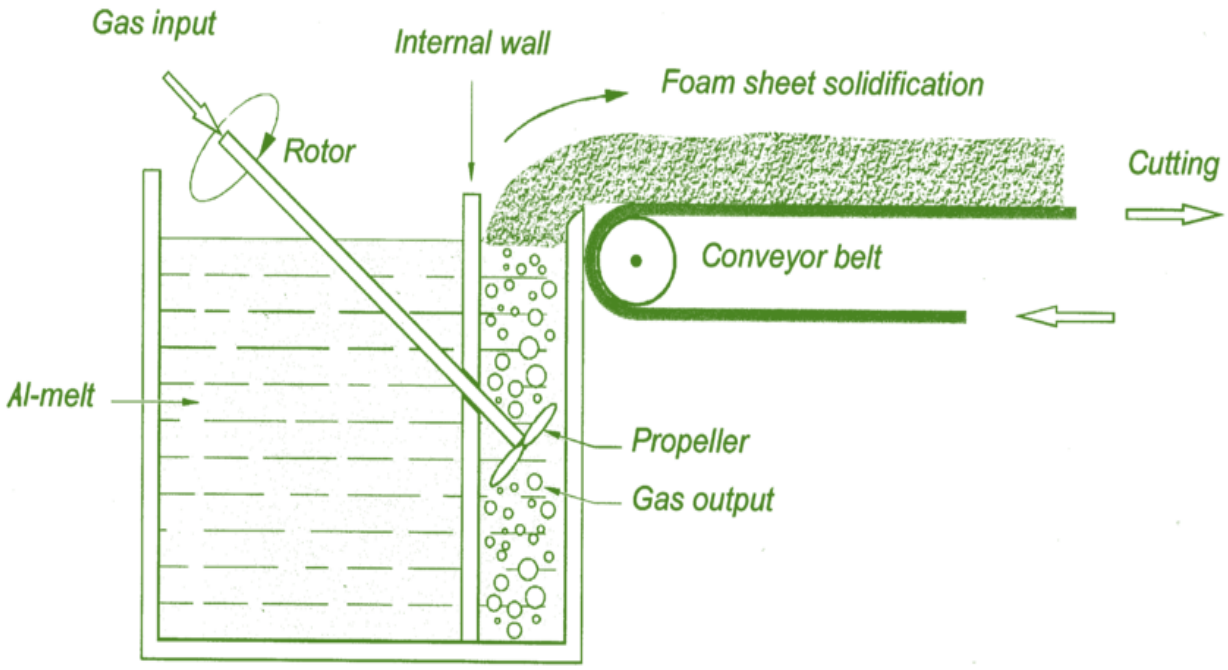

Figure I.6: Foaming of molten metal by gas injection [53].

An example of foam produced by this technique is shown in Figure I.7.

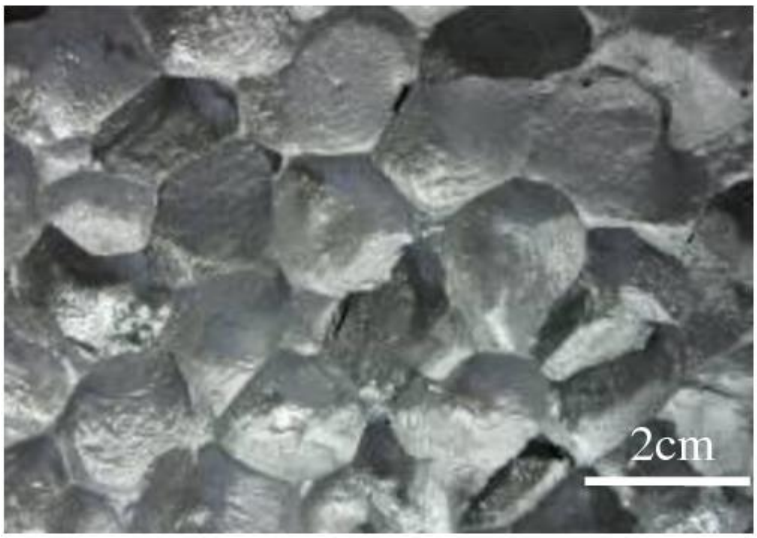

Figure I.7: SEM microstructure of produced composite foam by Melt Gas Injection Process with a density of 0.20 g/cm^3 [62].

b) Foaming of molten metal with a foaming agent

This process, shown in Figure I.8, involves adding calcium to molten aluminum at a temperature of 680 °C. The molten metal is then agitated for a period of time during which its viscosity significantly and continually increases. Once the viscosity is high enough, the titanium hydride emulsion is typically added, decomposes, and releases the hydrogen gas that creates the emulsion process.

Constant pressure is used throughout the emulsion process. The liquid foam hardens once the crucible has been cooled below the melting temperature of the aluminum alloy, allowing it to be withdrawn from the mold for later machining.

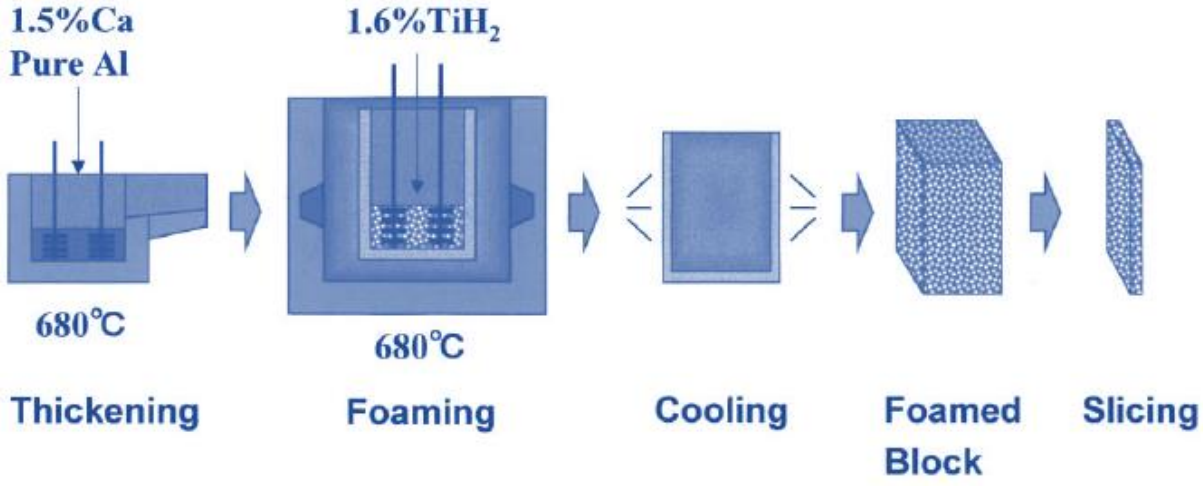

Figure I.8: Foaming of molten metal with foaming agent [55].

An example of foam produced by this technique is shown in Figure I.9.

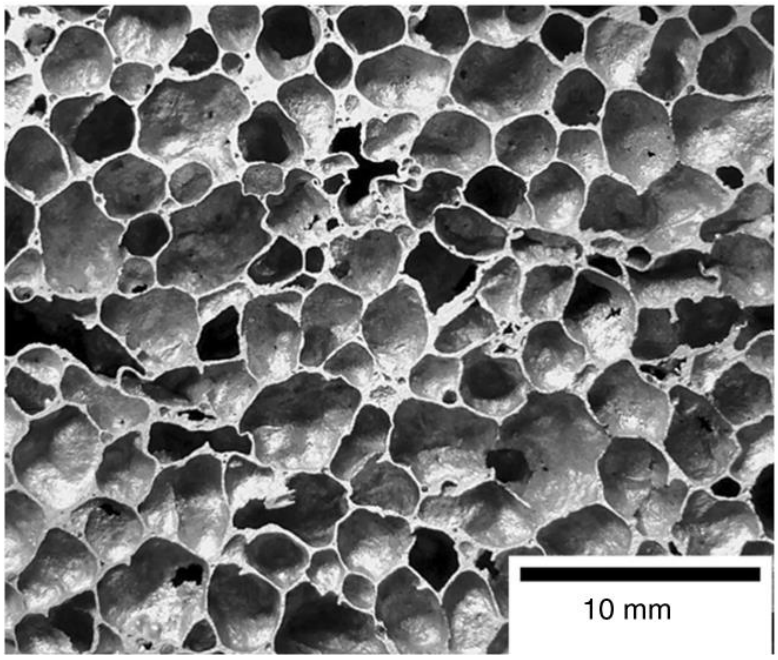

Figure I.9: Cross-section of an $AlSi_8Mg_4$ foam blown with TiH_2 [63].

c) Powder metallurgy

Figure I.10 displays a schematic diagram of the production process. It starts by mixing powdered aluminum alloy with foaming agent particles (usually titanium hydride). Following thorough mixing, the powder is cold compacted before being extruded into a bar or plate with a density that is close to that of theory. The powder is well mixed before being cold-compressed and extruded into a bar or plate with a density that is nearly identical to that predicted by theory. This "precursor" material is cut into small pieces, placed inside a sealed split mold, and heated to slightly above the solidus temperature of the alloy. The titanium hydride then decomposes, generating pressure-filled holes. These enlarge via semi-solid flow, the aluminum enlarges, and a foam is produced that fills the mold.

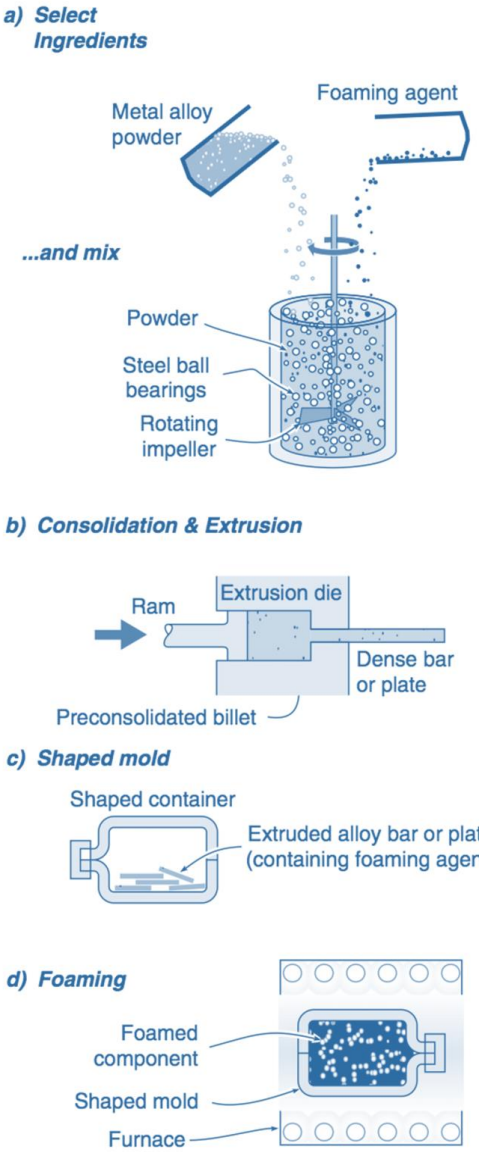

Figure I.10: The sequence of powder metallurgy steps used to manufacture metal foams by gas-releasing particles in semi-solids (the Fraunhofer and the Alulight processes) [64].

An example of foam produced by this technique is shown in Figure I.11.

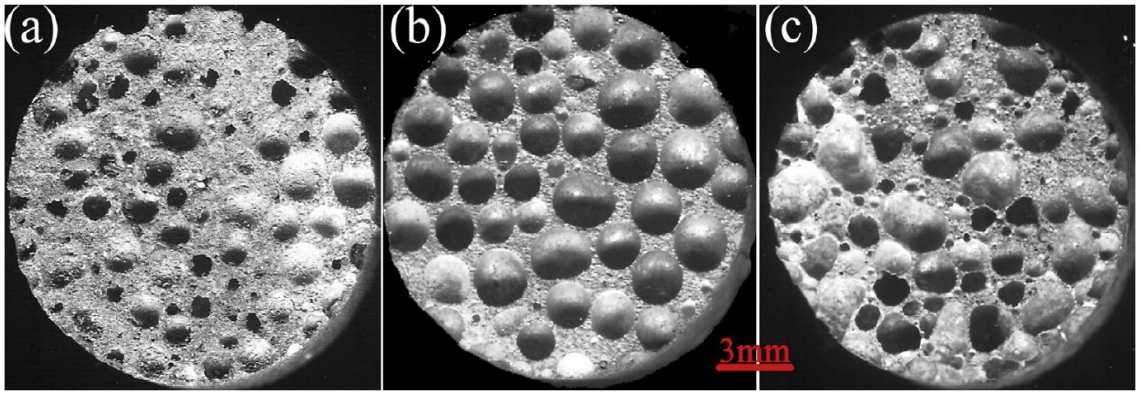

Figure I.11. Section images of Mg8Al2 foams fabricated at 620 ◦C with foaming time of (a) 90 s, (b) 150 s and (c) 180 s [65].

I.4.2. Manufacturing techniques of open-cell foams

a) Casting using a polymer precursor as a template

A variety of metals and their alloys can be cast into investment-casting molds made from open-cell polymer foams using them as templates. Figure I.12 provides a schematic illustration of the procedure.

- First, a mold template for open-cell polymer foam with the preferred cell size and relative density is chosen.
- The mold is then baked to remove the polymer template and harden the casting material, leaving behind a negative impression of the foam. Then a metal alloy is poured into this mold, and it is let to cool.

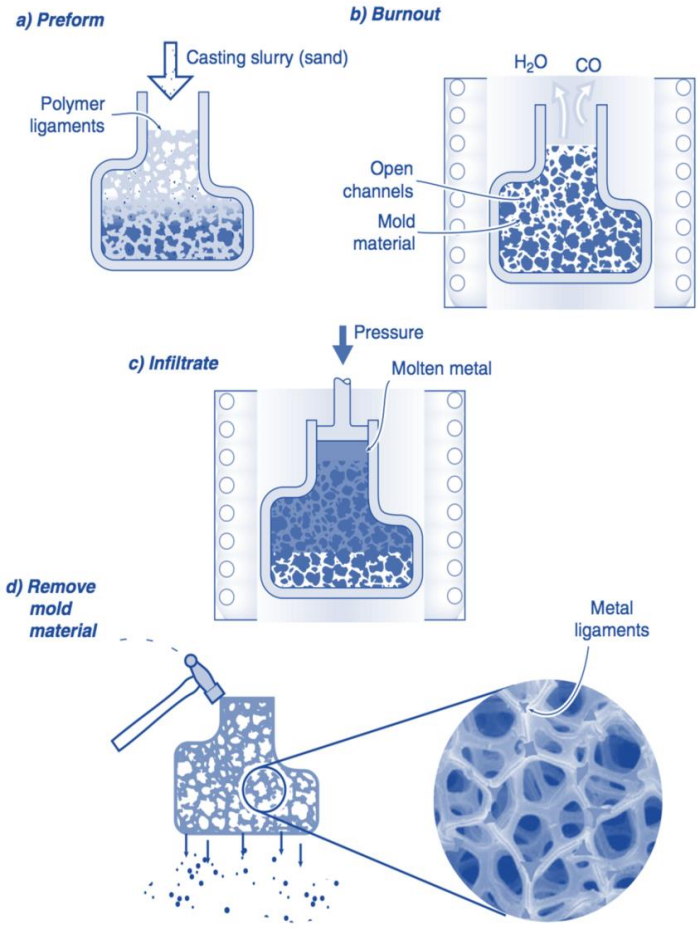

Figure I.12: Investment casting method used to manufacture open-cell foams [66].

An example of foam produced by this technique is shown in Figure I.13.

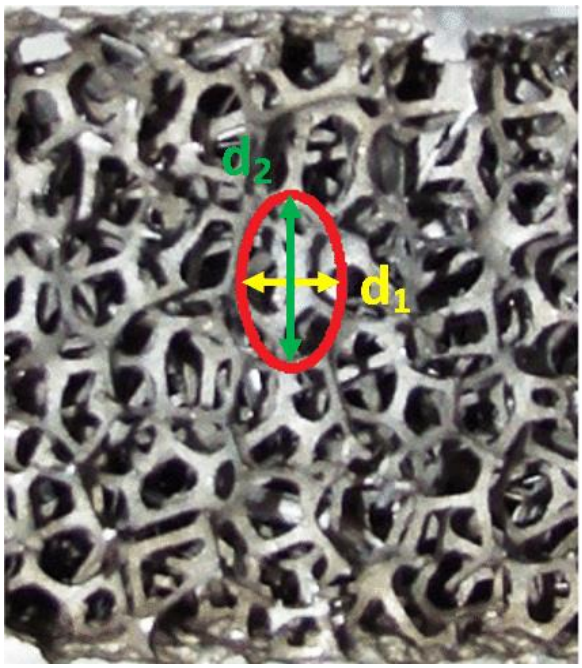

Figure I.13. Open-cell metal foam produced by investment casting from a polyurethane perform [67].

b) Metal deposition on cellular preforms

Open-cell polymer foams can act as templates for the electrodeposition, evaporation, or chemical vapor decomposition (CVD) of metals. Figure I.14 shows schematically a CVD reactor containing an open-cell polymer after nickel carbonyl has been introduced. At a temperature of about 100 °C, this gas decomposes into nickel and carbon monoxide, coating all heated surface that is exposed inside the reactor. To heat only the polymer foam infrared heating can be used. The metal-coated polymer foam is taken from the CVD reactor after several tens of micrometers of the metal have been deposited, where the polymer is burnt out through heating in the air.

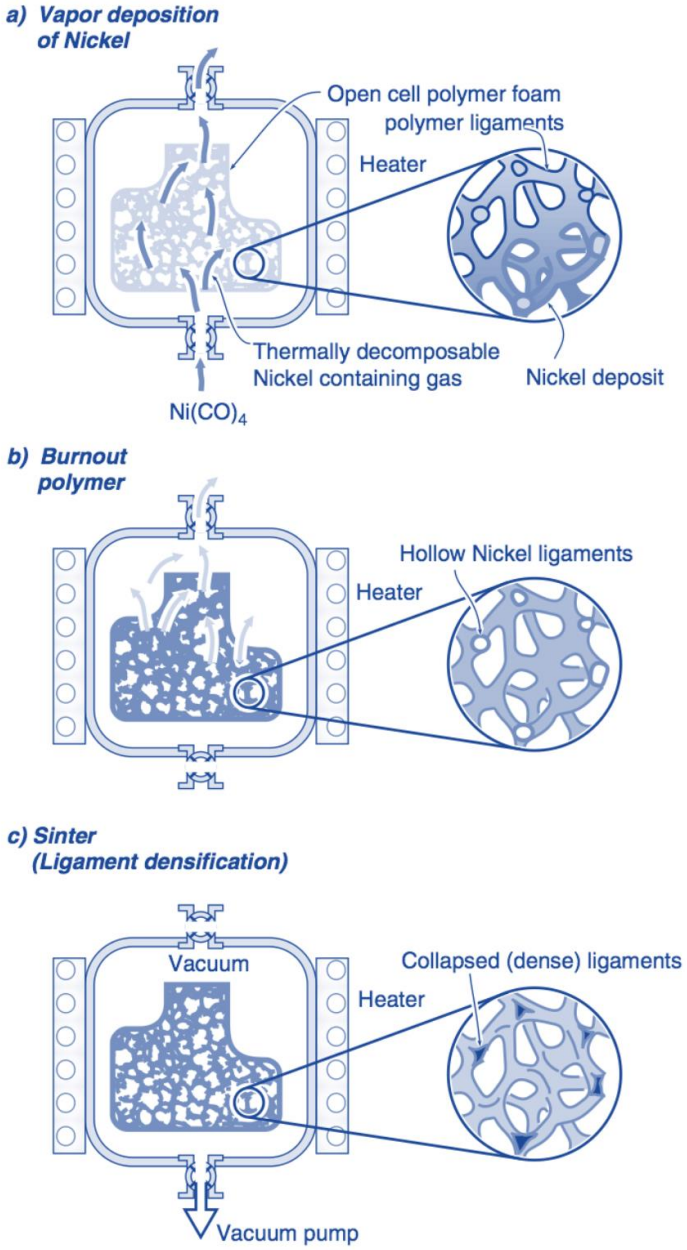

Figure I.14: Schematic illustration of the CVD process used to create nickel foams [66].

An example of foam produced by this technique is shown in Figure I.15 and Figure I.16.

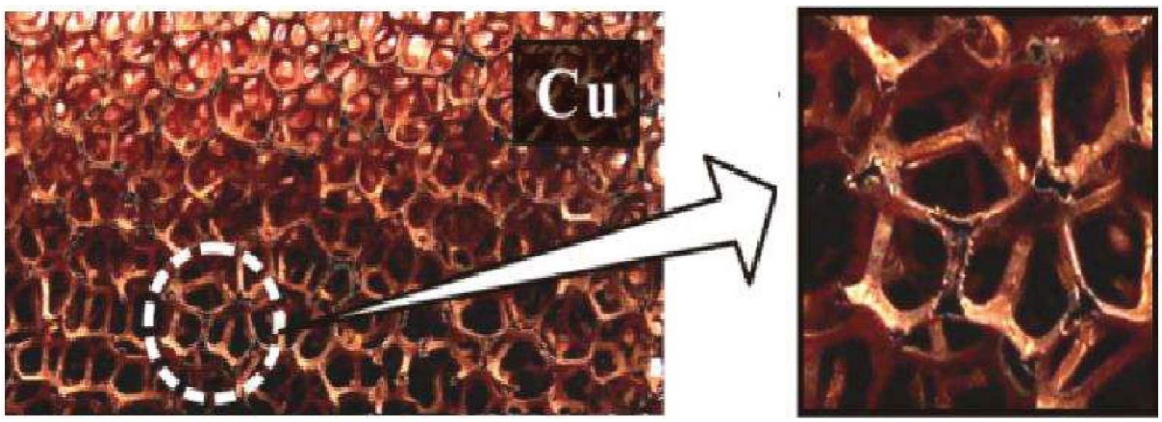

Figure I.15: Metal foam produced by electro-deposition method [68].

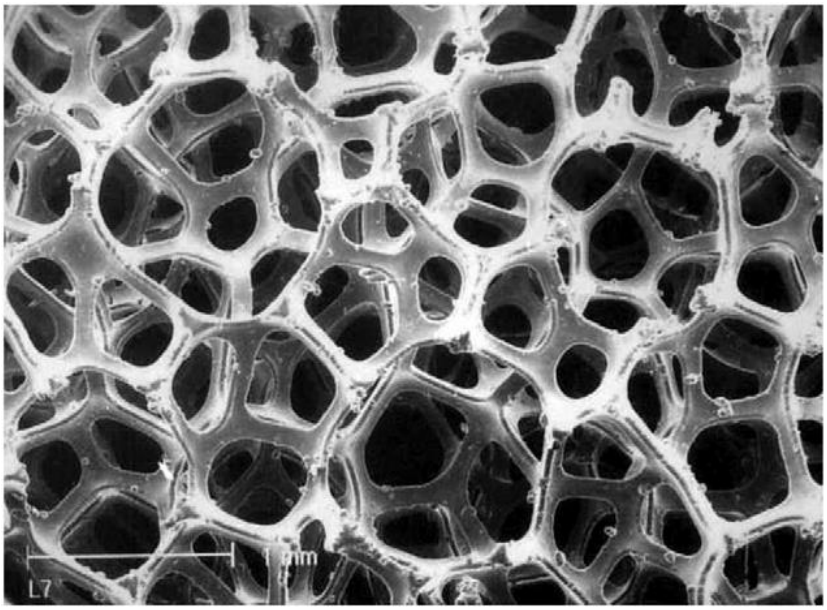

Figure I.16: Morphology of the nickel foam produced by electrodeposition. [69]

I.5. Additive manufacturing AM

The most widely used method for layer manufacturing of metallic objects is powder bed fusion. The principal setup is shown schematically in Figure 1, where a laser beam melts the metallic powder in accordance with a CAD file of the component to be built.

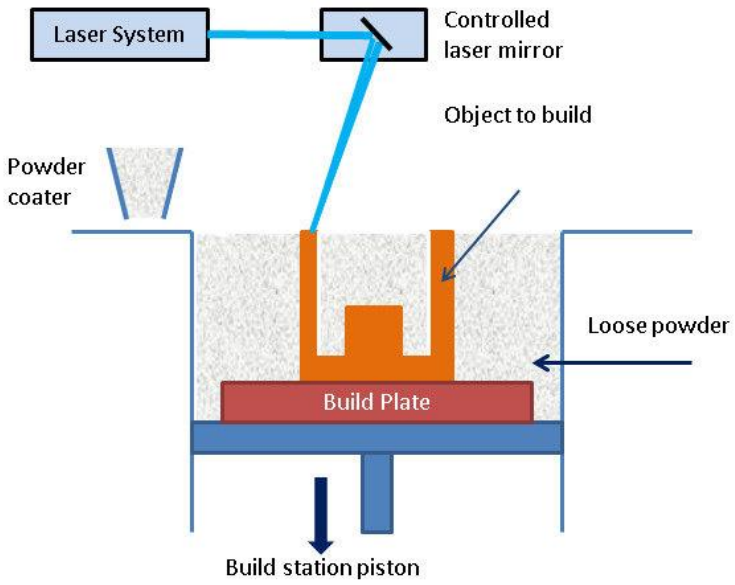

Figure I.17: Schematic representation of the powder bed fusion process.

An example of foam produced by this technique is shown in Figure I.18.

Figure I.18: Cylindrical random foams manufactured by means of LPBF [70].

I.6. Metal Foams applications

Depending on the nature of foams, their applications can be divided into two categories: functional and structural. Figure 1.19 displays the grouping of several potential uses according to the kind of porosity in the foam.

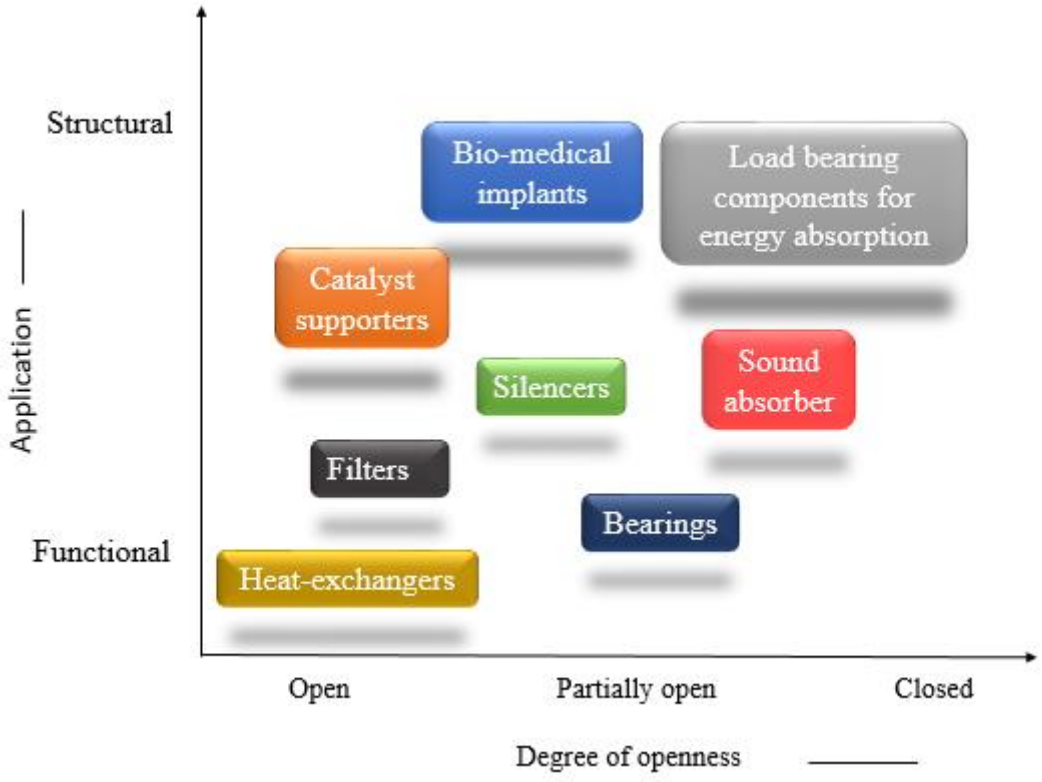

Figure 1.19 Applications of metal foams grouped according to the degree of open porosity needed and whether the application is functional or structural [71].

1.6.1. Light-weight construction

Metal foam research and development have recently seen a lot of activity in the automobile sector. As shown in Fig. 1.20 [72], there are numerous places in the bodywork where structural foams can be used.

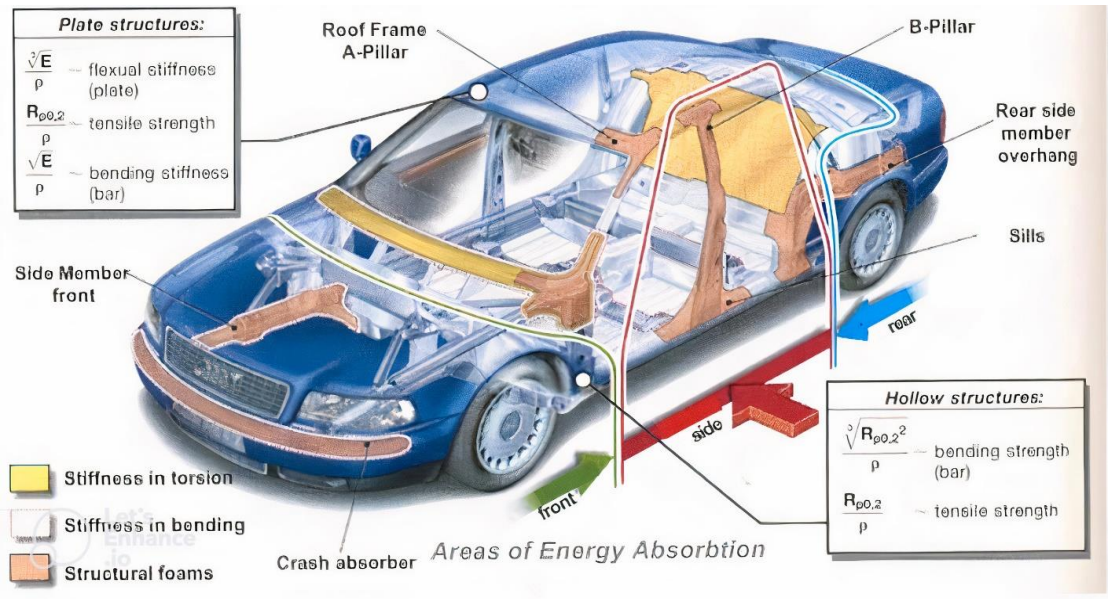

Figure 1.20 Numerous places in the bodywork where structural foams can be used [72].

Figure 1.21 illustrates a variety of open-cell metal foam-based products (filters) for functional applications that combine high temperature, chemical resistance, and sound-absorbing properties [73].

Figure 1.21 Open-cell metal foam-based products (filters) for functional applications.

I.6.2. Energy-absorbing applications

In order to increase the energy absorption capacity, aluminum foam is used as a filler material for tubular structures. For example, it replaces bulk metals or hollow tubular structures in car bumper system crashboxes [74].

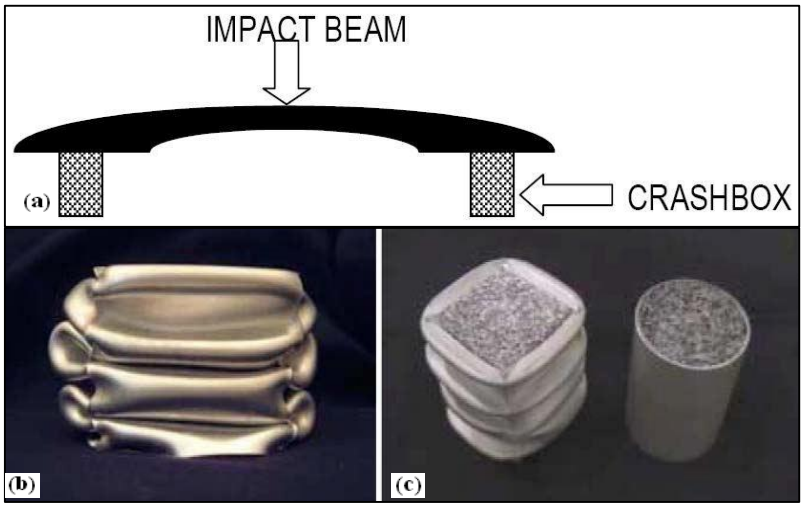

Figure 1.22 Aluminum foam (Cymat) filled crashboxes to be used in car bumper system [74].

Figure 1.23 shows an example of a fabricated Al foam-filled steel tube specimen and its cross-section, respectively [75].

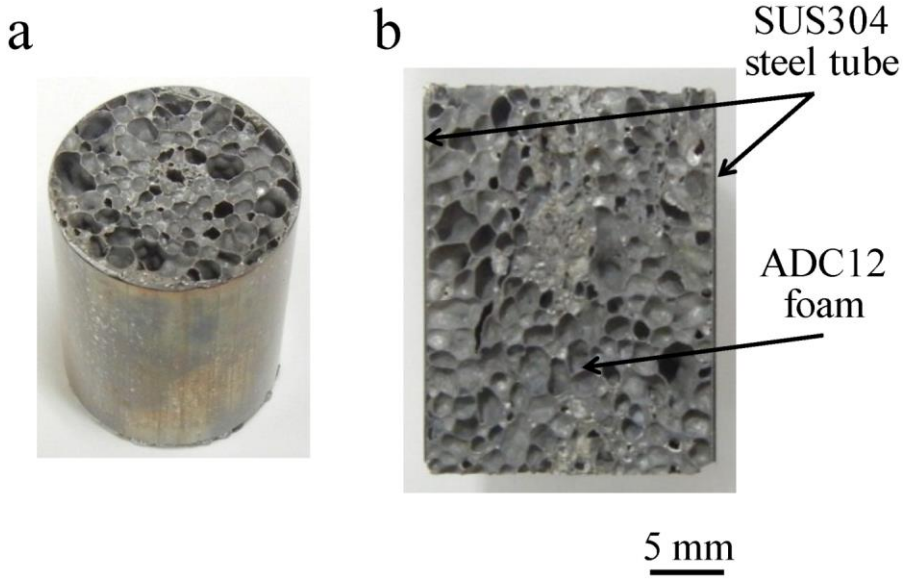

Figure 1.23. Fabricated Al foam-filled steel tube: (a) Compression test specimen; (b) Cross-sectional image of (a) [75].

A comparison of mechanical properties between steel tube, Al foam, and Al foam-filled steel tube is shown in Figure 1.24. As can be seen, the steel tube filled with aluminum foam had superior mechanical properties to both steel tube and aluminum foam.

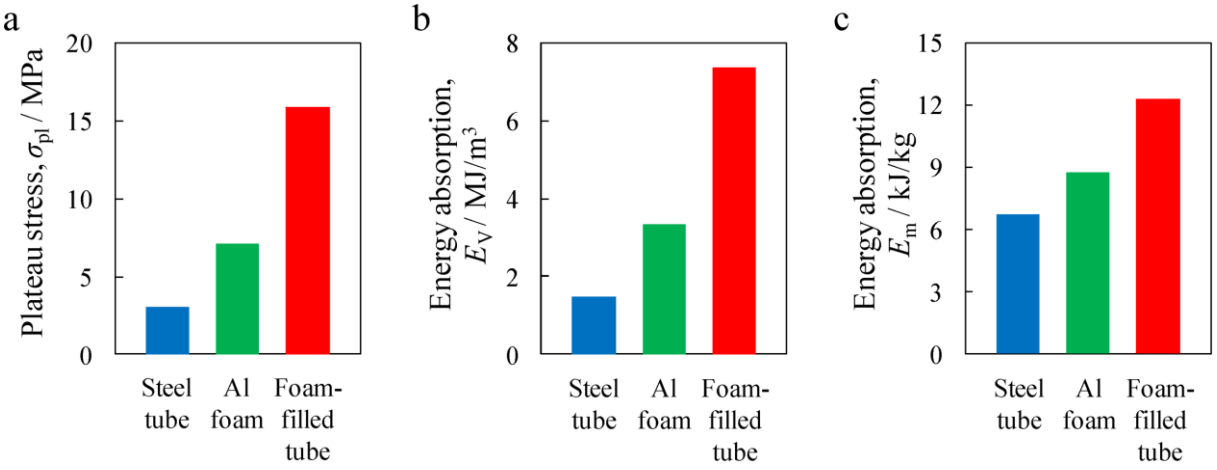

Figure 1.24. Comparison of mechanical properties between steel tube, Al foam, and Al foam-filled steel tube: (a) Plateau stress; (b) Energy absorption per unit volume; and (c) Energy absorption per unit mass [75]

I.6.3. Silencers

Industrial powder metallurgy applications frequently use parts to dampen sound, pressure pulses, or mechanical vibrations. For example, sudden pressure changes occurring in compressors or pneumatic devices can be damped with porous sintered elements (Figure 1.25) [71].

Figure 1.25: Example of aluminum foam silencer [71]

I.6.4. Fluid-fluid heat exchangers

Three crucial properties of open-celled metallic foams make them effective in heat exchange applications: a high surface area to volume ratio, a very complex flow passage through the foam, and strong solid-phase thermal conductivity [76]. It is used in a variety of devices, such as a small heat exchanger for the thermal stabilization of the electron scanning

microscope lens and thermal energy absorbers for laser medical applications (see Figuer I.26) [77].

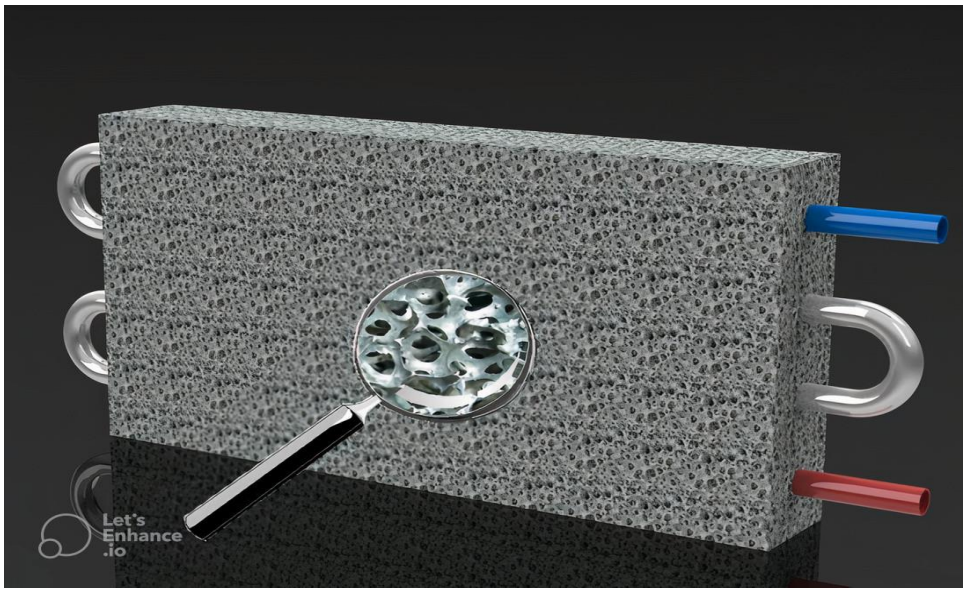

Figure 1.26 Open-cell aluminum foam (DUOCEL) used as heat-exchanging medium for the space shuttle atmospheric control system [77].

I.6.5. Sandwich panels

A foam sandwich is an innovative material that has many advantages such as a high bending stiffness at a low density and good energy absorption properties.

Figure I.27 shows Two different commercial aluminum alloy foam sandwiches have been investigated by [55], the first one (Schunk-Honsel Entwicklungsgemeinschaft) with faces obtained by extrusion (integral skins), the second one (Alulight® International GmbH) with faces bonded to the core by an epoxy adhesive.

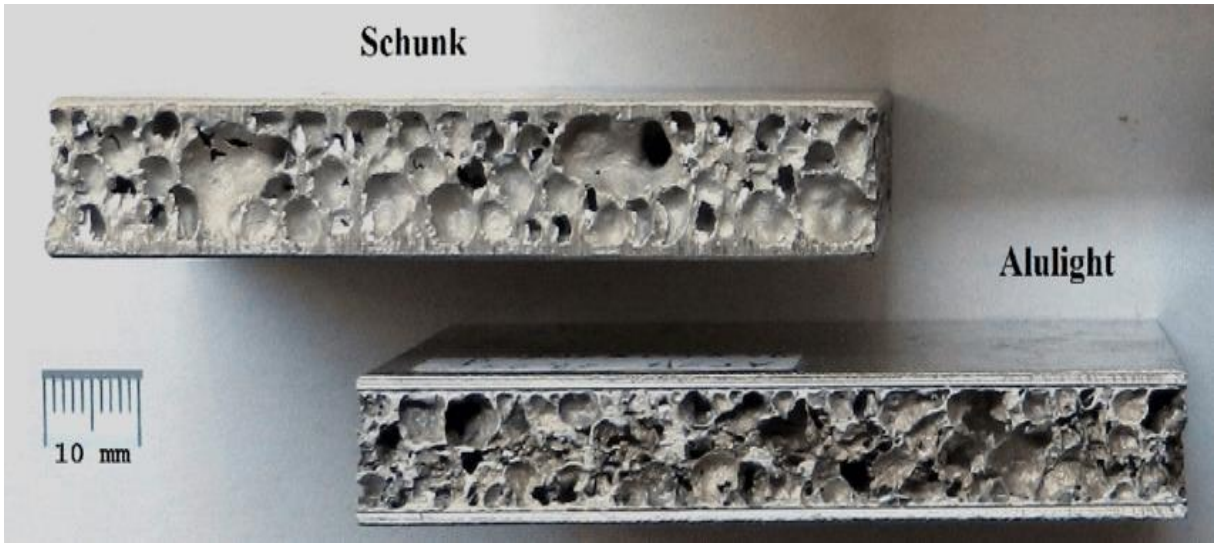

Figure 1.27: Aluminum foam sandwiches (AFS) panels structures.[78]

Table I.1 details a summary of some of the related applications of such sandwich structures. The typical applications reported in the literature are for low-velocity impact (perforation), shock wave, and crashworthiness applications [79]. For sandwich structure face sheets, typical materials used are either metals (stainless steel/aluminum) or fiber composites. For the core, the most common foam material used was aluminum. Some of the key findings are as follows:

- Graded metallic cores are better than uniform-density cores.
- Failure mechanisms of the face sheets and core play a vital role in the energy absorption capability.
- Parametric design is crucial to optimize the sandwich structure for energy absorption.
- For perforation applications, it was found that the sandwich panels performed poorly compared to the monolithic aluminum panel.
- Sandwich structures used for crashworthiness-related applications/testing conditions demonstrated progressive crushing.
- The blast resistance of the sandwich panels comprised of the composite face sheets outperformed the metallic counterparts.
- Strain rate of the foam core is important in defining the crushing behavior which is linked to the energy absorption capabilities.

Table I.1. Summary of some of the related applications of such sandwich structures [80]

Sandwich Construction	**Loading/ Application**	**Summary of Findings**	**Reference**
Spherical shell sandwich made from aluminum metallic foam cored with varying densities with outer and inner face sheet made from aluminum	Inner blast loading from the inner center of the structure (blast-simulation)	The arrangement of core foam density plays an important role in optimizing the blast-resistant response	[81]
Sandwich panels made from closed-cell aluminium foam cores	Low-velocity Impact	For perforation application, it was found that the sandwich panels	[82]

and aluminium face sheets	(perforation-simulation)	performed poorly compared to the monolithic aluminium panel.	
Sandwich panel consists of aluminum foam core with steel as face sheets	Air-blast loading (blast-simulation)	Specific energy absorption increases with the increase of foam thickness and the sandwich panel can reduce peak acceleration by 50% compared to steel plates.	[83]
Double wall tubular structure filled with metallic aluminum foam.	Compression test (Crashworthiness experiment and simulation)	(1) Strain rate of the foam core is important in defining the crushing behavior which is linked to the energy absorption capabilities. (2) Interaction between the foam and the tube wall enhance multiple propagating folds, which enhances crashworthiness performance.	[83]

I.6.6. Biomedical Implants

In recent years, metallic foams made of different metals have been used in different parts of the body. Metallic open porous foam structures have a significant potential in biomedical applications, especially since they show a similar structure to the tissue of the bone [84]. The used metal should not react with the tissue, bone or body fluids. It should not form toxic substances, not cause allergy, not contain carcinogenic substances and not release metallic ions. The foams produced from Ti, SS, Co-Cr alloys and Mg used in biomaterial applications exhibit compatible behavior with the body [85]. In addition, the porous structure of metallic foams has a structure similar to that of the bone, so that it can transmit body fluids increases adhesion to the tissue where the implant is located [86]

Table I.2 summarizes examples of metal foams used in biomedical applications.

Tantalum monoblock acetabulum [87]	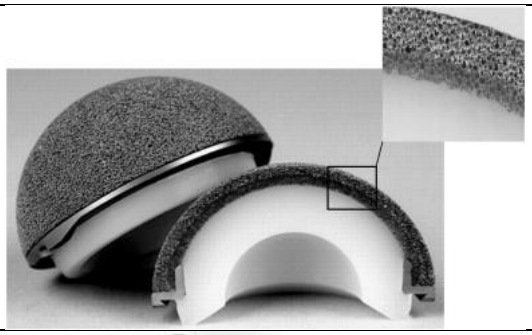
Osteonecrosis implant [87]	
Spine arthrodesis implants [87]	
Porous titanium component used in treatment of the flatfoot deformity [88] Figure ahead shows the bioactive titanium foam used for spinal interbody fusion. The component consists of titanium foam that produced with powder metallurgy technique placed in a dense frame.	
Titanium foam used for lumbar interbody fusion [89]	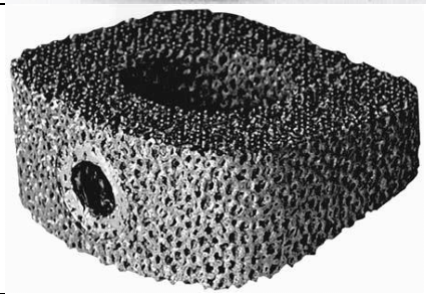
Dental implant developed by Zimmer Dental Inc. [86]	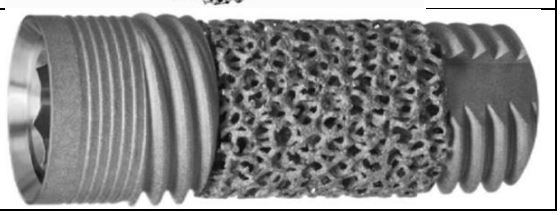

I.7. Summary of application and relevant features of metallic foams

A summary of the current and potential uses of metallic foams are summarised in table I.3.

Table I.3. Some applications of metallic foams and features of these materials that are relevant to end applications [91].

Application	***Relevant features of metallic foams***
Lightweight structures (sandwich panels etc.)	High specific stiffness and specific yield stress.
Mechanical damping, vibration control and acoustic absorption	Damping capacity is an order of magnitude higher than for solid metals. Vibration control and acoustic absorption characteristics are attractive on a specific basis.
Impact absorption	High energy absorption capability.
Thermal management and flame arrest	High surface area for heat transfer, combined with high thermal conductivity cell edges.
Filters	Controlled pores sizes can be produced in open cell foams.
Electrodes and catalyst supports	High surface area per unit volume in open cell foams.

I.8. Commercially available foams

Several foams have been developed commercially and used in various applications and are still in the phase of improvement. Table I.4 summarizes the commercially available foams and their mechanical properties.

Table 1.4 Commercially available foams and their mechanical properties [91,92].

Materials	Al–SiC	Al–Mg–Si	AlSi12	Al–5Ca–Ti	Al 6061 T6
Trade Name	Cymat, Alcan	Mepura, Alulight	Foaminal	Shinko Wire, Alporas	ERG, Duocel
Relative density	0.02–0.2	0.1–0.35	0.5–0.8	0.08–0.1	0.05–0.1
Structure	Closed cell	Closed cell	Closed cell	Closed cell	Open cell
Young's Modulus (MPa)	0.02–2.0	1.7–12	3.5–8.4	0.4–1.0	0.06–0.3
Poisson's ratio, ν	0.31–0.34	0.31–0.35		0.31–0.36	0.31–0.37
Compression strength (MPa)	0.04–7.0	1.9–14.0	7.9–22.8	1.3–1.7	0.9–3.0
Tensile strength (MPa)	0.05–8.5	2.2–30	2.76–5.99	1.6–1.9	1.9–3.5

Fracture toughness (MPa $m^{1/2}$)	0.03–0.5	0.3–1.6	0.03–1.19	0.1–0.9	0.1–0.2
Thermal conductivity (W/m K)	0.3–10	3.0–3.5	16.7	3.5–4.5	6.0–11

I.9. Advantages and disadvantages of metallic foams production procedures

Various production procedures and their outcomes are summarized in Table I.5 [93].

Table I.5: Various production procedures and their outcomes.

Process	Minimum density	Maximum density	Cell morphology	Major advantages	Major disadvantages
Powder metallurgy	0.04	0.65	Closed	High relative densities possible	
Injection molding with glass balls	0.48	0.66	Closed	High relative densities possible	Potential chemical reaction with glass, some glass can break in forming process
Oxide ceramic foam precursor	0.13	0.23021	Open	Foaming at room temperature, complex shape possible, standard equipment	
Consolidation of hollow spheres	0.04	0.95	Either	Very low relative densities possible, highly predictable and consistent behavior	High relative densities not possible
Working and sintering of bimaterial rods	0.05	0.95	Open	Wide range of relative densities possible, anisotropies are controllable	
Composite PM/ hollow spheres	0.32	0.43	Closed	Behavior is both predictable and strong, no collapse band until densification	

Slip reaction foam sintering	0.12	0.41	Open	Many optimizable manufacturing parameters, foaming at room temperature	
Polymer foam precursor	0.04	0.11	Open	Low density open cell structure for filter and sound absorption application	Too weak for most structural applications
Powder space holder	0.35	0.95	Closed	Porosity may be graded across a wide range	

I.10. Advantages and disadvantages of Metal foams

I.10.1. Advantages

- Metal foams provide excellent energy absorption features at a higher strength level as compared to foamed polymers

- Metal foams are easily processed by sawing, drilling, milling, etc,

- Metal Foams can be joined by adhesive bonding, brazing, and TIG and laser welding techniques.

-It does not erode, even under the effects of air flow or vibration.

- It is easily recyclable.

- Provides sound absorption at low frequencies at a smaller material thickness in comparison with other absorption materials such as glass or mineral wool fibers or polymer foams.

I.10.2. Disadvantages

- They are difficult to manufacture as precision manufacturing is required.

- Cost is a major factor

- Difficultly in manufacturing high temperature metal

- Knowledge about the metal foam is still not wide spread

- Once damaged it can not be repaired ,the whole metal foam has to replaced by new one.

I.11. Conclusion

In this chapter, the different types of metal foams and their production techniques have

been described. Metal foams are extremely light and highly insulation because they contain up to 95% air, they are also conductors of electricity, and their porosities can contain gases and powders. Depending on the shape, distribution, and connection of the pores, their properties vary and they have a wide range of uses.

Metal foams are divided into two types; closed or open according to the connections of the pores. This is the parameter that basically separates the areas of usage.

Today, metal foams are preferred in many structural or functional applications in different sectors such as transportation and construction, biomaterials and military materials, Since foams with closed pore structures have better mechanical properties, they are used in structural, impact, and sound insulation applications. Open porous foams are used in filters, catalyst carriers, and biomedical applications due to their permeability properties .

Applications of metal foams strongly depend on whether they are open-cell or closed-cell foams. Essentially, aluminium, steel, and iron foams are used in structural and aerospace industry. For biomedical applications, steel, cobalt–chromium, titanium, copper, and foams are popular for implants and tissue engineering. For chemical industry, nickel- and copper-based foams are extensively used.

This chapter further highlights that much work needs to be done to develop foams of .different materials and using manufacturing processes that are industrially viable, reproducible, and cost-effective.

CHAPTER II EXPERIMENTAL INVESTIGATIONS OF METAL FOAMS AND THEIR MECHANICAL PROPERTIES

II.1. Introduction

The aim of the present chapter is to collect different studies about the methodology for experimental investigations of metal foams and exploring the main microstructural parameters affecting the mechanical behavior of closed-cell foams. As consequence, the first part discusses the following experimental aspects and provides uptodate references for them:

- Determination of material characteristics and deformation manners with best methods to achieve it.
- Uniaxial, biaxial, and multi-axial tests in tension and compression as well as shear and twist tests;
- Specifications for sample size and shape as well as loading apparatuses with loading modes and strain measurements.

The properties of foams can be made to vary significantly by the choice of cell wall material, the volume fraction of the solid, and the geometry of the structure. Hence, it is important to understand and model their mechanical property variation with these parameters for optimum performance. For example, The role of cell morphology and of imperfections in governing properties such as stiffness, yield strength, crush behavior, and fracture resistance, notch sensitivity, and fatigue behavior have been studied.

II.2. Methodology for experimental investigations of metal foams

II.2.1. Sample characteristics

a) Sample size

Porous metals can be viewed as uniform materials when viewed at a macro level. If the scale length approaches the cell dimensions, which for the majority of metal foams range from 2 to 7 mm, the situation changes [94]. Sample size to cell diameter ratio is typically used to define specimen dimensions. Motz et al. and Andrews et al. [94,95] report on a study of size effects in ductile cellular solids and provide guidelines for the selection of specimen dimensions for various types of investigations. For uniaxial tension/compression testing, the sample size must be at least seven times the size of the cell. The same for twist tests. In the case of shear tests, the ratio should be greater than 3, and the ratio must be more than 7 for Young's modulus measurements [97].

b) Sample shape

The type of experiment that is conducted also affects sample shape. It is generally accepted that cylinders or prisms with a height that is two times the base length are sufficient for uniaxial strain testing. Flat rectangular specimens with a thickness-to-base size ratio of around 12 would be appropriate for shear testing [95,96].

c) Determination of basic cellular material characteristics

Prior to doing any strength tests, the whole structural features of the material must first be known, including its relative density, porosity, cell size, orientation, and shape, as well as its connectivity and distribution (specific surface). The density can be determined by weighing a sample with a known volume. While the other characteristics must be assessed using microscopy.

As an example, in the work of [49], the Olympus BX60m microscope was used to photograph the microstructures of closed-cell foam. Cell sizes were determined by measuring the diameters of the cell encircles. 473 cells' diameters were measured, and some of the measurements are shown in Figure II.1 (a). According to Figure II.2(a), the observed cell diameter roughly follows a lognormal distribution with an average of 256 µm and a standard deviation of 91.8 µm.

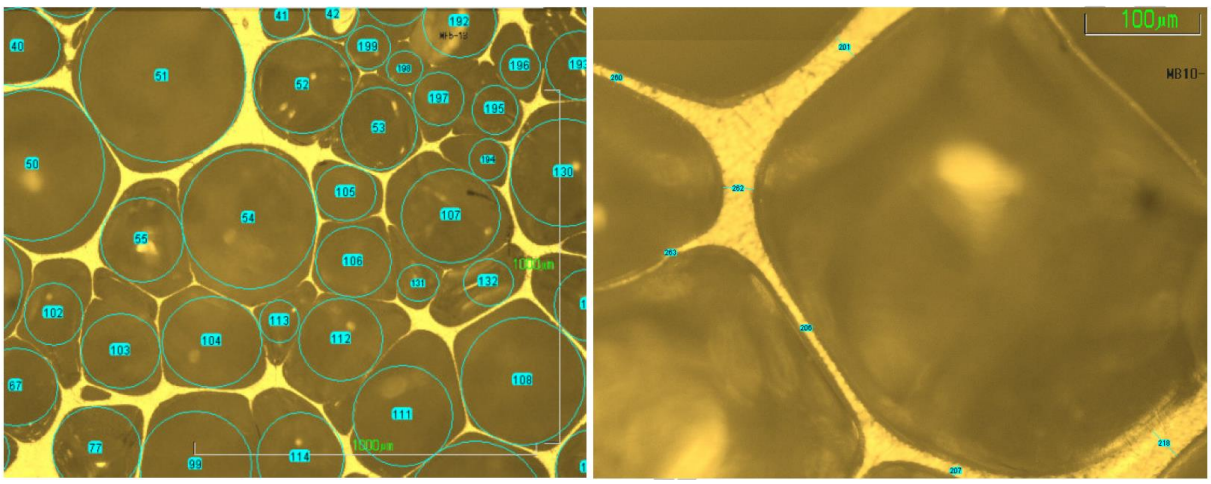

Figure II.1: (a) Cell size measurements, and (b) cell wall thickness measurements.

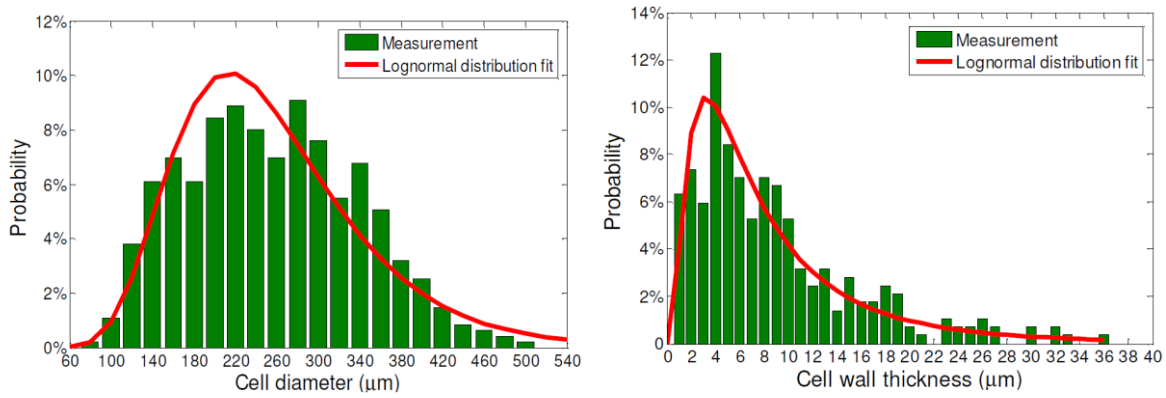

Figure II.2: (a) Measured cell size distribution and its probability distribution fit, and (b) measured cell wall thickness distribution and its probability distribution fit.

II.2.2. Uniaxial tests

a) Uniaxial compression test

Uniaxial compression tests are the most often performed experiments to evaluate the characteristics of metallic cellular materials because metal foams are typically utilized in applications where their compressive properties are important. In the compression test, the two sample ends touch loading platens while the sides of the specimen are free.

For illustration, en example of a quasi-static compressive experiment conducted in a microcomputer controlled electronic universal testing machine (model WDW-200E see Figure II.3) is shown in FigureII.4 .

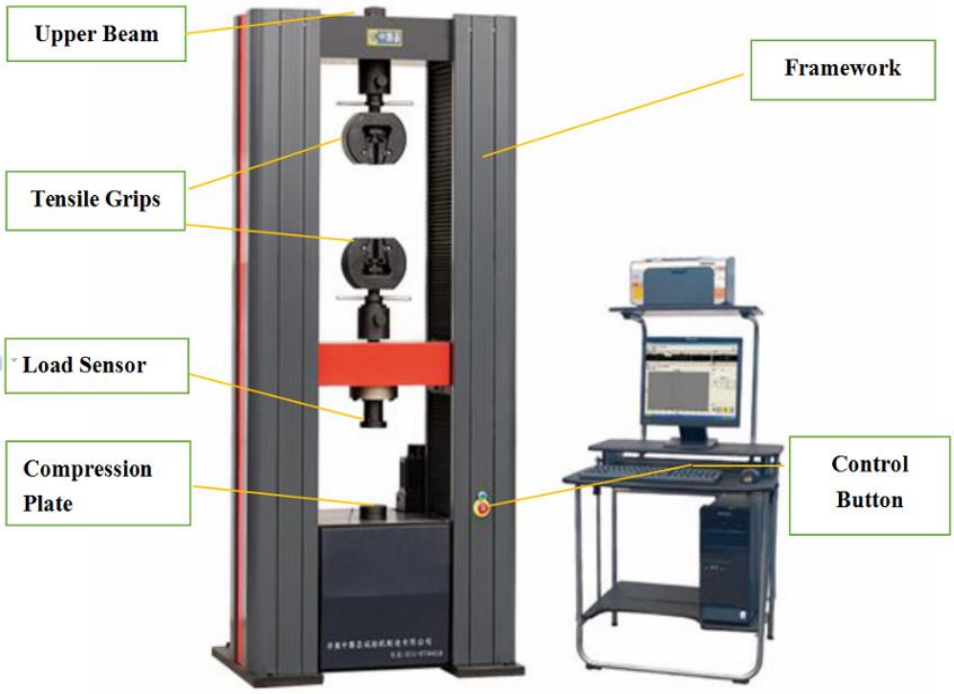

Figure II.3: WDW-200E Computer Controlled Electronic Universal Testing Machine.

The uniaxial compression loading was applied with a platen velocity of 5 mm/min (strain rate: 1.7 *10^{-3}) at room temperature. During compression, the load and displacement were automatically recorded by a computer, and the foam deformation process was also captured with a digital camera. The nominal stress was calculated by dividing the load with the initial cross-sectional area of the specimen (2500 mm2). The nominal strain was calculated by dividing the platen displacement with the initial specimen height (50 mm).

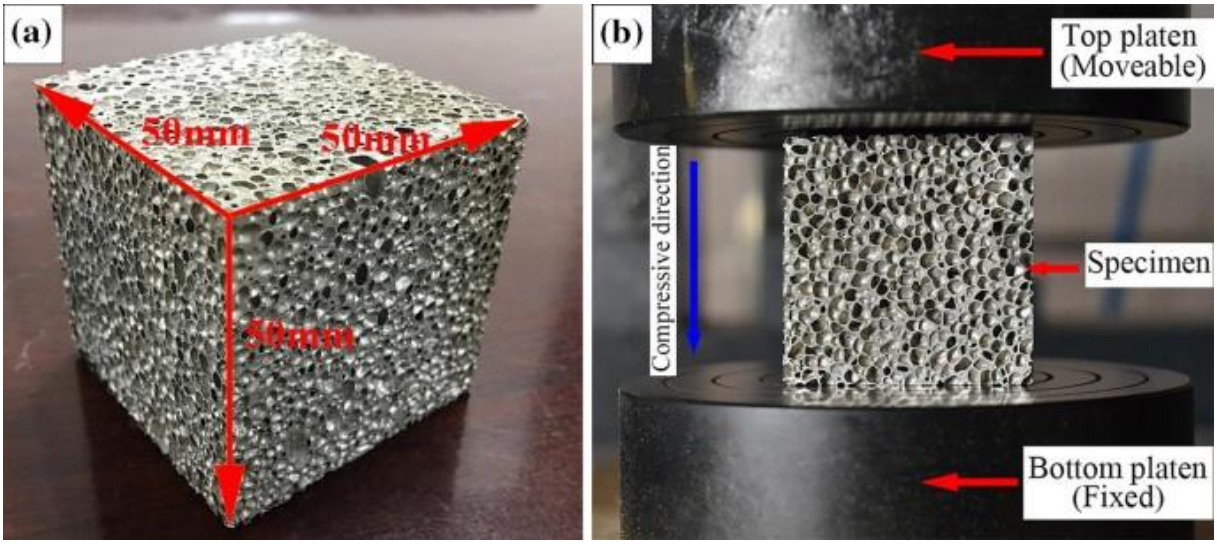

Figure II.4: Foam specimen and experimental setup for compression test: (a) foam specimen size; (b) experimental setup for quasi-static compression.

Figure II.5 shows the stress-strain curve of the test specimen and its corresponding macro deformation behavior. It can be seen from the obtained stress-strain curve that under compression test the specimen undergoes three distinct stages: a very short linear stage at the beginning, a long plateau region at the second stage, and finally a densification stage during which the stress increases rapidly with strain.

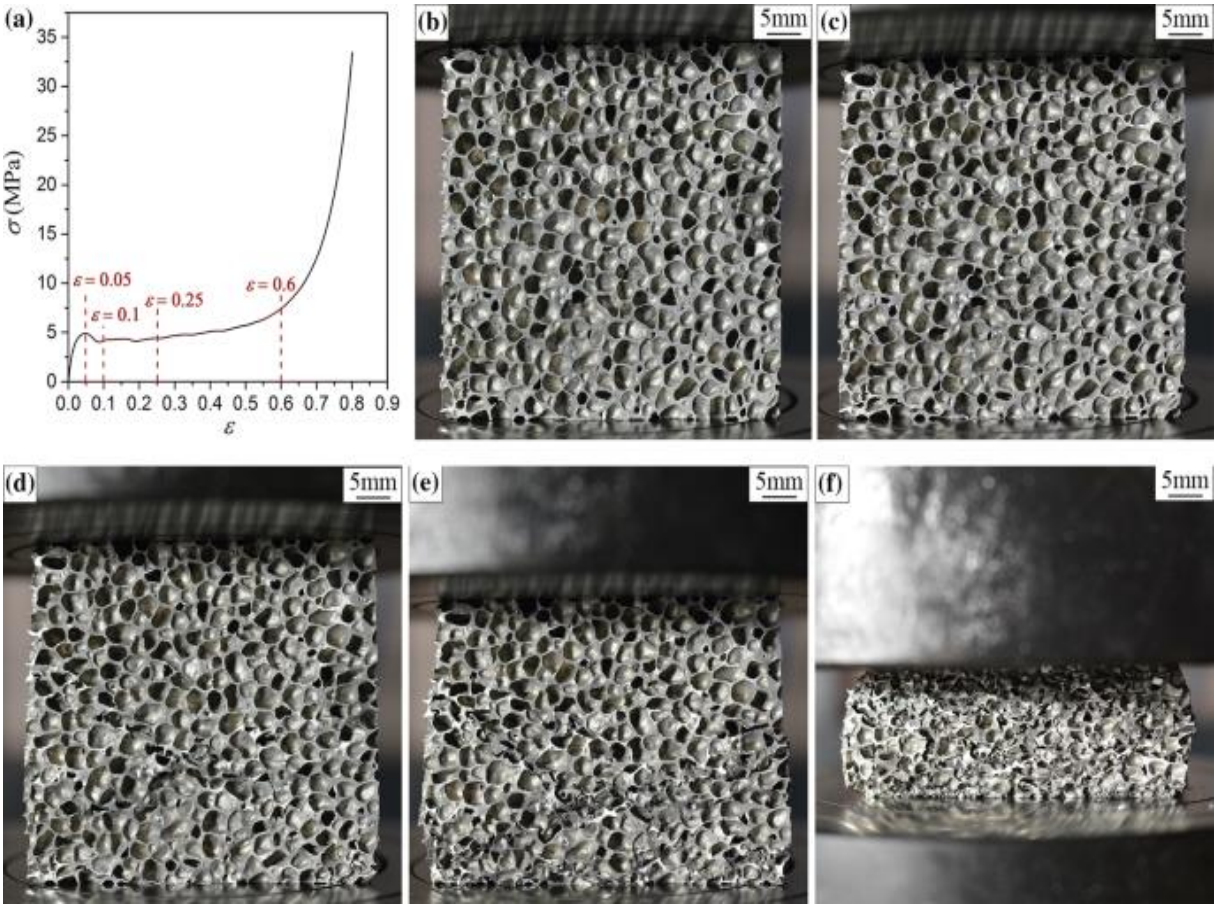

Figure II.5 Stress-strain curve and macro-deformation process of closed-cell foam specimen under quasi-static compression test and its corresponding macro-deformation process (a) ε = 0; (b) ε = 0.05; (c) ε = 0.1; (d) ε = 0.25 and (e) ε = 0.6. [98].

a) Uniaxial tension test

In a uniaxial tension test, the samples have usually a waisted shape (Figure II.6), though it is not necessary. The ends can be simple because the most important regions stay in contact with the machine grips.

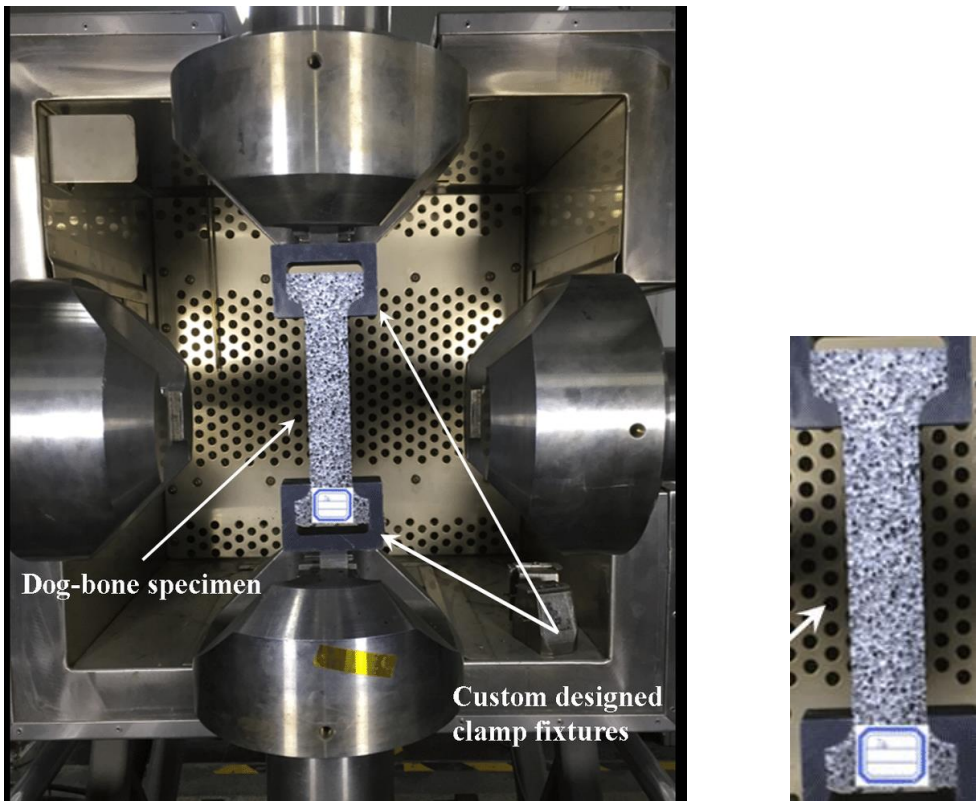

Figure II.6: Experimental set-up for uniaxial tension testing for closed-cell aluminum foam specimens [99].

The cross-section of the specimen can be circular or rectangular/square. The diameter or the thickness of the cross-section should be at least seven times the cell size. The ASTM E8-96a standard could be a useful resource for information on the specifics of tensile sample machining. The tensile strength is taken as the maximum stress on the stress-strain curve.

The following mechanical properties: Young's modulus, Poisson's ratio, ultimate tensile strength, and yield strength can be determined using the tensile test (see [100]). Figure II.7 shows a typical stress-strain curve for metal foams under a tensile test. The curve includes two points of interest: the yield strength and ultimate tensile strength point, and the quasi-elastic initial stiffness.

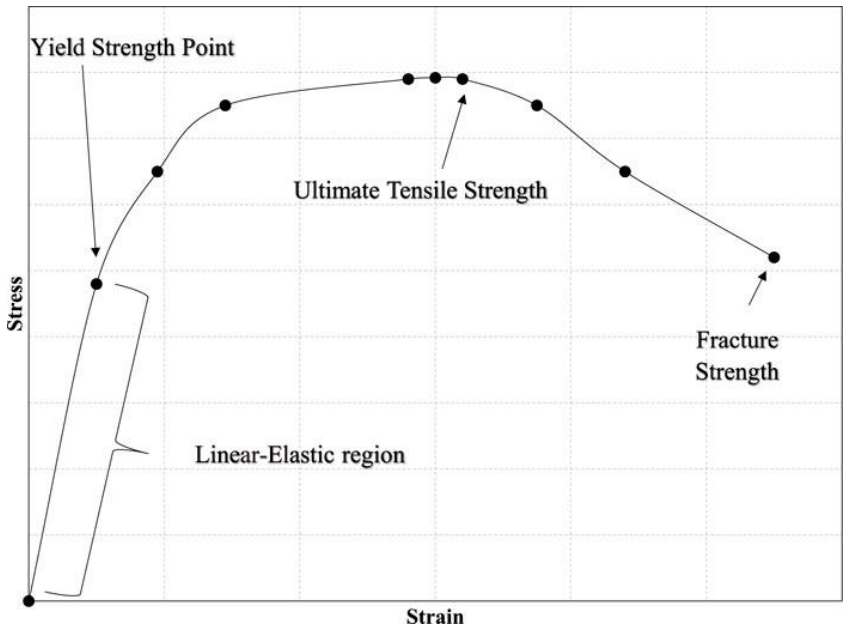

Figure II.7. Typical stress-strain curve for metal foams under tensile test [100].

The most typical material used in metal foam fabrication is aluminum. This can be due to its physical characteristics, such as its melting point, which make it possible to scale up the manufacturing of metal foams using reasonably manageable heat treatment processes.

A range of studies concerning the determination of structural and mechanical properties of aluminum foams can be found in the literature, e.g. ([8,95,101,102,103,104,105]).

II.2.3. Shear and torsion tests

Foam shear tests are rarely carried out because of several technological challenges. Low overall cellular material stiffness and maintaining the axial alignment of the apparatus-specimen assembly are the main issues. Shear tests and torsion tests, which are carried out more often, both allow for the measurement of shear strength.

a) Shear tests

Long, thin prisms with rectangular sections are used as specimens in shear testing. The length to thickness ratio may achieve 12 in this case. Width should be ca. 50 mm, while enough thickness t is above three times the cell size, typi- cally then $t \in (5 \div 30)$ mm.

As mentioned in [92] and utilized e.g. by [106], there are typically two testing modes. The first method is conducted according to the standard ISO 1922:2001 (formerly ISO 1922:1981.

In this test, the larger faces of the specimen are bonded to rigid plates (steel material) that should be fixed to the grips of a tensile machine where the assembly is put under tensile load producing shear in the foam sample as illustrated in Figure II.8 .

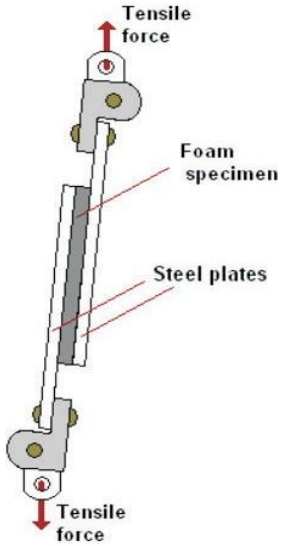

Figure II.8: Scheme of the assembly used for measurement of shear strength. The drawing is based on [92] – the method presented in standard ISO 1922:2001/ASTM C-273.

In the second method so-called double-lap configuration, two specimens and three plates are utilized. Two of the plates are adhered to the outside sample faces, and one plate is inserted between the foam samples. The set is then gripped and loaded in a tensile machine to create a shear condition in the material as shown in Figure II.9.

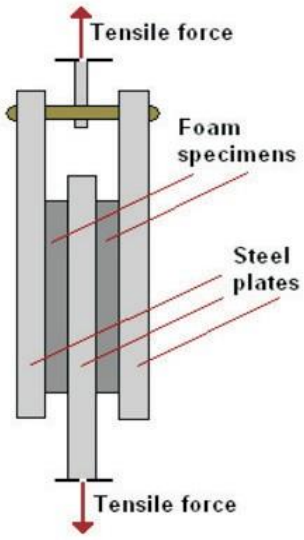

Figure II.9. Scheme of the alternative, double-lap assembly used for measurement of shear strength. The drawing is based on [92].

Displacement should be read either from crosshead displacement or by the use of LVDT. Shear strength is taken as the maximum stress from the stress-strain curve.

II.2.4. Twist method

In this type of experiment, specimens with a cylindrical form are employed. The minimum cross-sectional dimension should be larger than seven times the cell size [97]. Tension-torsion machines are employed for these kind of measurements.

The sample is held in the grips as shown in Figure II.10. Noting that it is very important that the axes of the sample and the machine stay collinear. This can be down using a dial gauges with a tolerance on the order of 0.1 mm [106].

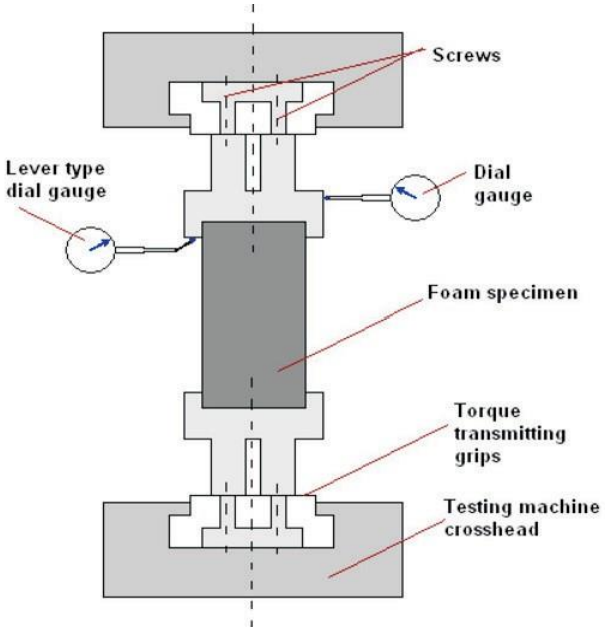

Figure II.10: Scheme of the assembly used for measurement of shear strength in torsional tests. The drawing is based on [106].

The displacement rate of an angular speed in these experiments may be as high as 0.1 o/s.

This kind of test necessitates the following actions be taken in terms of displacement and deformation measurements:

- Two wires should be attached to the specimen at one end and to an LVDT at the other.
- Change of the LVDTs position is then transformed into the angle of twist, allowing the shear modulus to be calculated [92,107].

The shear strength is considered as the limit of the linear elastic regime in the torque/angle curve.

A schematic of the shear experiment for Al foam [103] is shown in Figure II.11. The typical loading–unloading and load-displacement curves obtained are shown in Figure II.12.

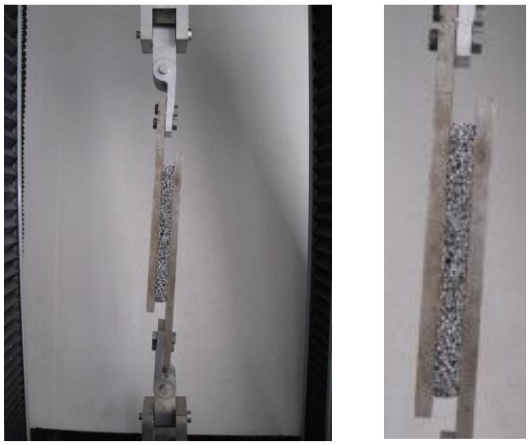

Figure II.11: Schematic of shear test setup for Al foam [103].

According to Fig. 4a, the initial loading part of the curve has a lower slope than the unloading curve. To this end, the unloading region of the load-displacement curve is used to calculate the shear modulus G.

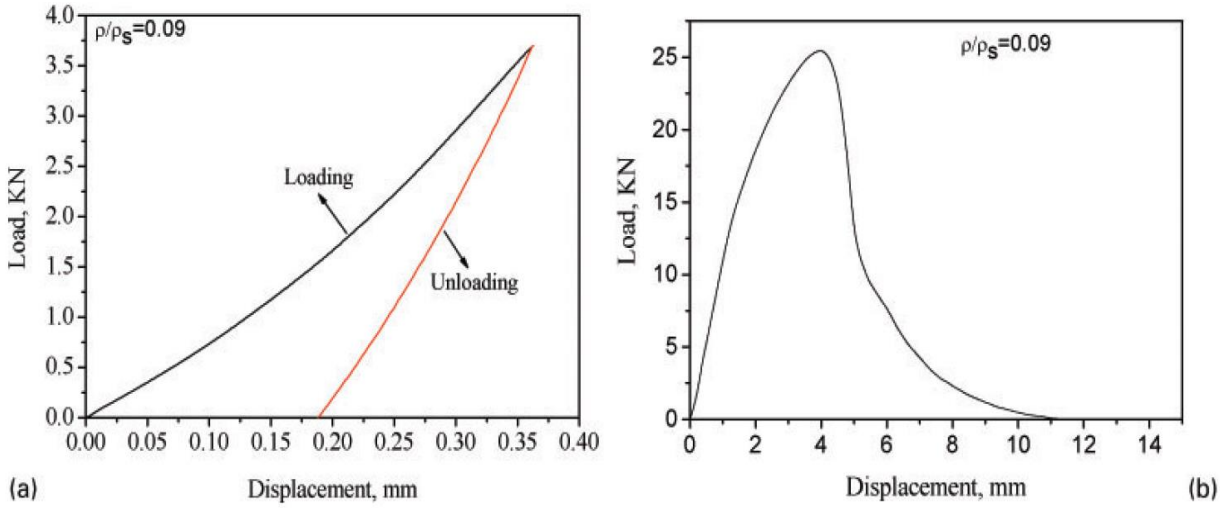

Figure II.12: Typical FWT stress–strain response of Al foam (a) loading–unloading response curve; (b) load–displacement response curve [103].

Figure II.13 depicts the related deformation process and failure mechanism of the tested closed-cell Al foam.

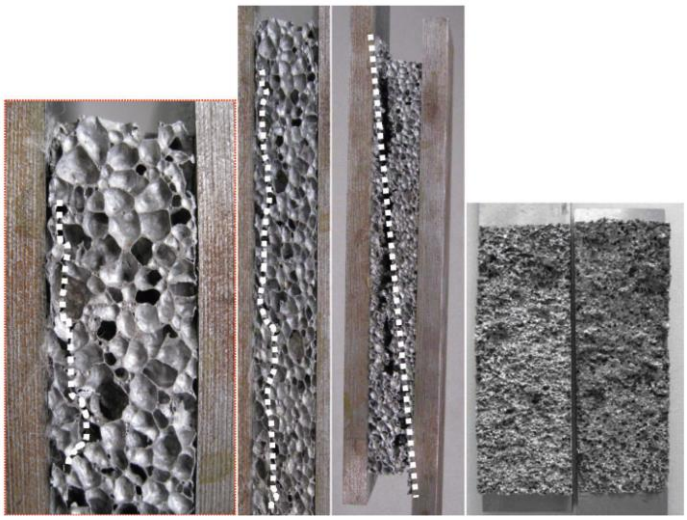

Figure II.13: Shear failure mechanism of Al foam: (a) Initial shear crack of Al foam; (b) shear crack propagation of Al foam; (c) entirely failure morphology of Al foam in shear; (d) failure feature of Al foam under shear [103].

Shear experiments may be used to determine two important mechanical parameters, shear strength τ_{max} (taken as the maximum stress) and shear modulus G. A range of studies investigating the mechanical properties of aluminum foams under shear test can be found in the literature, e.g. ([103 ,106,108,109,110,111]).

II.2.5. Biaxial tests

a) Biaxial compression-compression tests

Cubic-shaped specimens are required for biaxial compression-compression experiments. The linear size should be at least seven times the cell size. A typical uniaxial tension/compression machine applies the load in one direction, while a hydraulic cylinder loads the opposite way using two pairs of plates.

The sample is loaded by first moving one pair of plates using the tension/compression machine or jack at constant displacement, and then moving the second pair of plates [107,112].

A peak load can be used to determine ultimate strength; otherwise, it can be assumed from the point at which the slopes of the linear elastic and plateau regions intersect in the stress-strain graph.

a) Biaxial tension-compression tests

Dogbone-shaped specimens are required for biaxial tension-compression studies. The A minimum linear dimension should once more be seven times the size of a cell. A typical tension/compression machine is used to apply tension on the sample. Through a hydraulic jack, the foam is compressed in the opposite direction [107,112]. The specimen is loaded

consecutively in both directions. Measurements of displacement are analogous to tests using compression-compression. Also, ultimate strength is defined similarly.

II.2.6. Multiaxial tests

a) Torsion and tension/compression

The specimens utilized are cylinder-shaped and can be waisted if necessary to fulfill ASTM E8-96a requirements. The cross-sectional dimension should be at least seven times the cell size. The machine type used and mounting of the specimen in it is here similar as in twist tests.

During the succeeding torsion, the axial load can be applied and kept constant. Similar to sole torsion and sole tension/compression tests, strain rates and displacement measures are likewise analogous.

b) Triaxial tension-compression and compression

Triaxial tests require a special apparatus-either custom built or adapted (e.g. a soil mechanics triaxial cell, see Figure II.14). The particular conditions and details of the experiment can be found in ([92,107,113]).

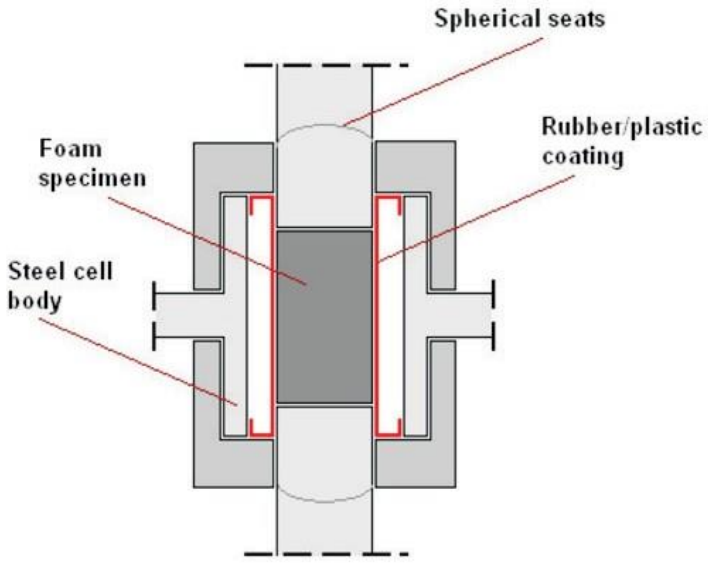

Figure II.14: Scheme of the assembly used for triaxial tests. The drawing is based on the method with the use of soil testing equipment. [113]

Triaxial tests must adhere to the basic guideline for tension/compression tests, which states that the specimen should be larger than seven times the size of a cell in its lowest dimension [95,96]. Samples must be cylindrical, which is a requirement of the testing instrument.

Two types of triaxial tests are considered, the first involves applying pressure in all three major axes, while the second involves applying pressure in two major axes (radially) and tension along the specimen axis.

II.2.7. Flexural Test

The sandwiches were subjected to the three-point bending test (3 PB) in accordance with the ASTM C 393-62 standard to determine the flexural properties , including core shear stress, face sheet compressive and tensile stresses, and deflections [114].

As an illustrative example, Figure II.15 shows a three-point bending test configuration according to the ASTMC 393–62 of sandwich panel specimen under loading reported in the work of [114]. A 100 kN capacity Devotrans® universal test machine was used for the test and recording of the force versus stroke values at a crosshead displacement rate of 2 mm/min.

Figure II.15: Three-point bending test configuration according to the ASTMC 393–62 b test specimen under loading[114].

An example of the main failure modes observed in the three-point bending experiments is illustrated in Figure II.16).

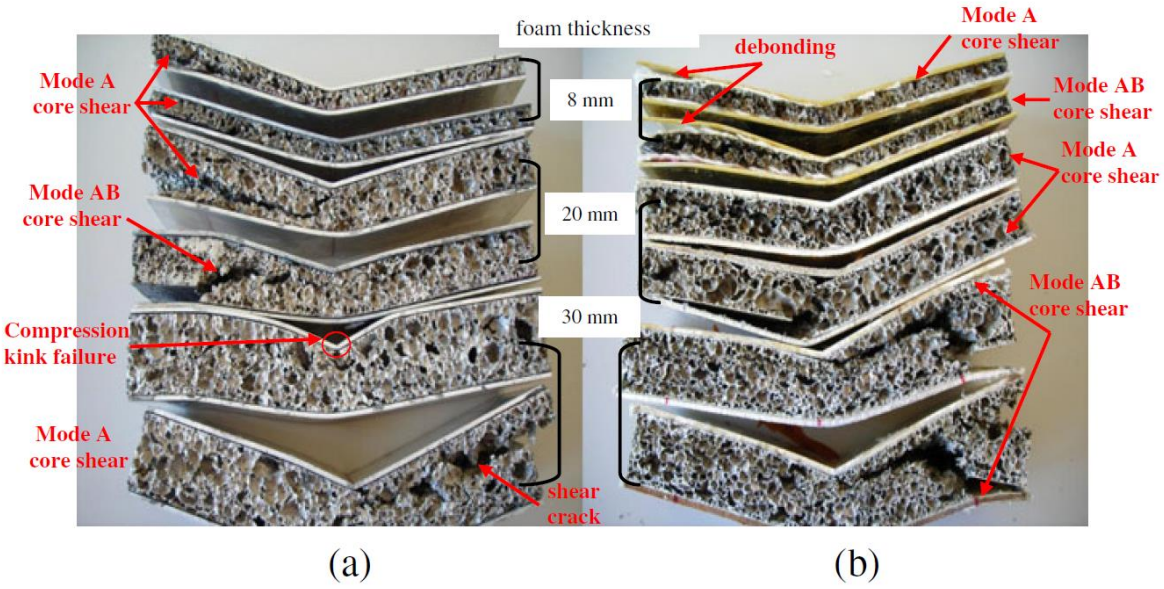

Figure II.16: Failure modes observed during flexural testing of (a) Al sheet/Al foam sandwiches integrated with epoxy adhesive (b) Al sheet/GFPP/Al foam sandwiches bonded after silane surface treatment [114].

II.3. Microstructural parameters affecting the mechanical behavior of foams

Closed-cell aluminum foams' mechanical response is significantly affected by microstructural factors such as cell size, aspect ratio, variation in cell wall thickness, cell wall geometry, and irregular cell shape. The effect of these microstructural factors on macroscopic properties is discussed in this section.

II.3.1. Effect of relative density

Relative density (RD) is the important parameter that controls the foam architecture [115]. It is defined as the density ratio of the foam to the solid material [115]. It is given by Eq. II.1:

$$\rho = {\rho^*}/{\rho_s} \qquad \textit{Eq. II.1}$$

Where ρ^* is the density of the cellular material and ρ_s is the density of the solid material from which the cellular material is created.

Several studies explored the effect of relative density on the stress-strain curves of metallic foams under various loading. Figure II.17 shows the effect of relative density on the yield strength and the flow stress of aluminum foams, which increase with an increased relative density as reported in [116].

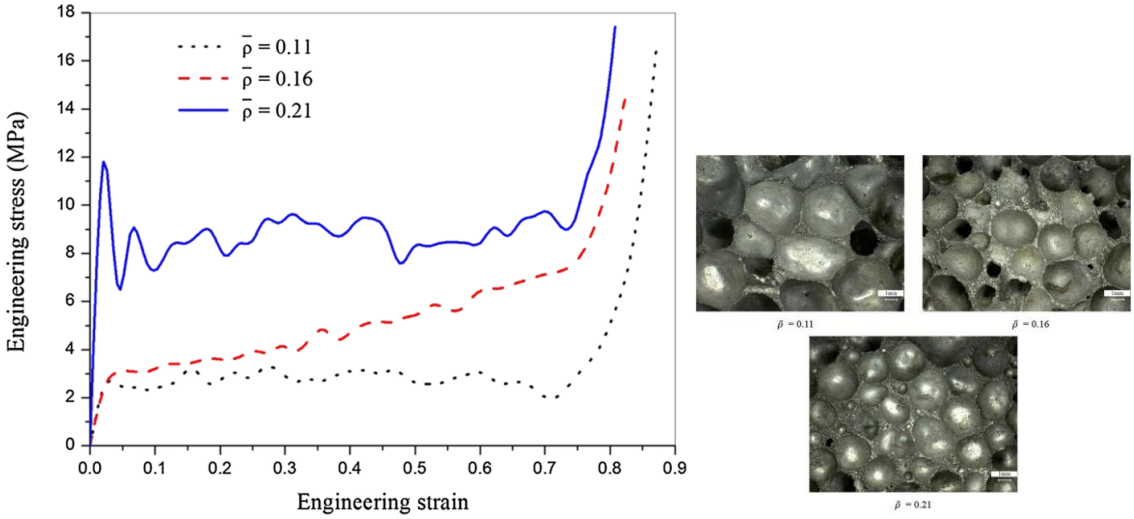

Figure II.17: Effect of relative density on the quasi-static compressive stress-strain curves of closed-cell aluminum foams.[116]

II.3.2. Effect of cell aspect ratio

In foams, the cell aspect ratio measures the geometric anisotropy of cellular microstructures, which may be relevant to compressive behavior since geometric anisotropy has been demonstrated to result in mechanical anisotropy [20,37]. This quantification is more challenging for closed-cell foams than open-cell foams due to the presence of cell walls.

The effect of geometric anisotropy on mechanical properties was examined by Jang et al. [117]. Three ALPORAS foam specimens with a similar relative density and three cell aspect ratios in each direction K12 and K13 > 1, K23 (longer in the direction D1 and had similar dimensions in the directions D2, and D3) were subjected to compression tests. Where each specimen was loaded in one of the three directions. The compressive responses in three loading directions for the tested specimens are shown in Figure II.18. It was observed that the specimen loaded in the direction in which cells are longer (D1) yielded the highest overall response.

The author concluded that foam specimens exhibit the highest response under a compression load in the directions with cell aspect ratio greater than unity [117].

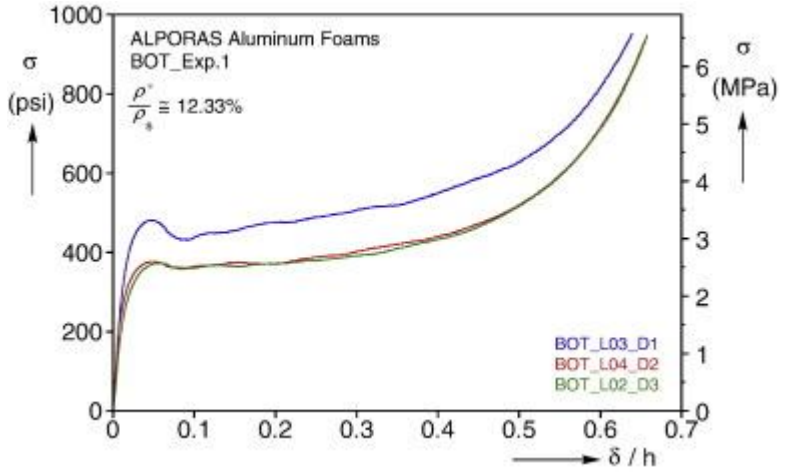

Figure II.18. Compressive responses in three loading directions for ALPORAS foam specimens with similar relative density. [117]

II.3.3. Effect of cell shape irregularity

The compressive deformation behavior of foams was demonstrated as strongly dependent on their inherent microstructural irregularity [6]. It was agreed that, As foam irregularity increases, the peak and plateau stresses clearly decrease. For instance, Shi et al. [6] investigate the microstructural irregularity in generated closed-cell Voronoi foam models for the same relative density of 10% and various irregularity values. From the obtained average compressive responses (Figure II.19) a significant increase in the plastic-collapse strength as the regularity of the foam model increases [6].

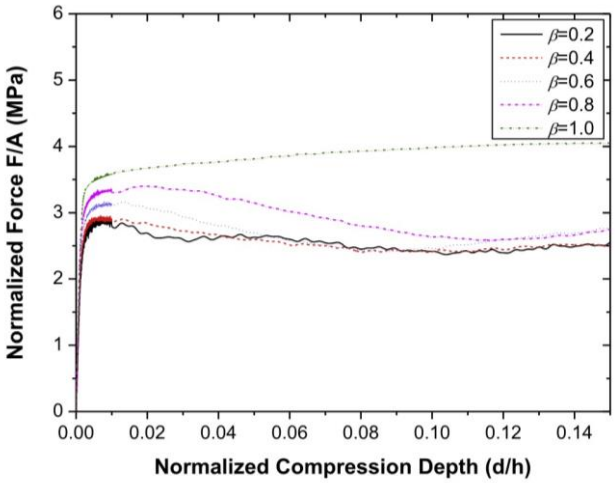

Figure II.19. Effect of regularity on the compressive response of Voronoi foam models. [6]

II.3.4. Effect of cell wall thickness variation

Real foams are characterized by a variation in cell wall thickness distribution. However, in most existing finite element micromechanical models, cell wall thickness is assumed to be

unvarying in order to simplify the models and reduce their computation time, as mentioned by Fang et al. [118] and Abdullahi et al. [119]. This simplification facilitates the control over the relative density of the foam models and reduces the analysis computation time, but it may lead to an overestimation of the mechanical properties of real foams, as demonstrated by various studies that have investigated this question [49].

According to Chen et al. [27], a larger dispersion of cell wall thickness distribution caused a greater number of cell wall bucklings during the elastic regime, resulting in a reduced peak stress of the foam.

II.3.5. Effect of cell wall geometry

Compared to variations in cell wall thickness, cell wall geometry has received less attention from researchers.

Cell wall geometry has received even less attention from researchers than cell wall thickness variation. The vast majority of numerical research assume that the thickness of each cell wall is constant along its length. However, such an assumption may not be quite appropriate.

For instance, Jang et al. [117] analyzed the cell wall geometry of ALPORAS closed-cell aluminum foams by means of stereomicroscopic images, and revealed that its thickness was not constant but varied in the longitudinal direction, as illustrated in Figure II.20.

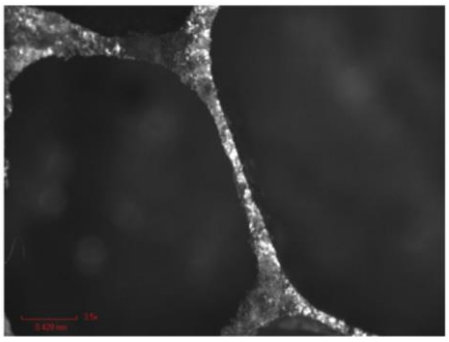

Figure II.20. A typical cell wall, significantly thicker at their ends. [117]

It was obsereved that, the cell walls are thinnest in the mid-span and become increasingly thicker toward their ends, eventually forming circular fillets at the intersections with the adjacent cell walls. Figure II.21 shows a schematic of this cell wall geometry, which consists of a rectangular section with a constant thickness and four circular fillets at the ends.

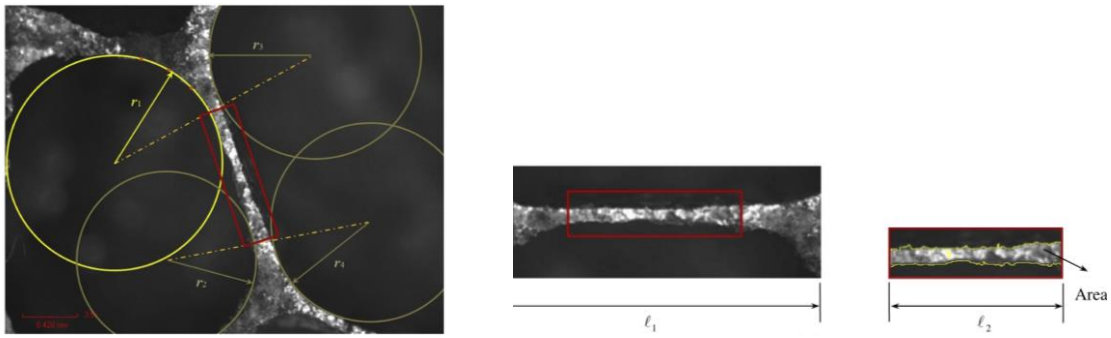

(a) (b)

Figure II.21. Schematic for measuring the fillet radii (a), and the lengths l1 and l2 (b) (Jang et al. [122]).

In the uniform thickness models, the cell wall plastic deformation may be captured by buckling mechanisms, as opposed to real foams, which have thicker cell walls at junctions as shown above.

II.3.6. Effect of strain rate

A considerable amount of research has been carried out on the strain rate sensitivity of foams. It was found that the mechanical behavior of foam is affected by strain rate. As an example, Yang et al. [120] studied the dynamic response of polyurethane foam subjected to different strain rates, and compared it with the quasi-static response [121] (Figure II.22). Comparing the quasi-static foam specimen to the dynamically deformed specimens reveals a longer stress plateau and a larger densification strain. Lockup occurs at around 44% strain in quasi-static deformed foam, while it occurs well below 20%, 18% and 14% strain for foam deformed at 80 s−1, 120 s−1 and 160 s−1, respectively.

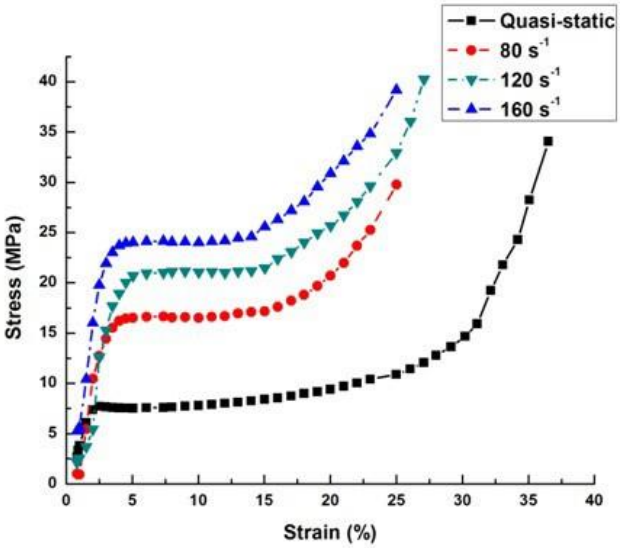

Figure II.22: A comparison of stress-strain curves for rigid polyurethane foam subjected to quasi-static and dynamic compression.[121]

II.4. Conclusions

In light of this literature, and beyond the specific focus of this study, it becomes apparent that there still are several pending challenges [20,21,22] in the fundamental research of closed-cell aluminum foams in order to improve the energy absorbing process, namely:

- Determining more precisely the influence of foaming process variables on the structural properties of foams (relative density, pore diameter, cell aspect ratio), which in turn govern their mechanical properties.
- Deepening our knowledge of the effect of cell topology on the compression behavior of foams.
- Better understanding the compressive deformation and failure process at cell level and their relationship with the macroscopic properties in order for a more thorough identification of the specific energy absorption mechanisms.
- Developing cheaper production processes of 3D-complex shapes for a more effective industrial application of foams as energy absorbing material.

CHAPTER III NOVEL DESIGN OF IRREGULAR CLOSED-CELL FOAMS STRUCTURES WITH RELATIVE DENSITY CONTROL

III.1. Introduction

This chapter describes the method proposed to generate three-dimensional (3D) realistic models of closed-cell foams. The mechanical performances of closed-cell foams have been studied experimentally under various mechanical loadings, essentially under quasi-static, dynamic uniaxial compression [2, 14, 15, 21-27] and three-point bending [29-31]. The main drawback of experimental studies is the difficulty to study the influence of each morphological parameter separately due to the complexity, and the high cost of manufacturing methods and experimental tests [33], which restrict the experimental methods and suggest adopting an alternative approach.

As a result, numerical modeling of foam materials based on trustworthy finite element models becomes a crucial strategy because it enables simple parameter investigation. Two categories of models can be recognized in numerical modeling: tessellation-based models and image-based models [34- 36].

Due to the high degree of randomness in the microstructure of real closed-cell foams, many numerical models reported in the literature are not able to capture precisely the local morphological features found in solid foams geometry. This is still the main impediment that restricts the investigation of this novel material and motivates the development of a sophisticated 3D solid model that describes properly the complex geometry of real closed-cell foams.

In this regard, this chapter presents first an overview of the geometrical modeling of closed-cell foam structures, followed by the efficient method proposed in this thesis to generate three-dimensional (3D) realistic models of closed-cell foams. The modeling approach was successfully verified by comparing the cell-morphological details of the generated models with those produced experimentally.

III.2. Overview of geometrical modelling of closed-cell foam structures

Numerical modeling of foam materials based on reliable finite element models becomes an important approach, it allows to investigate easily each parameter separately. In numerical modeling, two groups of models can be distinguished: image-based models and tessellation-based models [34- 36].

III.2.1. X-ray tomography

a) Principle

X-ray microtomography (µ-CT) is based on an X-ray beam that crosses the sample and is attenuated. The sample is rotated to measure attenuations at different angles. A reconstruction algorithm is then used to generate cross-sections of the sample's internal structure [122]. The most used algorithm is the Feldkamp algorithm [123]. Figure III.1 shows the general array of a microtomographic system. This technique had been used to analyze the internal structure of several kinds of materials, such as bones [124,125], rocks [126,127] and industrial foams [128,129].

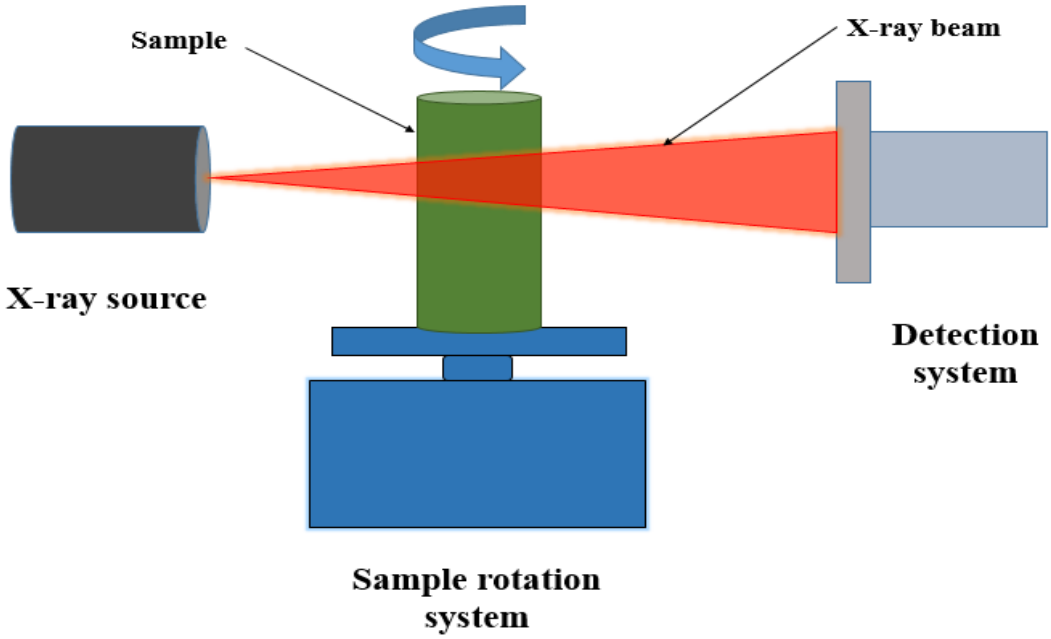

Figure III.1: Schematic of the X-ray microtomography system [130].

b) Structural analysis

To accurately describe the foam shape, the initial condition of the foam may be investigated. In fact, understanding foam morphology can affect which representative unit cell is selected to reflect the mechanical behaviour of foams [131, 132]. Noting that a sizable starting volume should be examined in order to acquire a statistically representative result.

The main parameters required to describe the microstructure of closed-cell foam will be discussed in this section.

- *Cell volume distribution*

Once the cells have been segmented, the first parameter that can be easily measured is the volume of each individual cell. This is done by counting the voxels that make up each cell. The cell volume can be more accurately estimated using a marching cube algorithm [133]. As an illustration example, Figure III.2 shows the cell volume distribution for an open-cell nickel foam structure analyzed using X-ray microtomography by Dillard et al. [134]. The distribution is mono-modal, as seen in this figure, with a peak at 0.08mm^3 and a center at 0.07mm^3, with an average cell volume of 0.071 mm^3. The average cell would have a diameter of 514 mm if the cells were spherical.

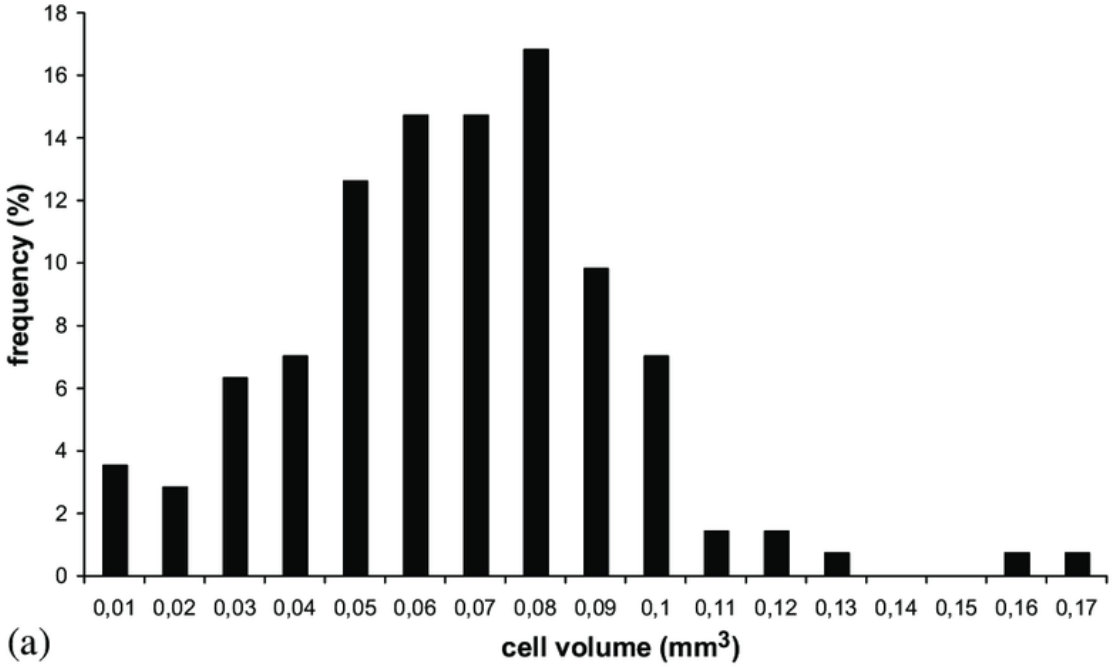

Figure III.2: Cell volume distribution in the initial state of open-cell nickel foam structure obtained by X-ray microtomography [135].

- *Strut length distribution*

After the 3D image processing is complete and the graph of the foam has been acquired, the length of the strut is calculated. The only information required to determine the length of the struts is the spatial coordinates of the nodes and node connectivity. Figure III.3 shows an example of the measured strut length distribution of nickel foams [135]. According to the figure, fifty percent of the foam struts range in length from 130 to 210 mm, with a mean strut length of 193 mm.

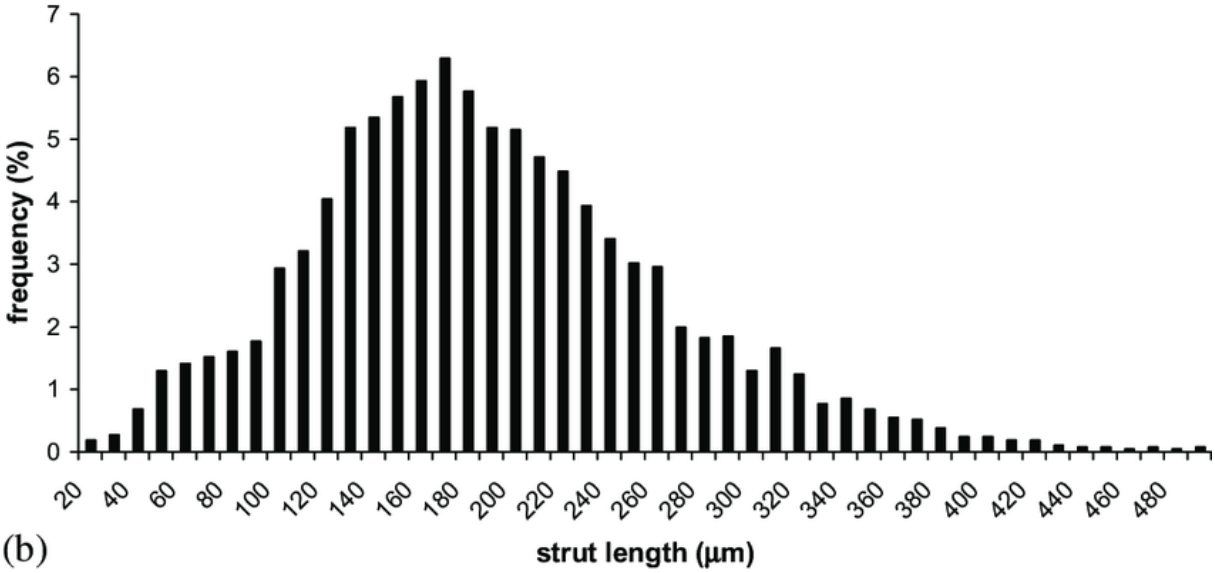

Figure III.3: Strut length distribution in the initial state of state of nickel foams [135].

c) Example of analyzed foam structure using a microfocus X-ray CT system

By way of illustration, an example of a foam structure analyzed using the X-ray CT system is shown in [135]. A sample of closed-cell aluminum foam ALPORAS (see Fig. III. 4) made by Shinko Wire Co. Ltd. using the direct foaming technique was analyzed to generate the 3D geometrical model. The modeling requires to use of a microfocus X-ray CT system, a 3D reconstruction program, and 3D scanned data processing software [135]. The specimen was prepared by fabricating several 10mm x 10mm x 10mm foam samples using the electrical discharge machine to ensure both flatness and clarity. Following this, a specimen without any visible structural defects was carefully selected using the VHX-100 digital microscope of KEYENCE Corp. The average cell size was d ¼ 4:36 mm and the relative density of the specimen was ρ/ρ_s = 0.0859. Here, q is the density of the Al foam, and ρ_s = 2.7 g/Cm3 is the density of the cell wall material.

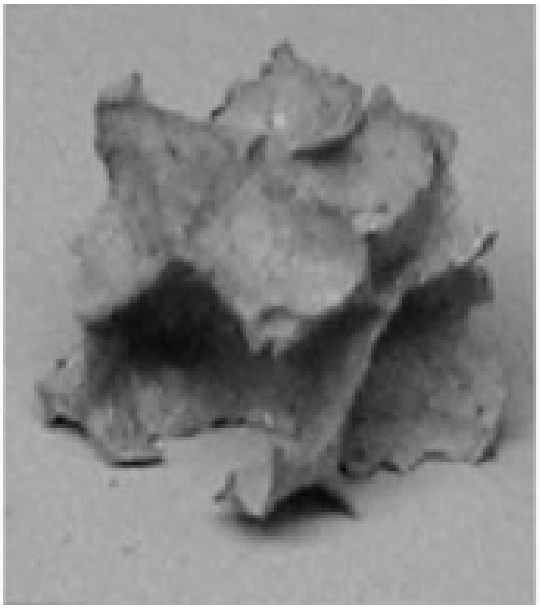

Figure III.4: Specimen of closed-cell Al foam ALPORAS of Shinko Wire Co. Ltd, fabricated with the direct foaming method [135].

To scan the external and internal structures of the selected foam a microfocus X-ray CT system of Shimadzu Corp was used. The scanned grayscale tomographic images are shown in Figure III.5.

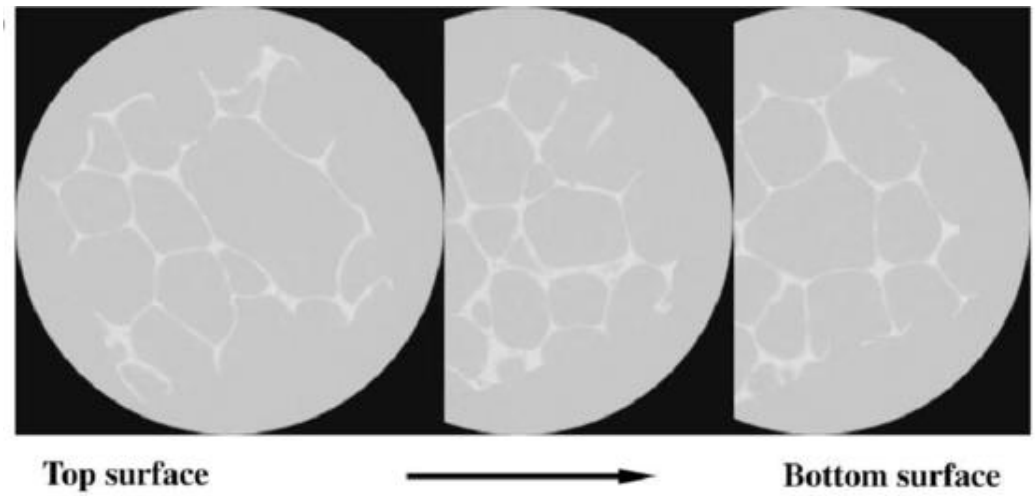

Figure III.5: Scanned grayscale tomographic images of the selected foam specimen [135].

These images were used to reconstruct the foam specimen using the 3D reconstruction program TRI/3D-BON of Ratoc System Engineering Co. Ltd.

Using this program, the tomographic images were binarized, and the isolated small particles from the solid cellular skeleton were removed from the binarized images.

The 3D cellular structure was then reconstructed using the marching cubes algorithm (see Figure III.6) [136].

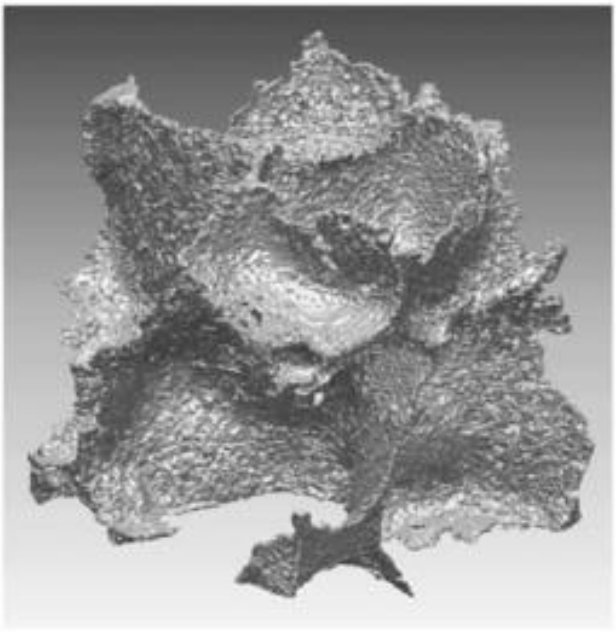

Figure III.6: 3D cellular reconstructed structure using the marching cubes algorithm [136].

Table III.1 shows examples of metal foams reconstructed by micro-computer tomography images.

Table III.1: Examples of metal foams reconstructed by micro-computer tomography images.

Volumetric representation of sample with 129 cells (a), extracted surface geometry (b), finite element shell model elements (c). [137]	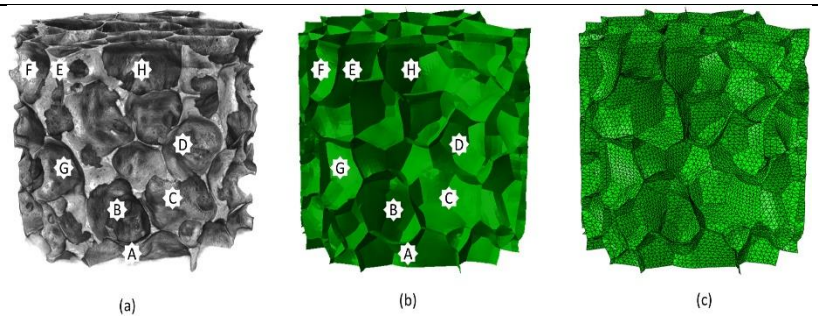

Numerical sample of the closed-cell foam based on CT scan images.[138]	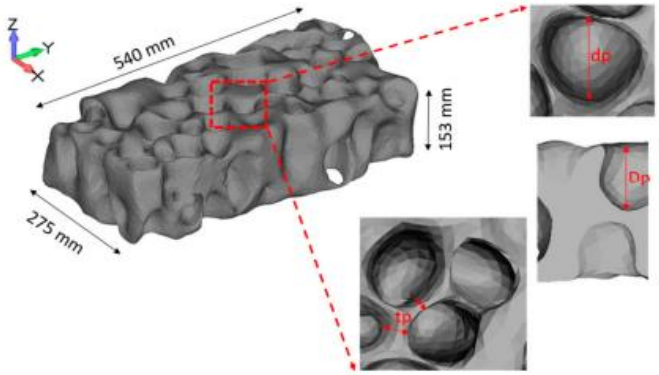
Aluminum foam with closed cells: a) cubic sample 20×20×20 mm, b) free face of the sample photo, c) visualization of data obtained from X-ray tomography [139]	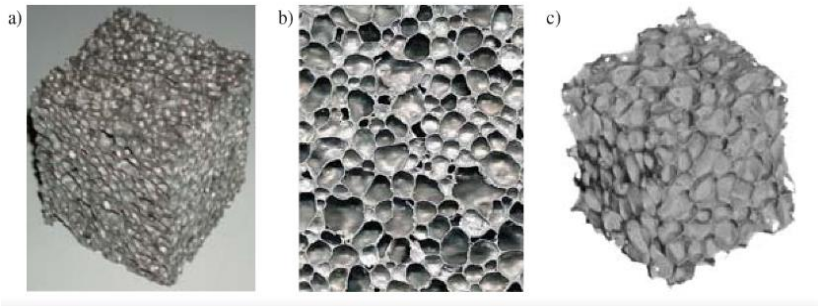
3D modeling of the closed-cell aluminum foam samples: (a) CT scan device and foam samples, (b) extracted CT scan 2D images of the foam samples, (c) 3D modeling of the foam sample from 2D images using Mimics software [140]	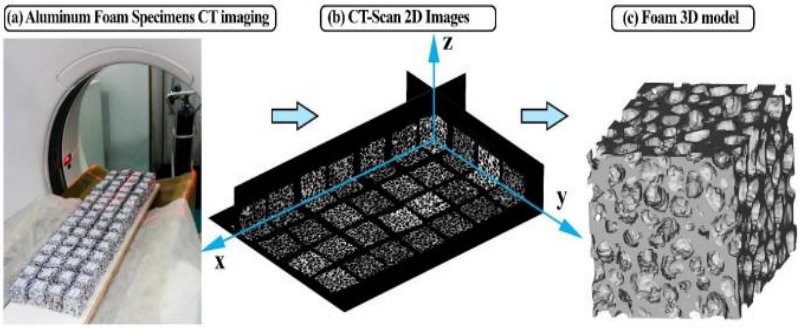
Reconstruction of cubic model of closed-cell Al foam specimen for uniaxial and tri-axial as well as compression-shear tests. [11]	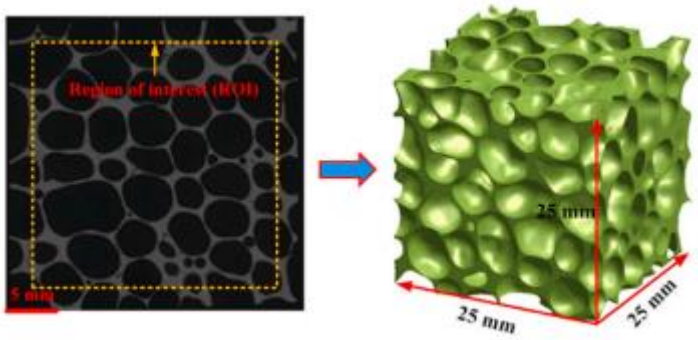

3D mode of of closed-cell aluminum foam sample [141]	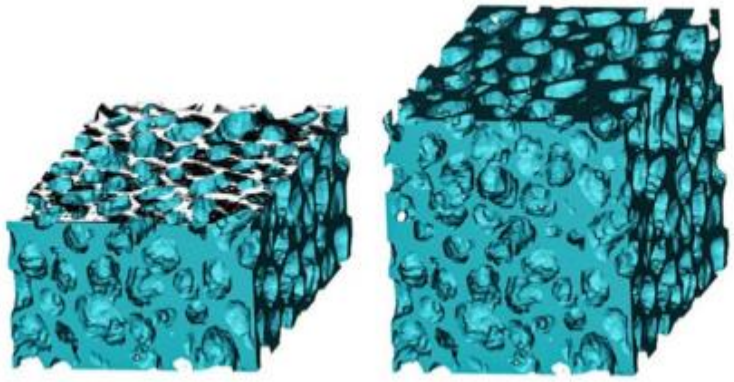

The reconstruction of real foam geometry using X-ray tomography is the most accurate method to give it a quantitative description [37]. Furthermore, the final geometrical body is meshed as a solid element. Although it provides valuable results, such studies encountered the same kind of problems as experimental ones like cost and time of sample preparation, time of scanning, and data post‑processing, which limit the study in terms of samples number, and also it requires high geometric discretization to capture accurately the small features existing in the original body, which demands much computational time. That's why in some studies, the simulated foam structure is often reduced to a small structure including only 2 or 3 cells in each direction, see for example [38], or only 5% of compression strain is calculated, and the densification regime is not addressed, see [13].

III.2.2. Tessellation-based models

a) Principle

Tessellation-based models are generated using algorithms such as Random Sequential Addition (RSA) and Random Close Packing (RCP). The principle of the algorithms is inspired from the foam formation process, where bubbles are inflated until each one meets its neighbors with a uniform rate (Voronoi) or a non-uniform rate (Laguerre) [142]. Figure III.7 shows a schematic diagram of a Voronoi tessellation modeling procedure [119].

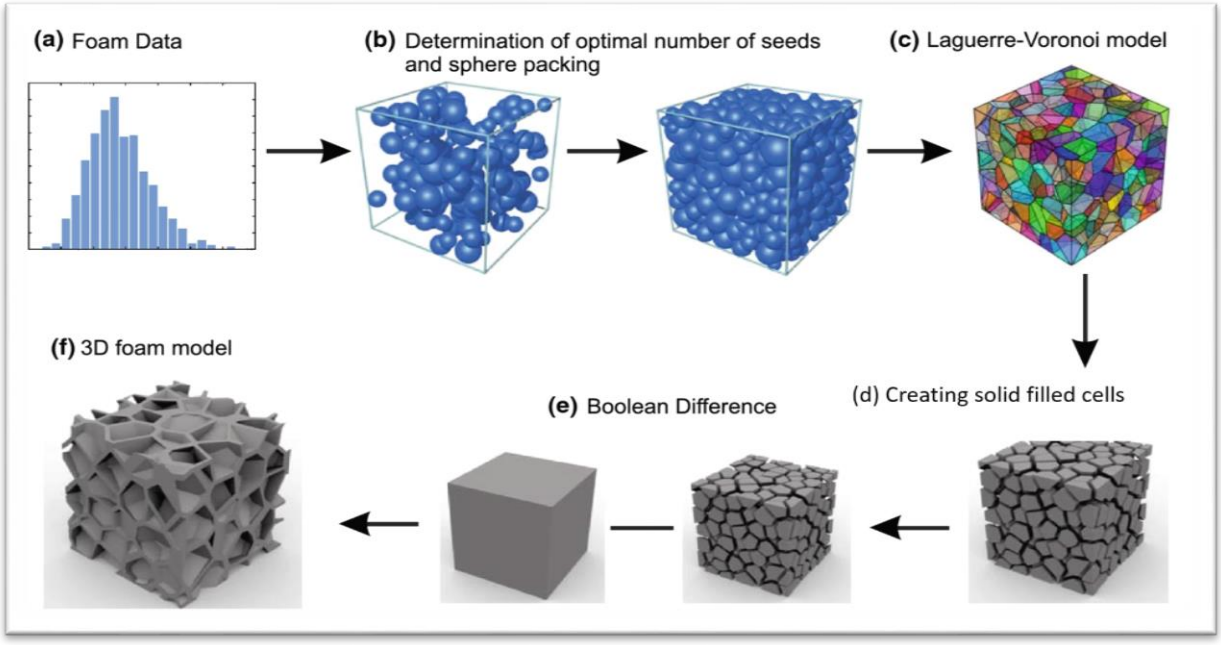

Figure III.7: Schematic diagram of a voronoi tessellation modeling procedure [119].

These models has been lately introduced by researchers to analyze the effect of the cell shape irregularity [143], cell wall thickness variation [144], and relative density [49] on the deformation mode and energy absorption of foams. Table III.2 shows examples of foam microstructures generated by the Voronoi tessellation technique.

Table III.2: Examples of foam microstructures generated by the Voronoi tessellation technique.

Tomographic data of the irregular closed-cell structure: (a) a tomography slice (400 × 400 px2); (b) 3D rendering after reconstruction (400 × 400 × 400 px3) [145]	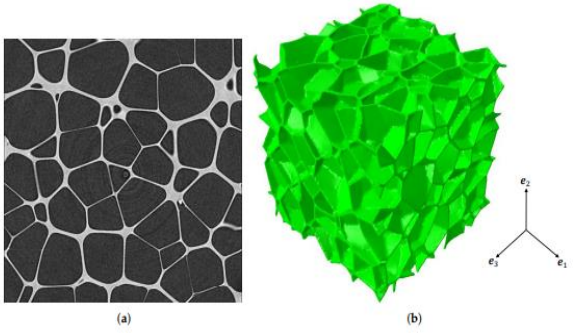

(a) Closed-cell aluminum foam; (b) 3D Voronoi foam model; (c) cross sections of the Voronoi foam model. [146]	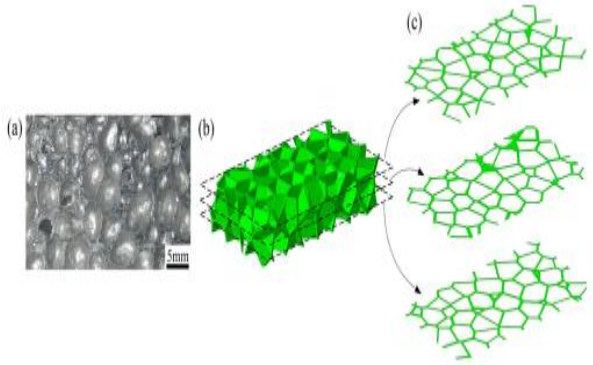
Numerical 3D Voronoi model of metal foam.[147]	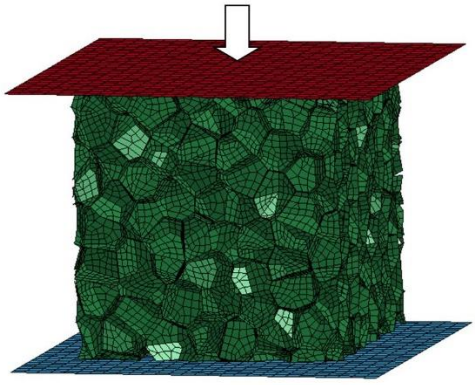
Laguerre tessellation based on random closed packing. [148]	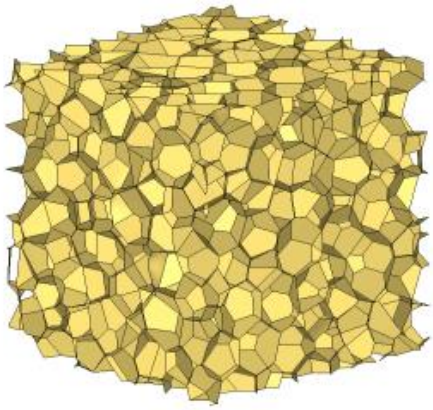
3D foam model [119]	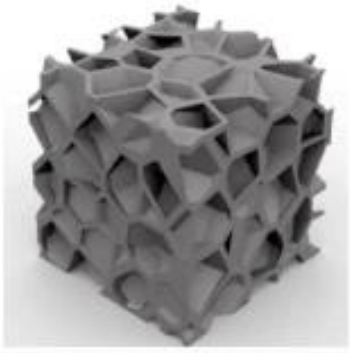

Voronoi foam model [149]	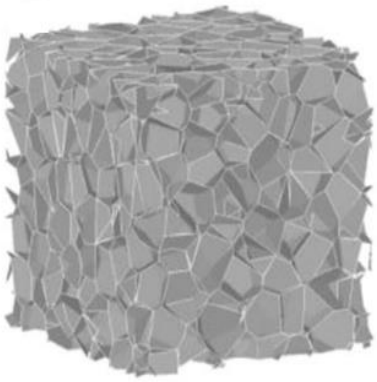

Comparing to real foams, the main disadvantage of the Tessellation models based on shell formulation is the lack of some important features such as wall irregularities and thickness variation which limits the functionality of these models, especially in medium-density foams. These imperfections led to the demand for a proper method to generate realistic RVE models, which can capture the real foams geometry more precisely.

III.3. Novel design of irregular closed-cell foams structures with relative density control

III.3.1. Methodology

In General, whatever the fabrication method of closed-cell foams, the obtained geometries are consisted of a solid metal that contains a large proportion of air (generally from 70% to 95% of volume). The gas bubbles formation technique is an efficient way to rise quickly the air phase volume and achieve a high foam porosity.

Therefore, in this work, the air phase reaches up to 96% of foam porosity was created by applying a fluid cavity pressure to inflate a packed random of thin spherical shells in a dynamic FEA using the Abaqus software, which governs the relationship between cavity pressure, volume, and temperature. The proposed technique allows to inflate quickly the bubbles and control the air phase volume constructing a real shape of closed-cell foam.

The 3D closed-cell foam generation is built on three main steps:

a- Generate the initial geometry of the inflatable structure

The initial geometry of the inflatable structure was considered as a Random Close Packing (RCP) of 220 thins spherical shells (Figure III.8). The geometry was generated using the proposed technique in the previous study of Benhizia et al. [150], where several input

parameters can be given, including RVE size, spheres number, required volume fraction, minimum distance of the non-overlapping spheres, shell thickness , and required realizations number. In the presented example, the sample has a site of 100''' 100* 100 mm3, with a minimum distance d of the non-overlapping spheres of 0.05 mm, and an oi‘igina1 spherical shell thickness of 0.15 mm.

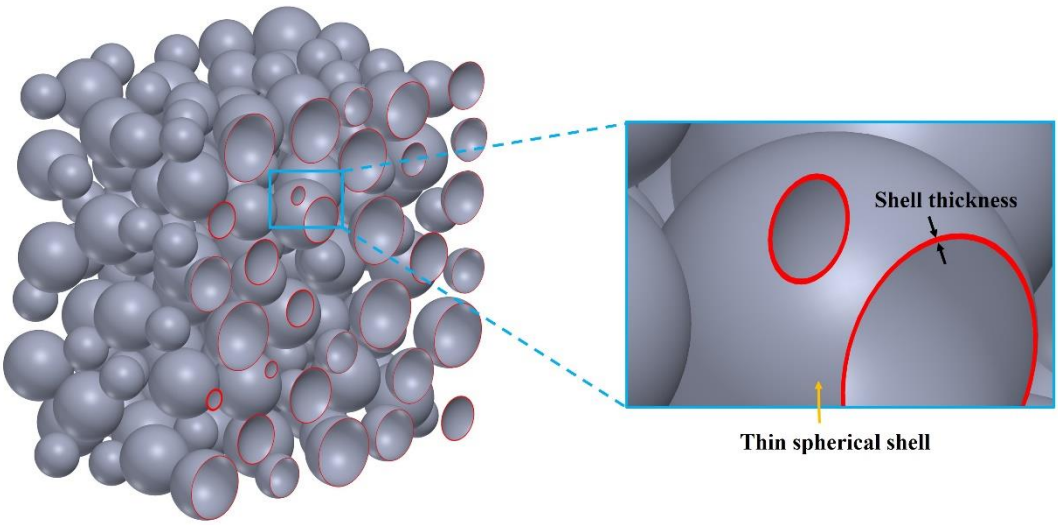

Figure III.8: Initial geometry of thin spherical shells.

A flow chart of the algorithm used to generate random non-periodic distribution particles is presented in figure III.9.

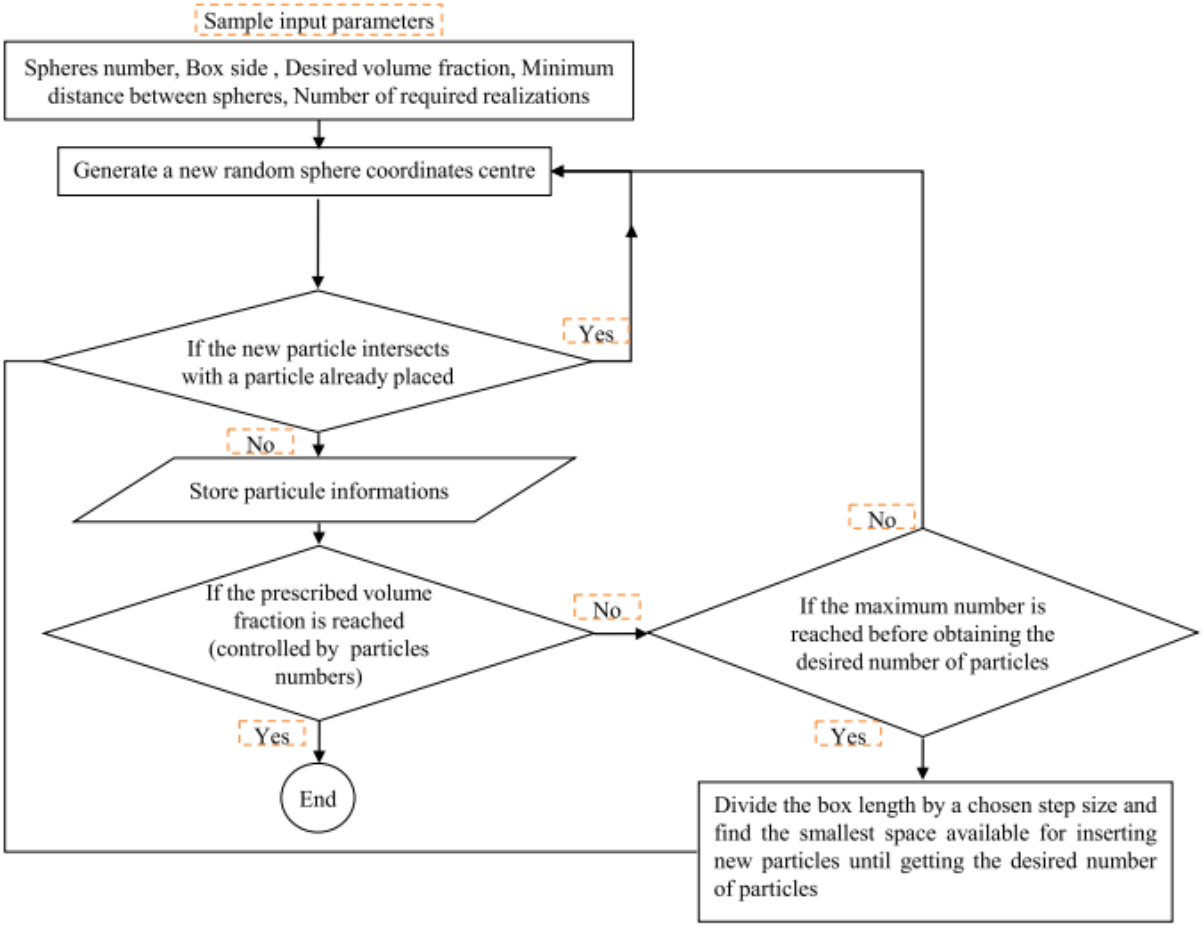

Figure III.9: Flow chart outlining the algorithm generating random non-periodic distribution particles [150].

b- Inflate the spherical particles

At this step, the generated spherical particles were inflated in a rigid cubic cell until each one meets its neighbors, using the surface-based fluid cavities in dynamic FEA (Figure III.11). The Finite element modeling was performed using the commercial software ABAQUS/Explicit package. The simulation was started with the initial shape of the thin spherical shells subjected to an internal pressure to reach the expanded possible shape. The modeling of the surface-based fluid cavities requires the definition of:

- Cavities surface: the volume surrounded by the enclosed surfaces is modeled by an empty rigid cubic cell as an external cavity (Figure III.10 (a)), where the enclosed inner surfaces of the thin spherical shells was defined as a fluid cavities to represent the volume being subjected to an internal pressure (Figure III-10 (b)).
- Cavity reference node: The internal pressure was imposed as a boundary condition to the cavity reference node, which is selected arbitrary from the geometry.

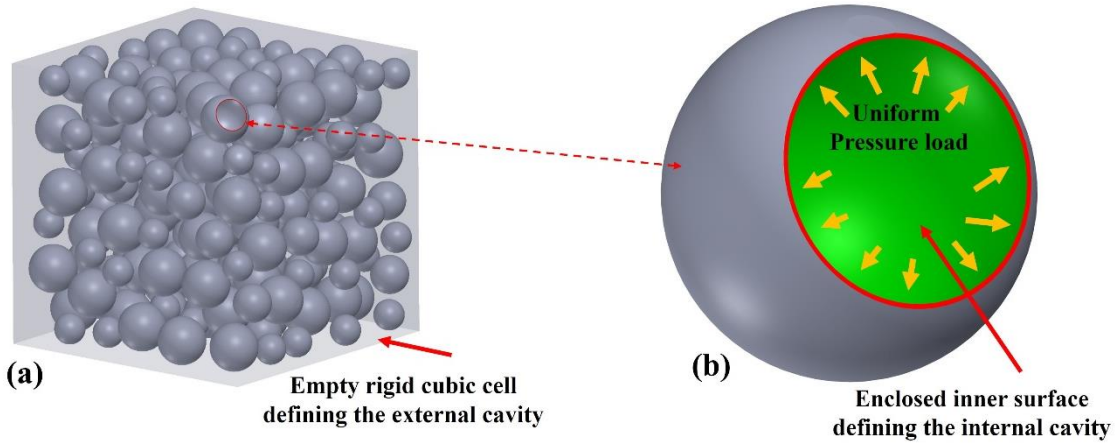

Figure III.10: Enclosed surfaces subjected to an internal pressure.

Figure III.11 shows an example of particle evolution during inflation. The interaction between the particles during inflation ensures that deformation occurs in any direction that dramatically changes the initial shape of the particles.

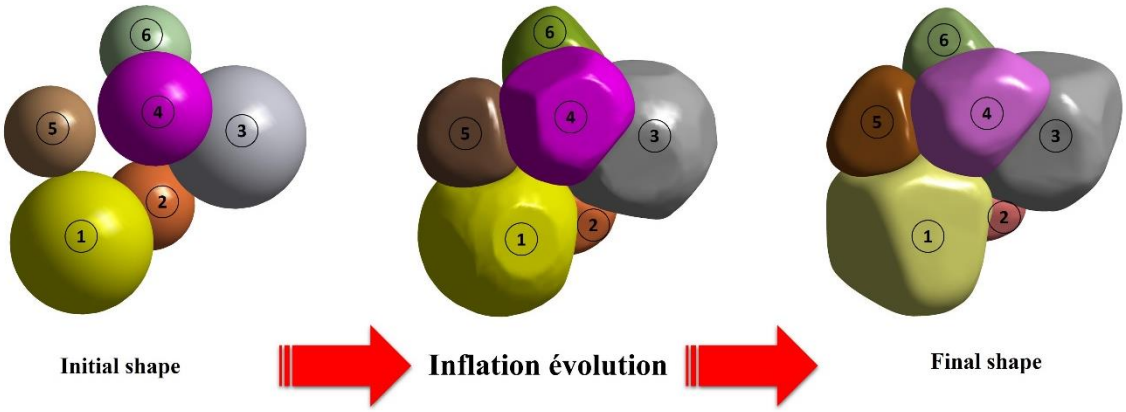

Figure III.11: Example of particle evolution during the inflation process.

c- Subtract the inner inflated particles geometry

The obtained deformed geometries of inflated particles stored in the output database are imported as a new part for a Boolean operation, where the inner inflated particle geometries were subtracted from solid cube to create the solid cell wall geometry of the foam (Figure III.12).

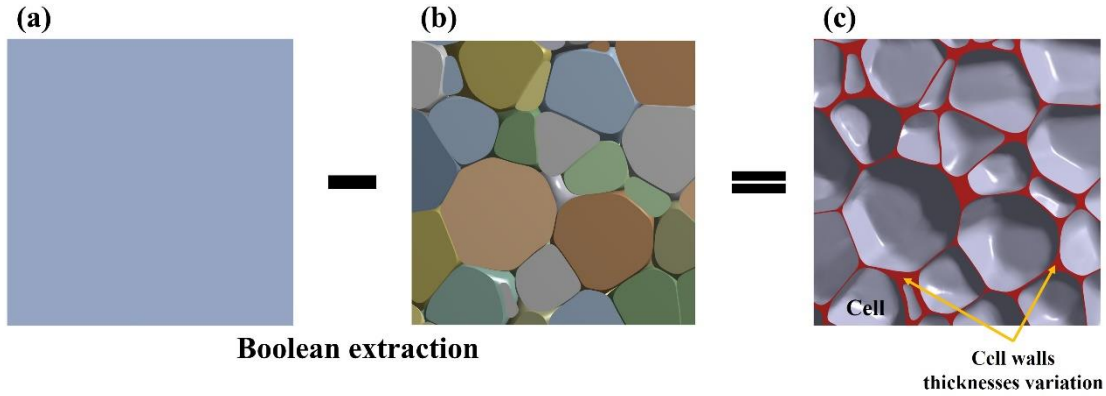

Figure III.12: Boolean operation used to create the solid closed-cell foam geometry: a) solid cube, b) Deformed geometries of the inner inflated particles, c) solid closed-cell foam geometry.

The proposed procedure is summarized in Figure III.13, for illustration an example of 220 thin spherical shells with deferent diameter size was inflated to obtain the final closed-cell foam geometry presented in Figure III.13 (c).

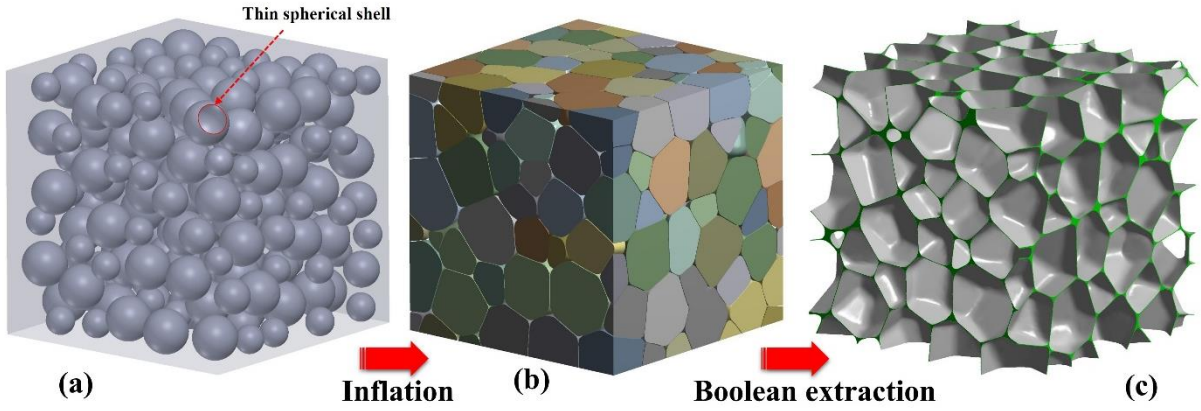

Figure III.13: 3D RVE closed-cell foam modeling steps: (a) Random close packing of 220 thin spherical shells, (b) Inflated spherical particles, (c) 3D generated solid model of closed-cell foam.

III.3.2. Illustrative example of designed foam with a high number of cells

In order to obtain a 3D solid model of closed-cell foam with a high number of cells, a random close packing with 1000 thin spherical shells was inflated to create the solid body of the foam as shows in Fig. 14. For a realistic display, the obtained closed-cell foam model was rendered in the software Solidworks (Figure III.14 (c)), this figure, illustrates the complex morphological features as in real foam.

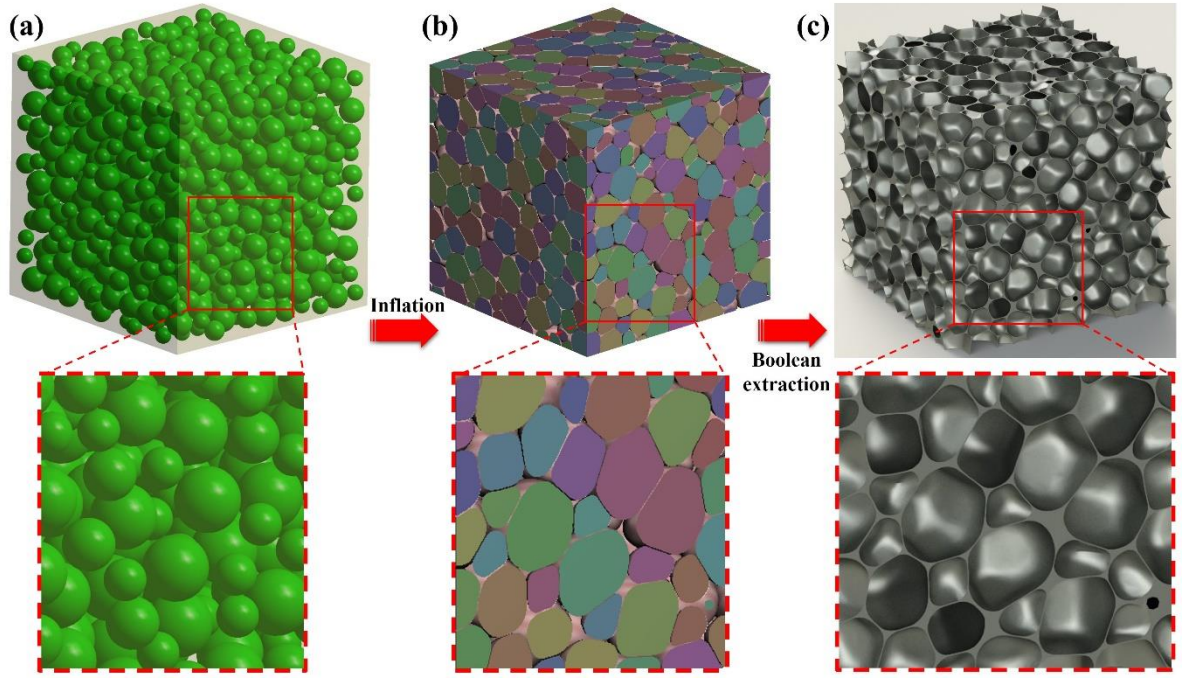

Figure III.14 : Example of 3D solid model of closed-cell foam with a high number of cells: (a) Random close packing with 1000 thin spherical shells, (b) Inflated spherical particles, (c) Rendered image of the obtained closed-cell foam model.

III.3.3. Comparison with real foam structure

To validate the generated numerical models, the obtained cell-morphological details were compared with those of the real foams. For illustration, Figure III.15 shows a comparison of a generated cylindrical closed-cell foam model (Figure III.15 (a)) and a studied cylindrical specimen (figure III.15 (b)) of closed-cell aluminum alloy foam produced by casting method and cuted using Electro Discharge Machine (EDM), with a same relative density of 159c and dimension of 20 mm diameter, 20 mm height [36]. This comparison shows that, the complex morphological features of the obtained foam are similar to the real one.

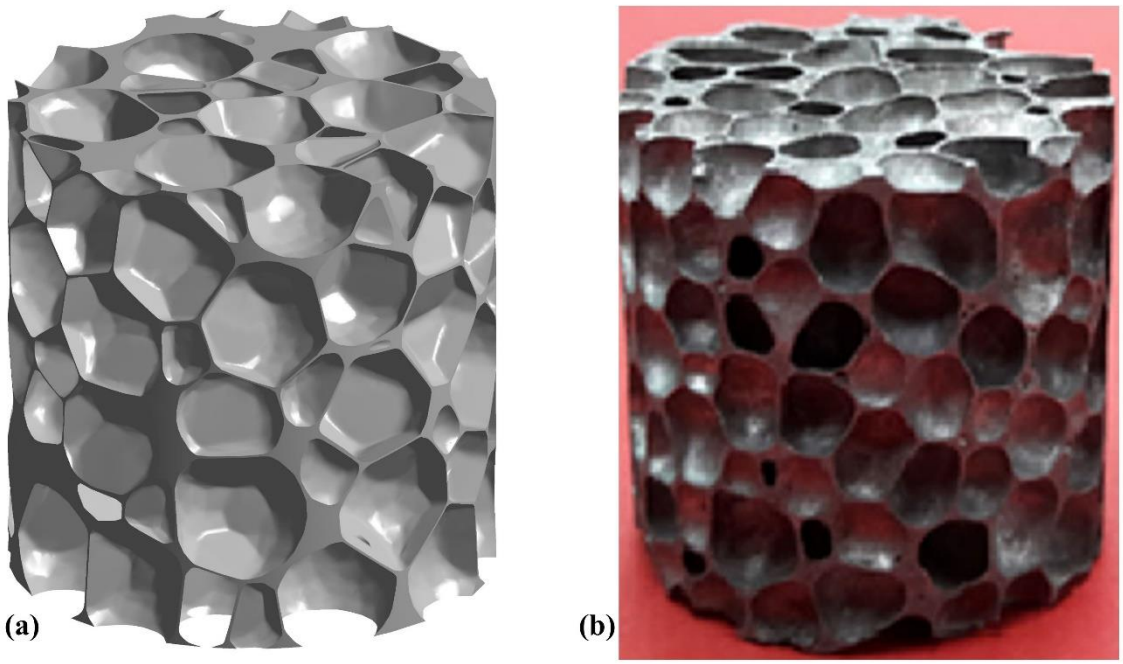

Figure III.15: Comparison of: (a) generated cylindrical closed-cell foam model and (b) specimen of closed-cell aluminum alloy foam.

For more demonstration, in another example, the non-uniform cell wall thickness and the unequally geometric distribution in a generated model (Figure III.16 (a)) are compared with those of an electron microscope photograph microstructure of closed-cell aluminum alloy foam (Figure III.16 (b)) manufactured by the China Shipbuilding Industry Corporation (CSIC) [151], as shown in figure III-16 . It is clear from this figure that these characteristics are well agreed in both the generated model and the produced aluminum foam.

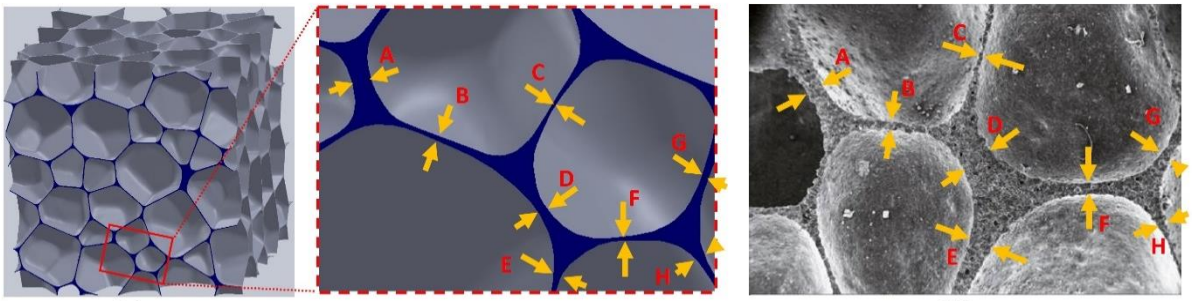

Figure III.16 : Comparison of non-uniform cell wall thickness and unequally geometric distribution in (a) generated model and (b) an electron microscope photograph microstructure of closed-cell aluminum alloy foam [151].

III.3.4. Evaluating the design for Additive Manufacturing (AM)

To validate experimentally the geometry of the proposed closed-cell foam models, a 3D designed CAD models (Figure III.17 (a)) were printed in the laboratory of mechanic of structures and Materials (LaMSM) as shown in Figure III.17 (b) using Geeetech AU 3d printer (PLA filament, 0.2 mm nozzle diameter and 0.14 mm layer thickness) for the cylinder specimen and Zortrax M200 3D printer (Z-Ultrat filament, 0.4 mm nozzle diameter and 0.14 mm layer thickness) for the cube specimen. For a good comparisons between designed and 3D-printed models, the irregular cell wall thickness distributions was indicated with arrows. As seen in Figure III.17, the complex structure of the foam with irregular cell wall thickness was successfully printed.

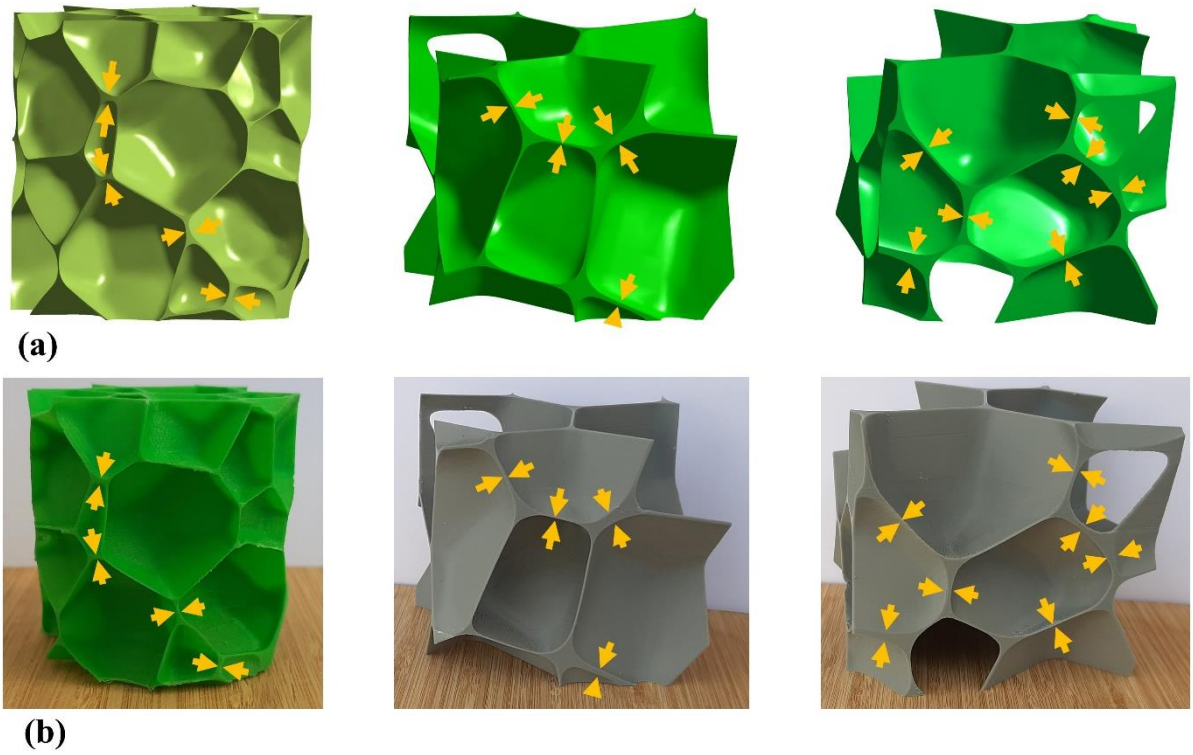

Figure III.17 : Comparison between (a) Designed models and (b) 3D-printed models of closed-cell foam structures.

Also, the relative densities of the manufactured and designed samples are compared as listed in Table III.3. It was shown that the relative densities of the manufactured samples are very close to the designed ones.

Table III.3 Comparison of relative density between the designed and 3D-printed models of closed- cell foam.

Sample	Dimensions(mm)	Relative density	
		Designed sample	**3D-printed sample**
Cylinder	50*50	0.068	0.069
cube	70*70*70	0.066	0.067

III.3.5. Foam Relative density control

Relative density (RD) is the important parameter that controls the foam architecture [26, 152]. It is defined as the density ratio of the foam to the solid material [153]. The deviation of the relative density is still the main problem in the reconstructed CT-based foam models, which is considered the most accurate method. This is due to the neglected tiny pores and the excessively thin cell walls in the numerical modeling process [11].

In the present study, spherical particle inflation is investigated to calculate the exact foam relative density. At each increment step, the foam geometry is extracted from the inflated particles and its relative density is calculated, aiming to plot the relative density evolution as a function of inflation time.

For illustrative purposes, Figure III.18 represents an example of extracted foam geometries from three different increment steps, with calculated relative densities of 0.57, 0.15, and 0.04, respectively.

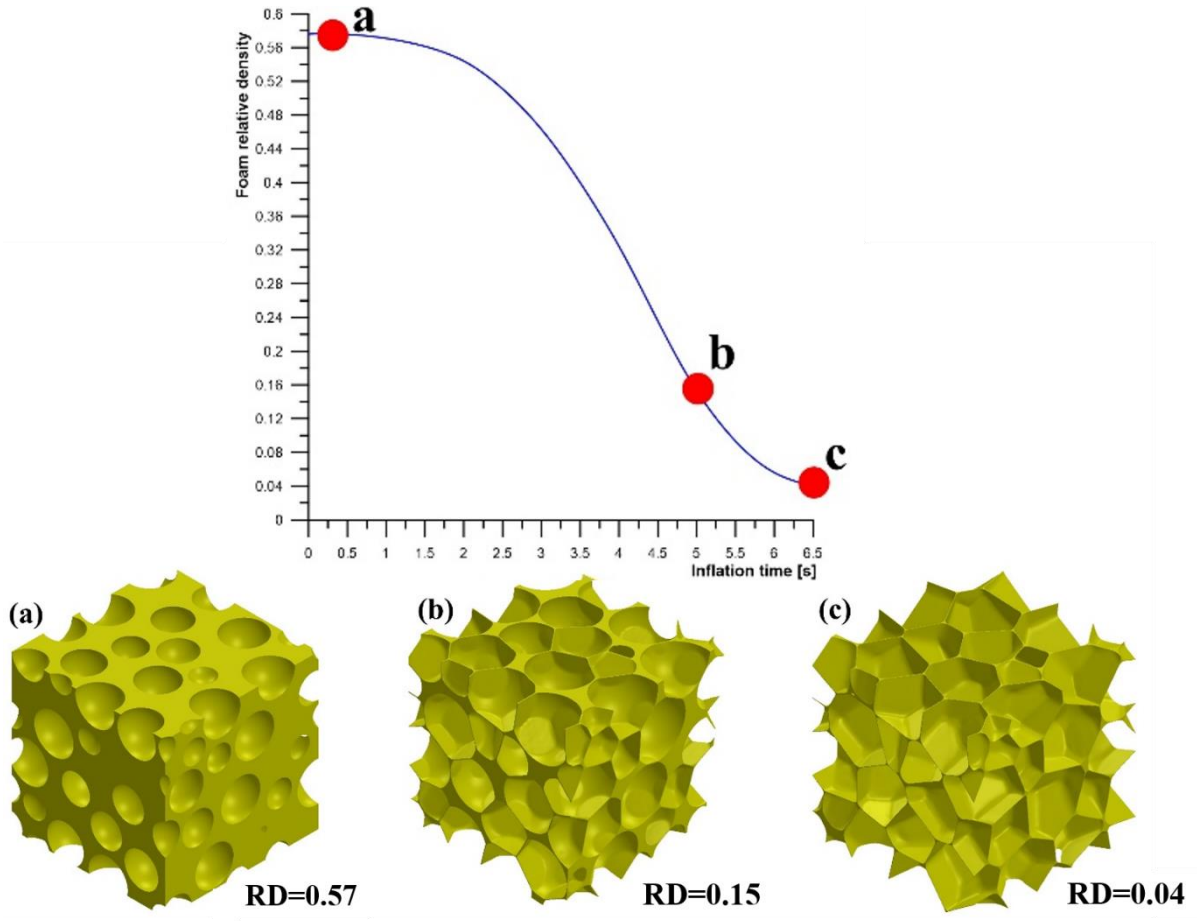

Figure III.18: Example of extracted foam geometries from three different increment steps, with calculated relative densities of (a) 0.57, (b) 0.15, and (c) 0.04.

To take into account the effect of random, number and size of panicles, the inflation simulation of four different random close packings (RCP) of 112, 155, 191, and 220 spheres respectively were analyzed. The relative density evolution curves in the four studied models are shown in Figure III.19.

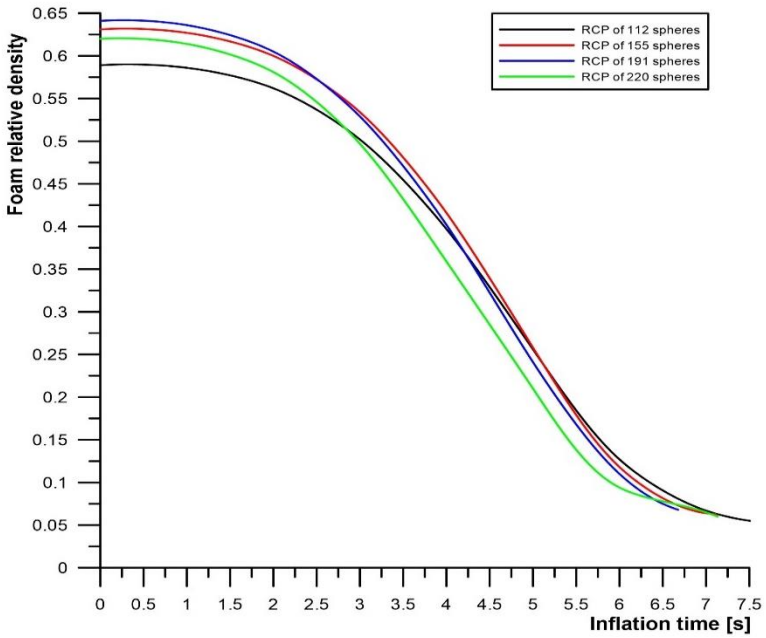

Figure III.19: Relative density evolution curves in the four studied models.

The important contribution of these curves is that it allows to choose the structure of closed-cell foam with an exact relative density.

This numerical analysis conducts to highlights another important advantage of the proposed technique, it was shown that the evolution of spherical particles during the inflation process can produce varying relative densities of foam due to the gradual decrease in the gap between the inflated particles (see Figure III.20), this makes the geometrical model of the foam suitable for studying the effect of local morphological characteristics on the mechanical performance of closed-cell foam material.

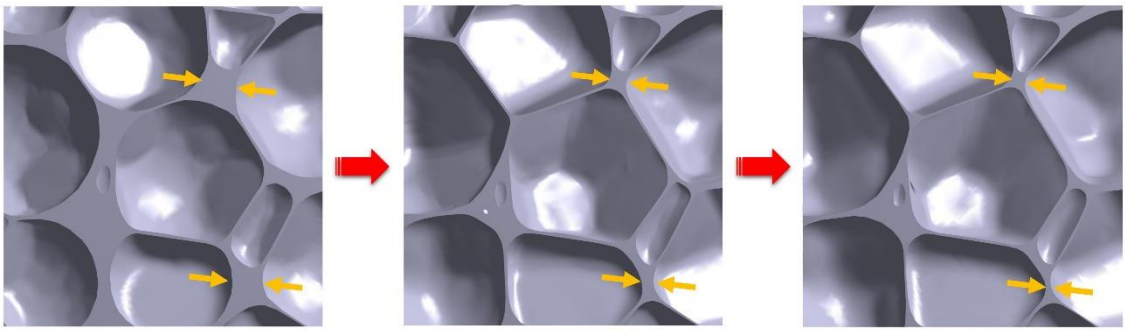

ρ=0.2 **ρ=0.094** **ρ=0.072**

Figure III.20 : Representation of cell wall thickness decrease during the inflation process and the obtained relative densities.

III.3.6. Cell size distribution

In this study, the cell size is quantified by the volume of the inflated particles extracted from different inflation times. Figure 14 shows histograms of the measured cell size in the initial geometry (Figure III.21 (a)) and in the final geometry (Figure III.21 (b)) of an inflated specimen of 220 spherical particles and dimensions of 100 x100x l00mm.

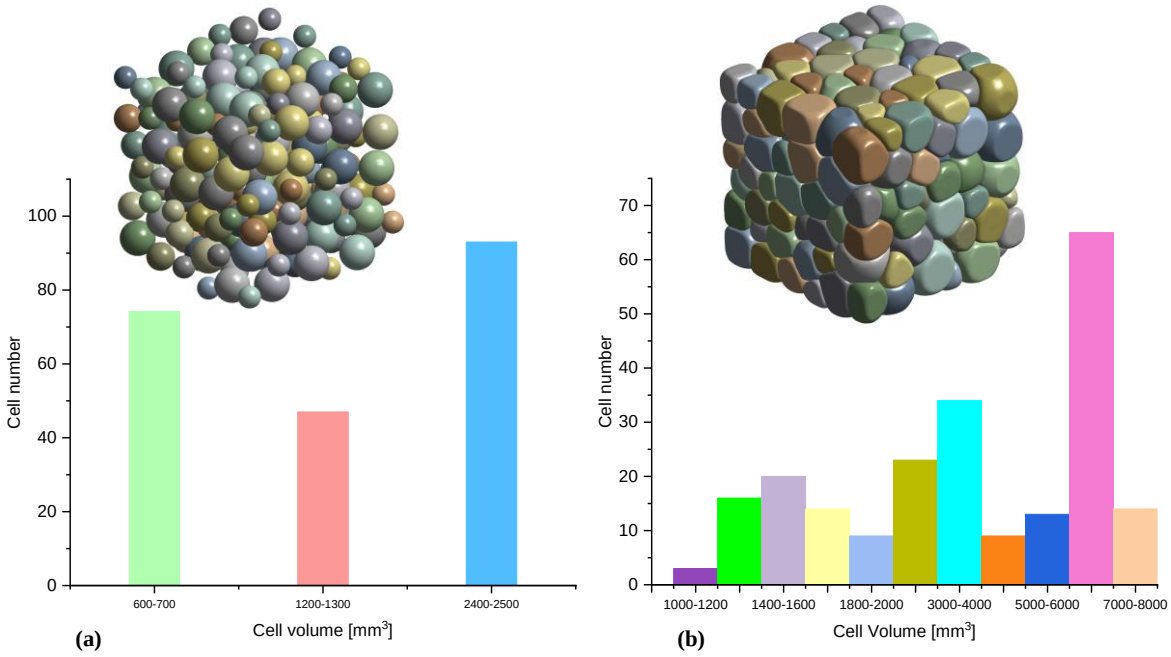

Figure III.21 : Histograms of measured cell size during inflation simulation: a) initial geometry, and b) final geometry.

The comparison of measured cell size shows that during inflation, the cell size became larger and non-uniform with more thickness ranges.

III.3.7. Cell wall thickness distribution

The average cell wall thickness is analyzed as a function of inflation time in five different random close packings (RCP) of 106, 112, 155, 191, and 220 spheres respectively as shown in Figure III.22 (a). The measured cell wall thickness distribution in the initial geometry and in the final one is shown in Figure III.22 (b). The initial geometry is characterized by medium and thick walls, while the geometry at the linal stage of inflation is characterized by a high percentage of thin walls (75%).

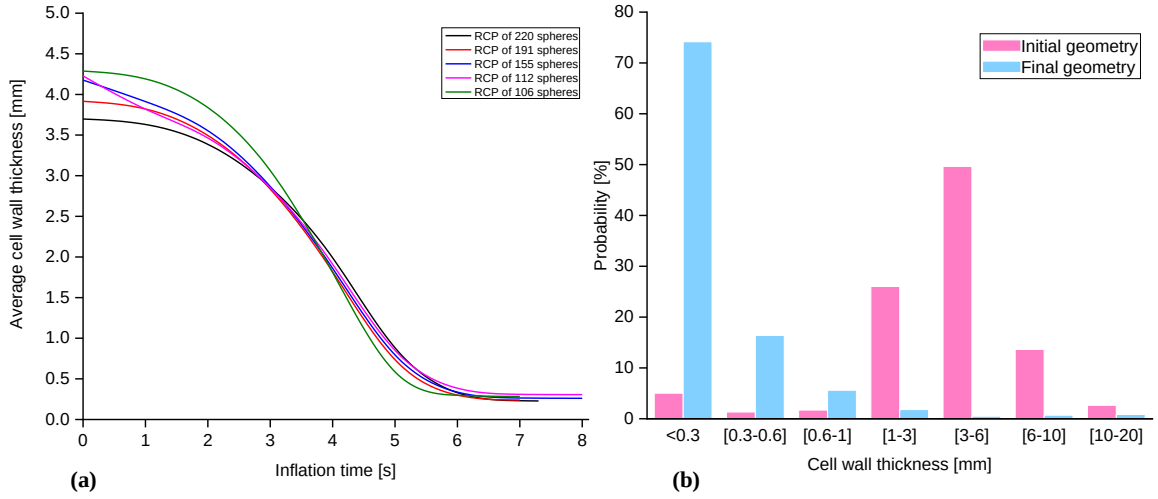

Figure III.22: Measured cell wall thickness distribution: (a) average cell wall thickness as a function of inflation time in five different random close packings (RCP) spheres, and (b) cell wall thickness distribution and its probability in the initial geometry and final geometry.

III.4. Conclusion

This chapter reviews the methodology devoted to generating 3D solid models of closed-cell foams and its validation through comparison with available experimental data from literature and by 3D printing tests.

Due to the high degree of randomness in the microstructure of real closed cell foams, many numerical models reported in literature not able to capture precisely the local morphological features found in solid foams geometry. This is still the main impediment which restricts the investigation of this novel material, and motivates the development of a sophisticated 3D solid model, that describes properly the complex geometry of real closed-cell foams. Additionally, the literature offers few 3D solid RVE modeling of real closed-cell foam microstructure. For this purpose, some efforts have been devoted with simplifying assumptions in geometry, some proposed models lack to cell walls irregularities and thickness variation, in other cases it was meshed with a regular grid, whereas a tetrahedron element type is required to mesh properly the cellular geometry due to the fact that cellular morphology and topology were fairly complex. Furthermore the porosity range is small and limited, and the models are not implemented in a hard test e.g. compression up to densification regime.

At this regard this work presents an efficient method to generate a three dimensional (3D) realistic models of closed-cell foams. The constructed RVEs solid models resemble to the real foams, in terms of local features such as, cell walls irregularities and thickness variation.

The RVE generation is based on the natural foam formation process, which is the efficient technique to rise quickly the porosity and to control the foam geometry. The air phase which is reached up to 96% of foam porosity was created by applying a fluid cavity pressure to inflate a packed random spherical particles in a dynamic FEA using the Abaqus software. The modeling approach was successfully verified by comparing cell-morphological details of the generated models with those produced experimentally.

CHAPTER IV MECHANICAL PERFORMANCE EVALUATION UNDER QUASI-STATIC LOADING

IV.1. Introduction

The influence of microstructural features on the mechanical behavior of foams has been demonstrated based on several examples illustrated in the precedent chapter. It was confirmed that the mechanical behavior of foams is strongly dependent on their relative density and on spatially variable geometrical features, such as the cell size distribution, the cell wall thickness distribution, cell wall curvatures, and the anisotropy in cell shape.

The main drawback of the experimental investigations is the difficulty to study the influence of each morphological parameter separately due to the complexity, and the high cost of manufacturing methods and experimental tests [33], which restrict the experimental methods.

Compared to real foams, the main disadvantage of models based on shell formulation is that it still lacks to the important spatially variable geometrical features found in real foams, such as the cell size distribution, the cell wall thickness distribution, cell wall curvatures, the anisotropy in cell shape. This disadvantage limits the functionality of these models, especially in medium-density foams. Computed tomography can only model the specific type of an individual foam and dramatically increases the computational time and economic expenses. That's why in some studies, the simulated foam structure is often reduced to a small structure including only 2 or 3 cells in each direction or only 5% of compression strain is calculated, and the densification regime is not addressed.

As presented in the precedent chapter, in this thesis the constructed 3D solid model describes properly the complex geometry of real closed-cell foams in terms of local features such as cell wall irregularities and thickness variation.

The evolution of spherical particles during the inflation process was found that it can produce varying relative densities of foam, this makes the geometrical model of the foam suitable for studying the effect of local morphological characteristics on the mechanical performance of closed-cell foam material.

For a developed closed-cell foam model, the biggest challenge to predict the mechanical response under quasi-static loading is capturing the densification stage.

To demonstrate that the compressive performance of the proposed closed-cell foam models can be controlled by relative density, 3D foam models were extracted from different inflation times and then subjected to quasi-static compression tests up to densification using the Abaqus software.

IV.2. Quasi-static compression test

To investigate the validity of the generated models in finite element analysis, a numerical simulation of a generated closed-cell aluminum foam under quasi-static loading is performed up to the densification stage, which is the range of deformation routinely utilized in engineering applications [154].

The foam sample with a dimension of 20x20x20 mm is supported by a rigid fixed plate and loaded by a rigid moving cylindrical impactor at a constant velocity of 13.2 m/s [155] as illustrated in Figure IV.1 (a), which are the approximated conditions of cellular materials under quasi-static test. The contact between foam cells, and between platens and foam, was modeled using the general contact algorithm with a friction coefficient of 0.2 [45].

The geometrical model of the closed-cell foam is meshed using the C3D10 tetrahedron element type with a mesh size of 0.7 mm as shown in Figure IV.1 (b).

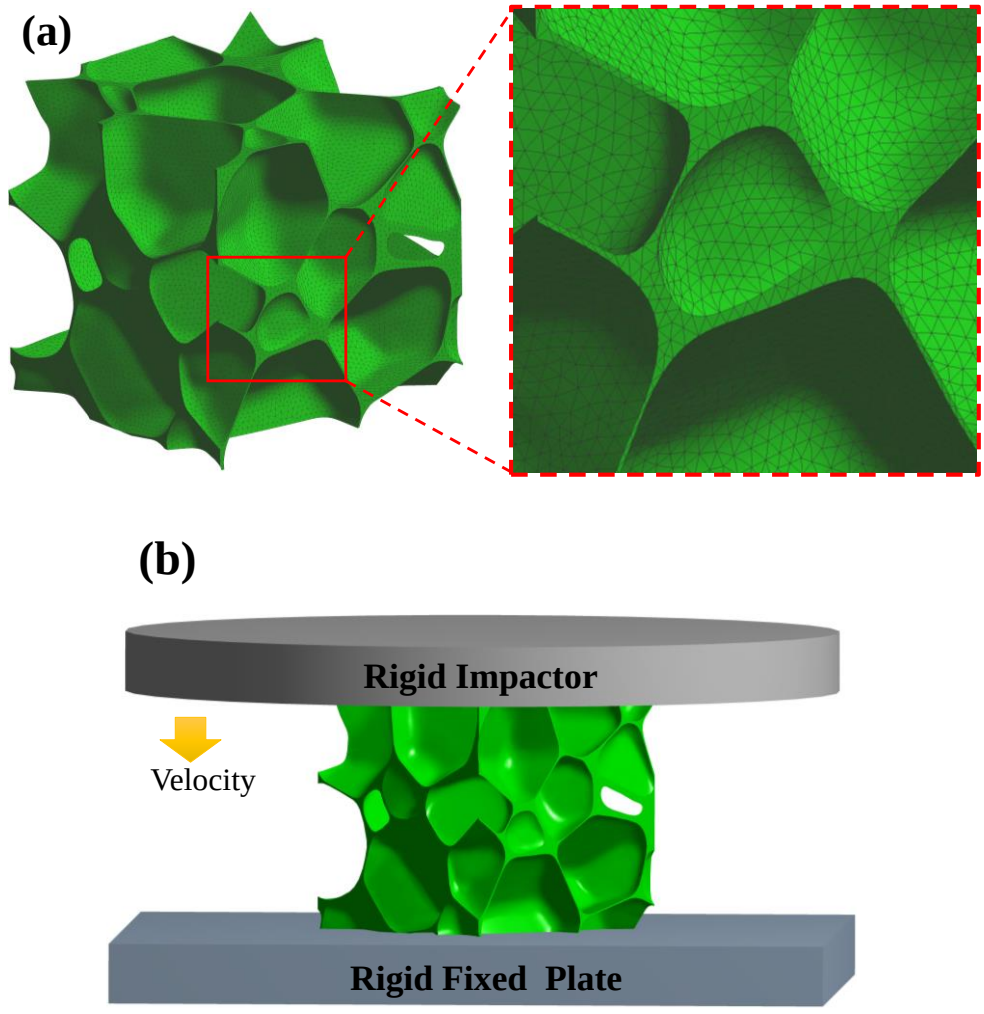

Figure IV.1: Illustration of (a) constructed specimen foam and quasi-static loading boundary conditions, and (b) 3D finite element mesh.

In order to obtain an efficient and an accurate results in the quasi-static simulation, the experimental mechanical properties of solid closed-cell aluminum foam provided in [156] were employed. The details of this mechanical properties are listed in Table IV.1.

Table IV.1 Aluminium material properties used in FE study [156].

Density (kg/m^3)	2710
Young's Modulus (GPa)	69
Yield Stress (MPa)	49.75
Poisson's Ratio	0.3
Stress (MPa)	**Plastic-strain**
49.75	0
54.4	0.00539
63.69	0.0135
70.47	0.0216
76.53	0.0327
84	0.0529
90.39	0.0761
96.05	0.102
104.87	0.156
107.33	0.174
110.81	0.22
112.84	0.268
111.31	0.3
109.84	0.326

IV.3.Results and discussion

IV.3.1. Mechanical response

The effective von misses stress distribution in foam sample for three different deformed configurations were presented in Figure IV.2.

The obtained reaction force-displacement curve is illustrated in Figure IV.3, it can be observed that it exhibits three different stages, started with a short linear stage, followed by long plateau region at the second stage, and finished by a densification stage.

This curve is similar to the typical force-displacement curve of real closed-cell aluminum foam under compression loading (e.g. see [157]).

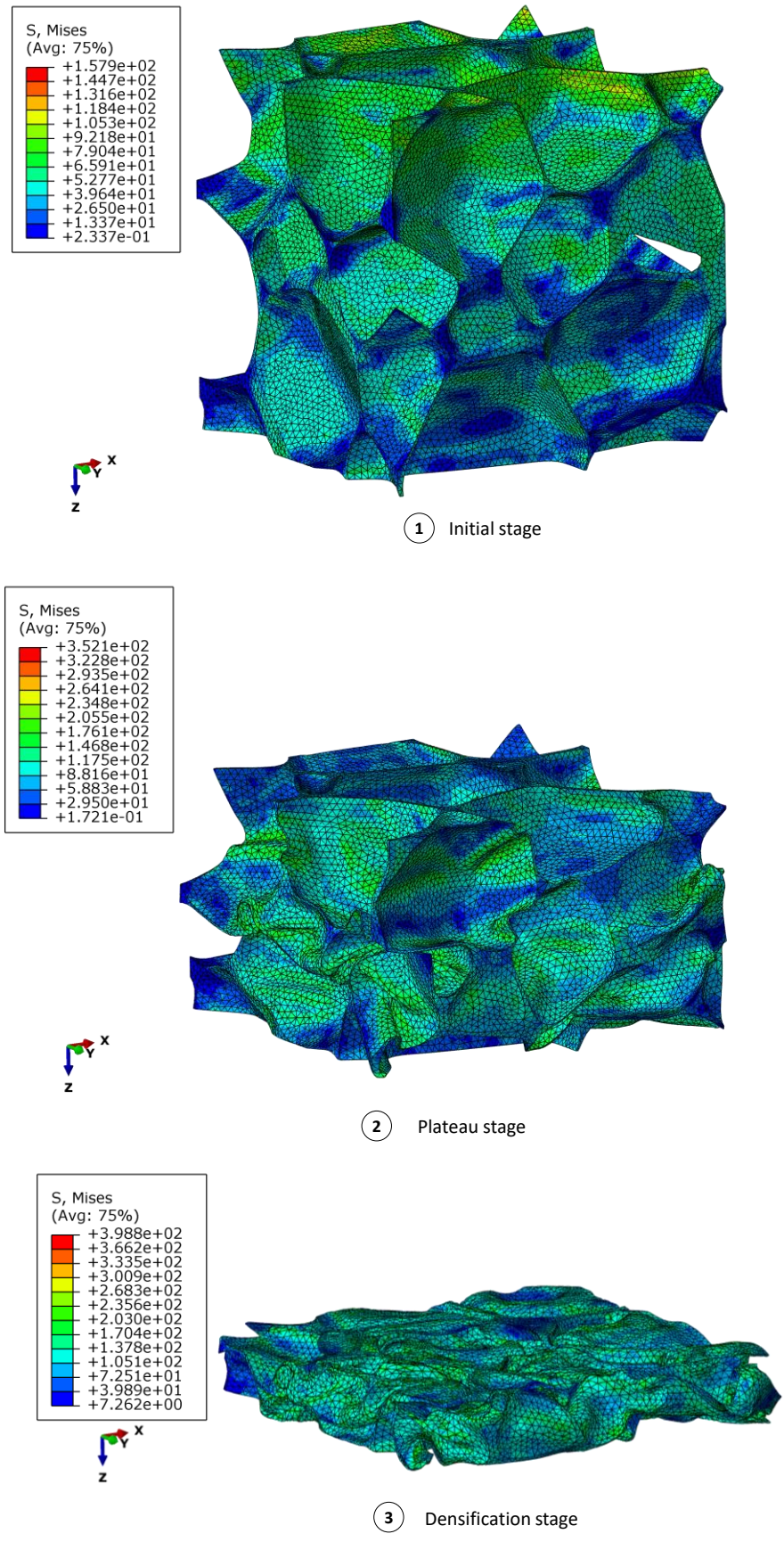

Figure IV.2: Effective von misses stress distribution in foam sample for three different deformed configurations.

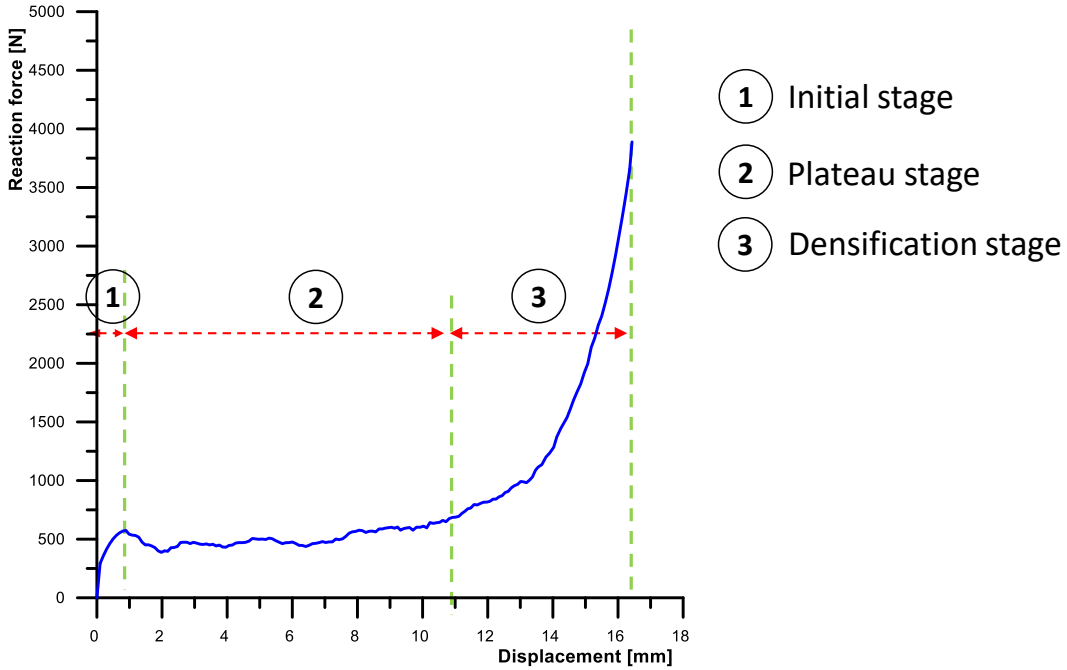

Figure IV.3: Obtained reaction force-displacement curve.

From the obtained results, it was shown that the compressive deformation process up to the densification stage of the tested foam model was successfully simulated.

IV.3.2. Compressive performance control

As demonstrated in the literature, the relative density has a major influence on the plateau region level (yield point), and on the plateau region length as shown in Figure IV.4.

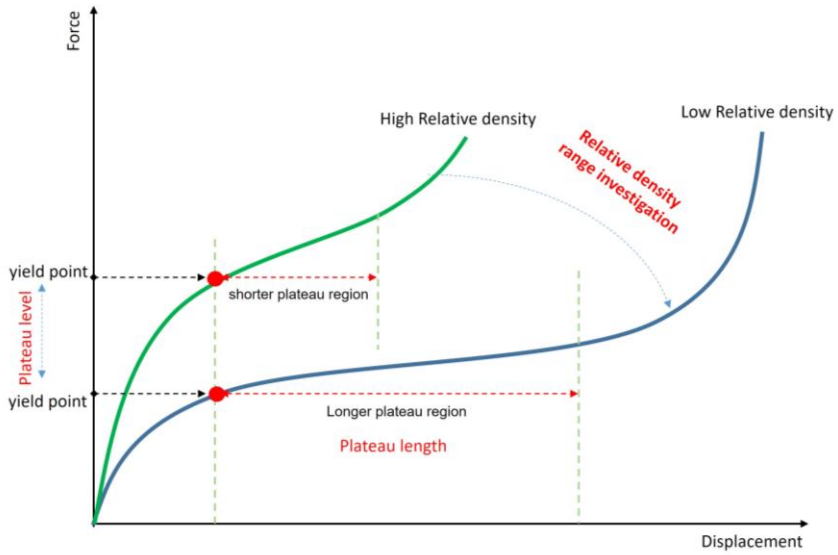

Figure IV.4: Illustration of relative density effect on quasi-static compression response of closed-cell aluminum foam.

To analyze the quasi-static compression load of closed-cell aluminum foam as a function of relative density, samples of foam with a dimension of 20x20x20 mm are extracted from different inflation times using the relative density evolution curve. The relative density was ranged from 0.07 to 0.2.

Examples of extracted foam geometries and their FE models are shown in Figure IV.5. It is evident from this Figure that the cell wall thickness decreased progressively.

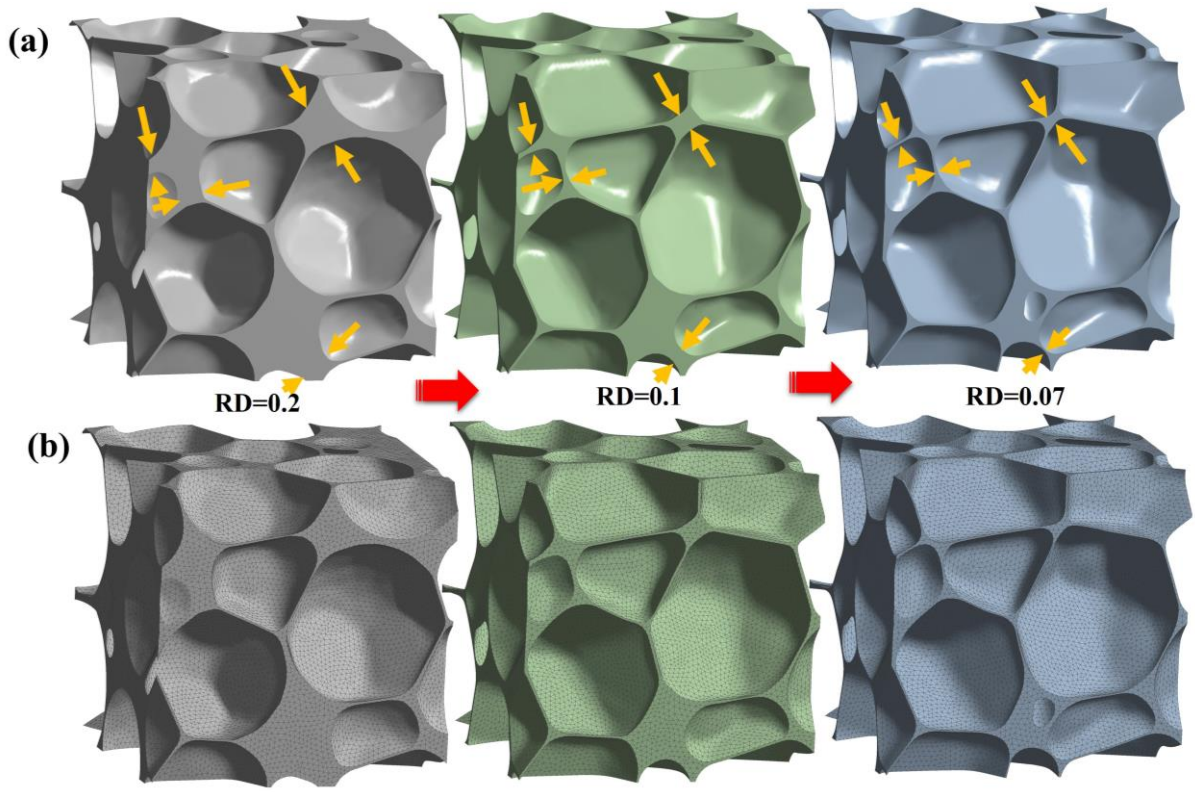

Figure IV.5: Illustration of: a) Extracted foam geometries and b) FE models.

IV.3.3. Reaction force-displacement curve

The obtained reaction force-displacement curves in the studied range of relative density are illustrated in Figure IV.6. Four foam specimens with relative densities of 0.07, 0.1, 0.15, and 0.2 respectively are selected for comparison.

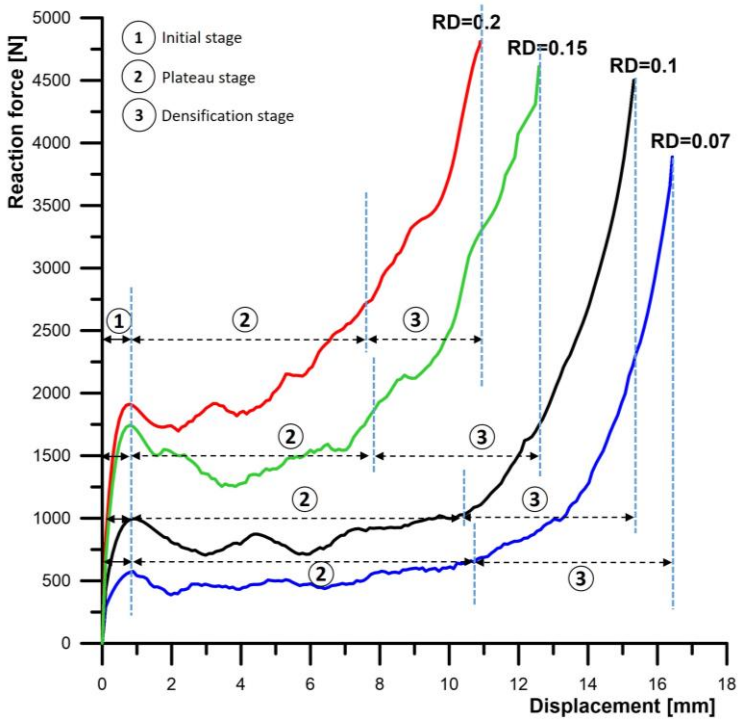

Figure IV.6: Quasi-static compression response of the studied closed-cell aluminum foam for different relative densities.

Comparing the curves, it is clearly observed that increasing the relative density will increase the plateau level and decrease the plateau length of the aluminum foam. As illustrated in Figure IV.3, the lower relative density value (RD=0.07) possesses a less-level plateau and an extended plateau length, which leads to later densification of the foam, in contrast, the higher relative density value (RD=0.2) has a high-level plateau, a shorter plateau length, and earlier densification.

IV.3.4. Compressive mechanical properties

Figures IV.7, IV.8, and IV.9 show the effective von misses stress distribution and observed cell wall deformation mode under uniaxial compression for the constructed foam with different relative densities.

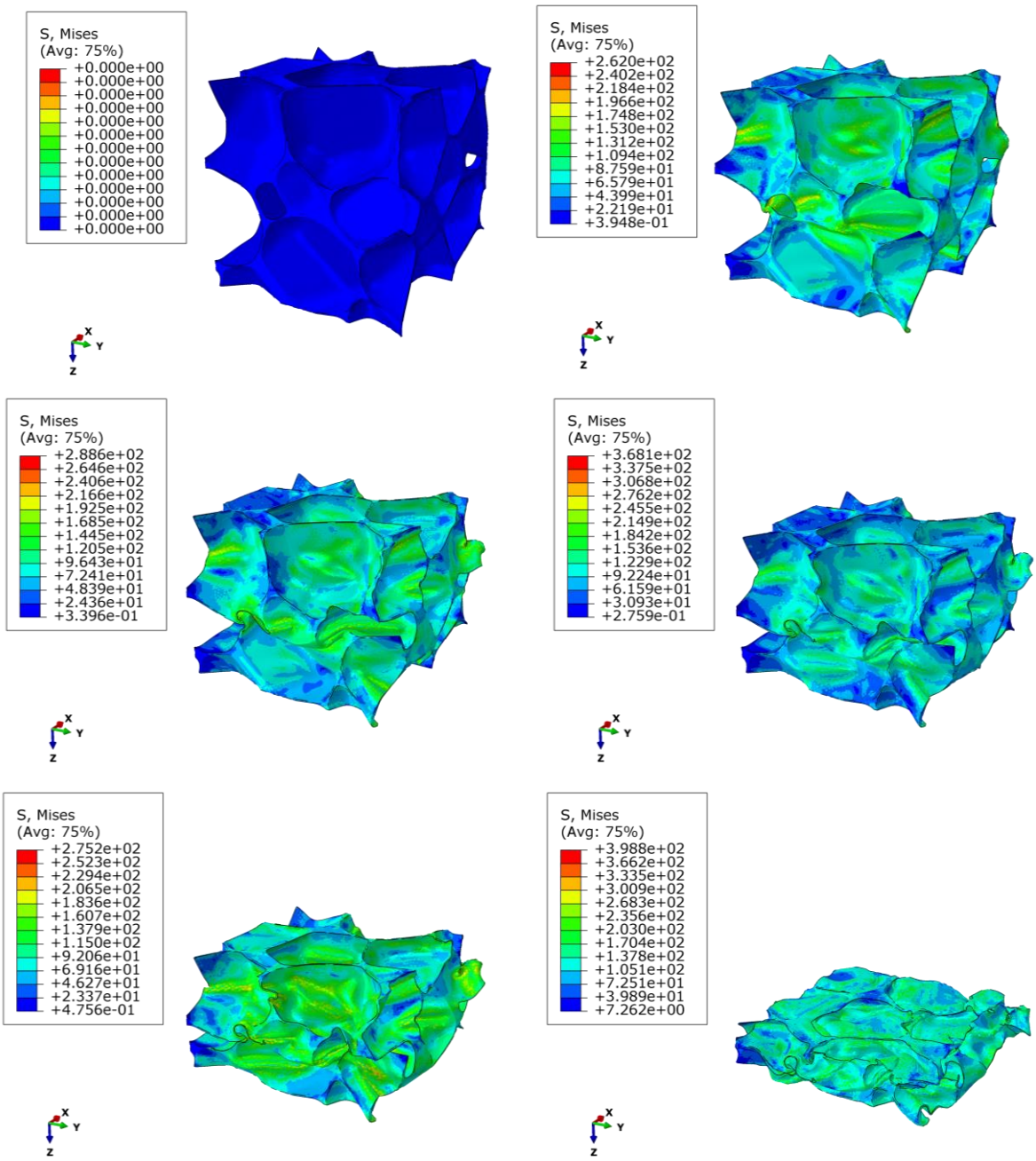

Figure IV.7: Effective von misses stress distribution and observed cell wall deformation mode under uniaxial compression for constructed foam with relative density RD=0.07.

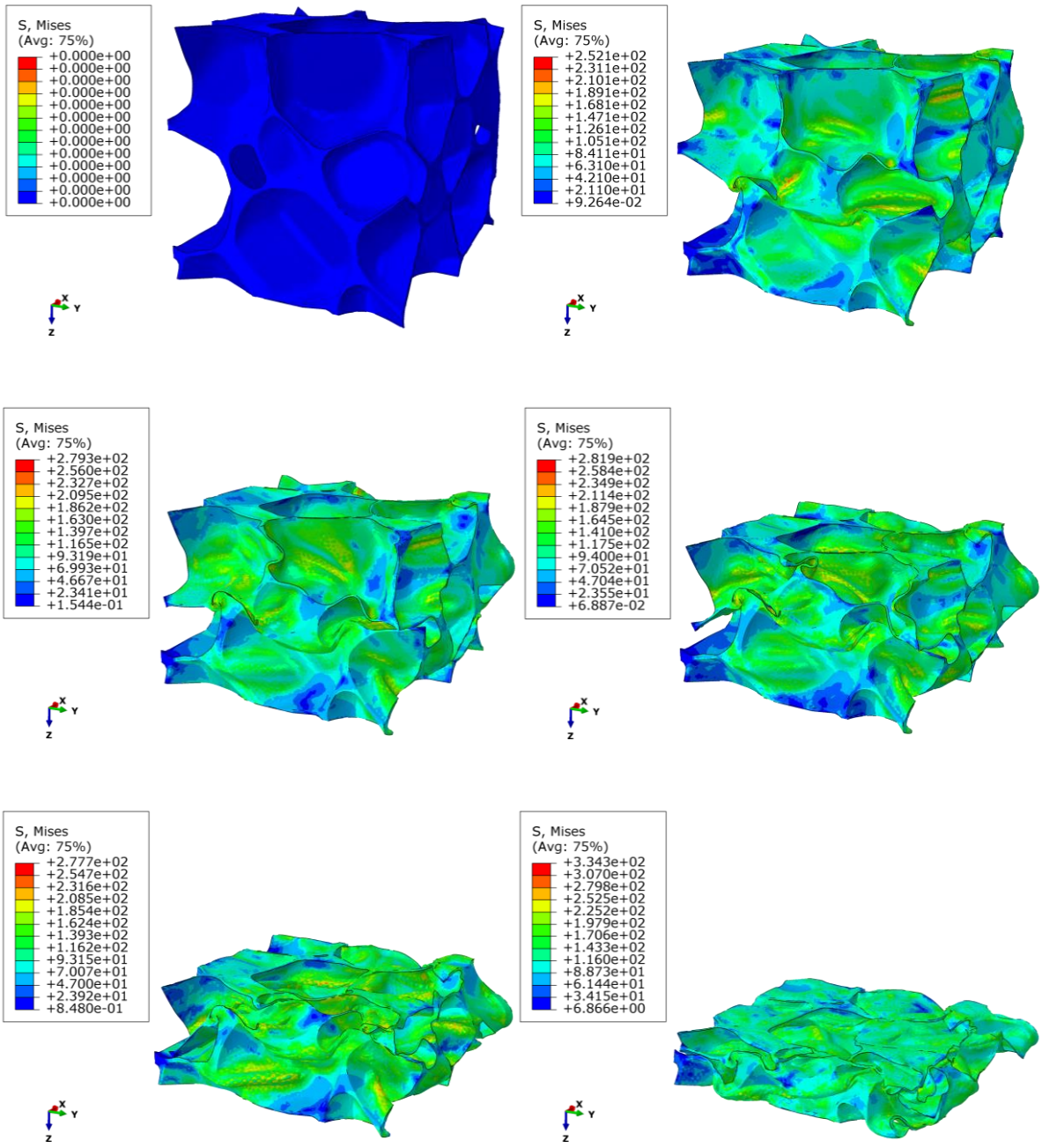

Figure IV.8: Effective von misses stress distribution and observed cell wall deformation mode under uniaxial compression for constructed foam with relative density RD=0.1.

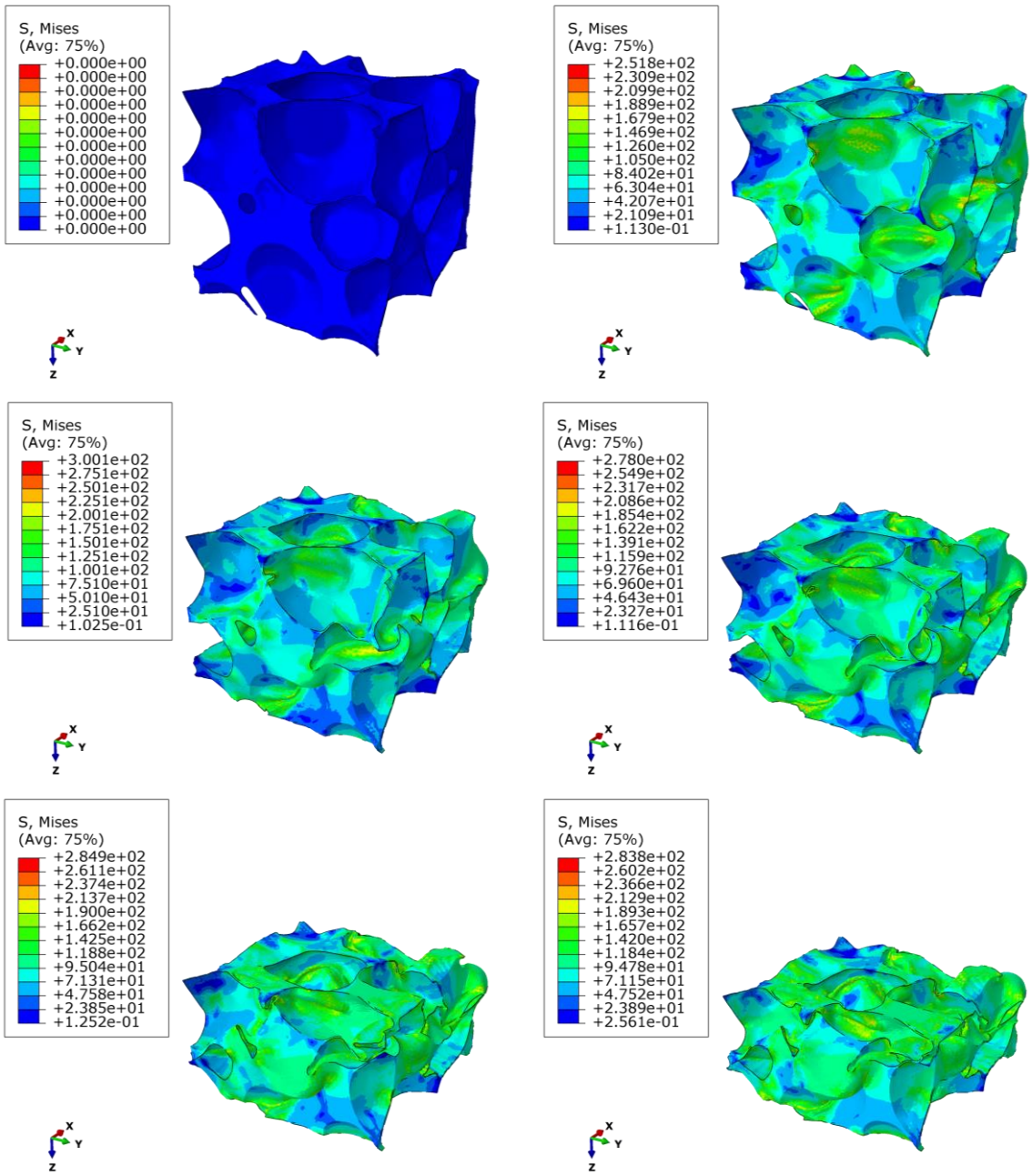

Figure IV.9: Effective von misses stress distribution and observed cell wall deformation mode under uniaxial compression for constructed foam with relative density RD=0.2.

Figure IV.10 shows the quasi-static compression stress-strain curves for aluminum foams with different relative densities.

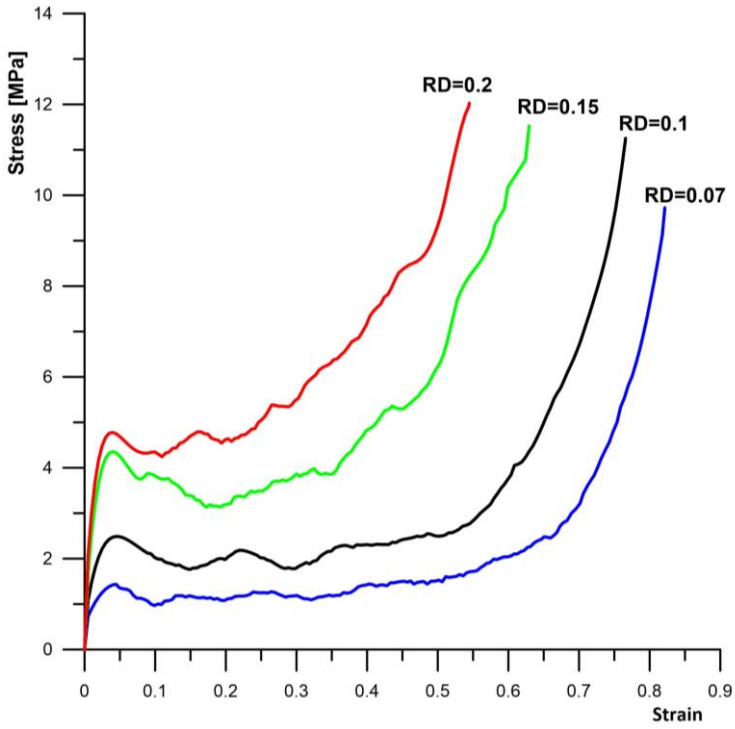

Figure IV.10: Quasi-static compression stress-strain curves for aluminum foams with different relative densities.

The main mechanical properties of the studied foams are calculated from the stress-strain curves (Figure IV.10 according to ISO 13314 standard [158] and listed in table 3. Where the first maximum compressive strength is the compressive stress corresponding to the first local maximum in the stress-strain curve, the plateau stress σ_{pl} is calculated as the arithmetic means of the stress at the strain of 0.2 and 0.4, and the densification strain corresponds to the strain where stress reaches 1.3 σ_{pl}.

Table IV.2: Summary of calculated mechanical parameters for Al foams under compression.

Relative Density	**First maximum compressive strength (MPa)**	**Plateau Stress (σ_{pl}) (MPa)**	**Densification Strain (ε_D)**
0.07	1.44	1.27	0.56
0.1	2.49	2.14	0.54
0.15	4.36	3.84	0.44
0.2	4.78	5.91	0.41

IV.3.5. Plateau stress variation

According to several literature references [e.g. 32, 159, 160, and 161], the relation between the plateau stress and relative density of aluminum foam could be fitted with a power function as:

$$\sigma_{pl} = A\sigma_{ys}\left(\frac{\rho^*}{\rho_s}\right)^B \quad \text{(IV.1)}$$

Where σ_{ys}, and ρ_s are the yield stress and density of cell-wall base material; *A* and *B* are the two material constants.

The equation proposed by Santosa and Wierzbicki [162] can be used for closed-cell aluminum

foams with a strengthening coefficient A =1.33 and a power of the term $\frac{\rho^*}{\rho_s}$ approximately 1.5 according to some researchers [32, 163], the equation can be written as:

$$\sigma_{pl^*} = 1.33\sigma_{ys}(\frac{\rho^*}{\rho_s})^{1.5} \quad \text{(IV.2)}$$

The calculated plateau stress σ_{pl^*} values using the Eq. (IV.2) were plotted along with the numerical results obtained from the investigated closed-cell foam in the present study as shown in Figure IV.11. Noting that the formula was verified in the studied range of relative density from 0.07 to 0.2.

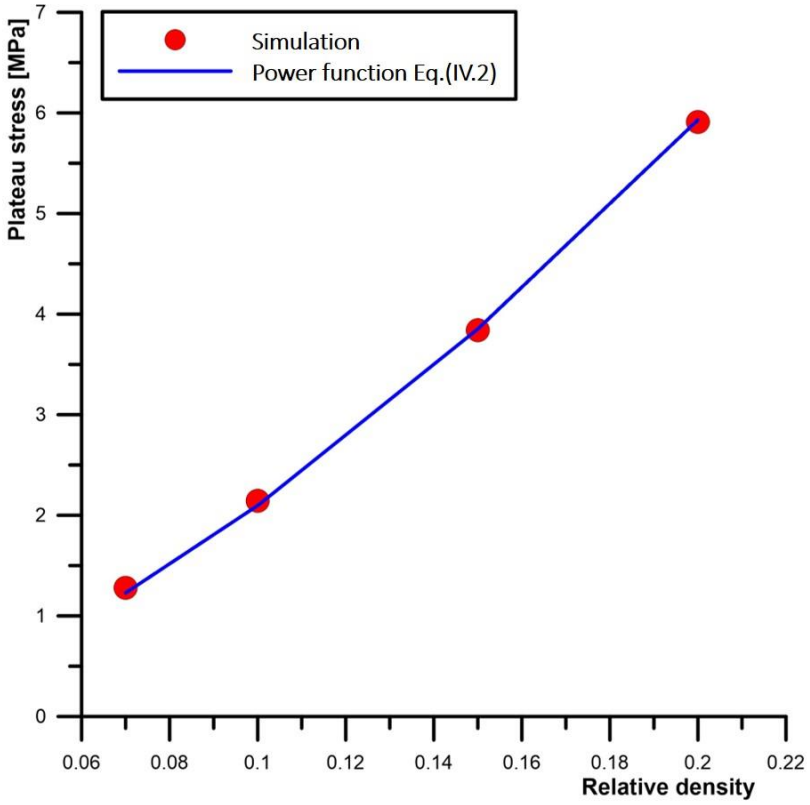

Figure IV.11: Evolution of Plateau stress as a function of relative density - comparison between obtained numerical results and those calculated by the Eq. (IV.2).

As seen in Figure IV.11, it can be concluded that the results of simulations are well-fitted to the power formula.

The obtained numerical results demonstrate the effectiveness of the designed models and the possibility of controlling the compressive performance of closed-cell foam. With the proposed technique an optimum value of relative density foam can be easily found and adjusted for a given application.

IV-3-6- Effect of loading direction on compressive behavior

To analyze the effect of loading direction on the compressive behavior of designed models, the foam specimen with a relative density of 0.1 was selected as an example. Figure IV.12 plots the reaction force-displacement curves under uniaxial quasi-static compression in the three orthogonal directions X, y, and Z respectively.

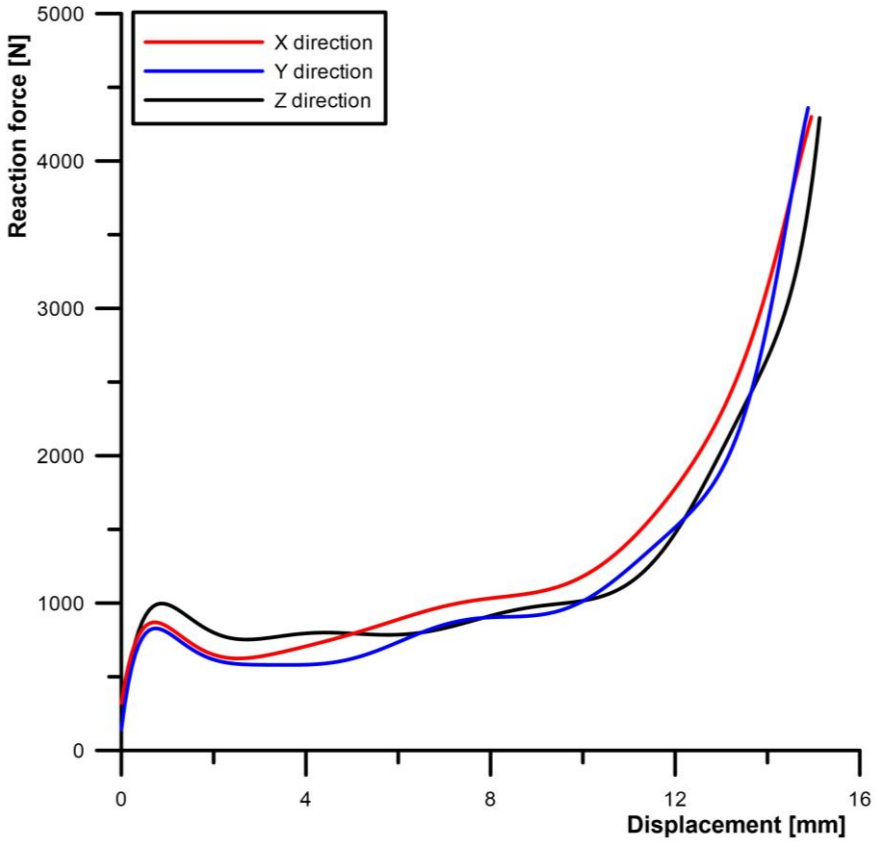

Figure IV.12: Reaction force-displacement curves under uniaxial quasi-static compression in the three orthogonal directions X, Y, and Z.

From Figure IV.12, it can be seen that the difference in the three tested directions is small, which implies that the studied closed-cell foam is largely uniform and isotropic in nature, as revealed in existing experimental works [see e.g. 11, 151].

IV.3.7. Effect of cell wall thickness non-uniformity

The effect of cell wall thickness non-uniformity was numerically investigated in [164], by comparing the deformation mechanism of developed uniform cell wall thickness Voronoi foam models with CT-based reconstructed models. The comparison shows an overestimation of the maximum stress value with remarkable delayed densification in the response of the Voronoi model. The authors related these differences to the buckling deformation mode of the cell walls observed in the reconstructed CT-based model, whereas it deforms in bending for the Voronoi foam model. The plastic buckling mechanism of cell walls is observed, with a stress-strain response close to that of the reconstructed CT image model when introducing non-uniform cell wall thickness into the Voronoi model.

In the present study, the effect of cell wall thickness non-uniformity is evaluated by comparing the quasi-static compression stress-strain curves of a constructed non-uniform cell-wall thickness foam model based on spherical particles inflation simulation (Figure IV.13(a)) and a constructed foam with identical cell-wall thickness (Figure IV.13(b)) having the same cell irregularity and relative density (RD=0.09) and the dimension of 15x 15x 15 mm. For better comparison, the centers and diameters of the inflated spheres were used as input parameters to create the foam with a uniform cell-wall thickness using the Voronoi technique. The geometrical models are meshed using the C3D10 tetrahedron element type with a mesh size of 0.7 mm.

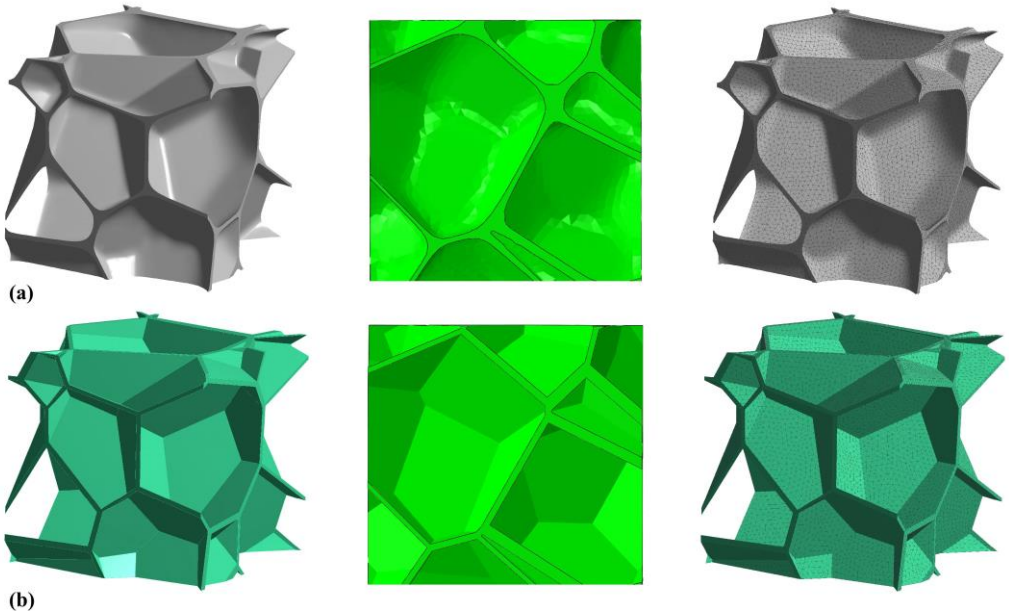

Figure IV.13: Geometric model and finite element mesh of (a) constructed non-uniform cell-wall thickness foam based on spherical particle inflation and (b) constructed foam with identical cell-wall thickness.

The deformation mechanism during the uniaxial compression tests obtained in foam samples with uniform and non-uniform cell wall thickness distribution is compared as shown in Figure IV.14.

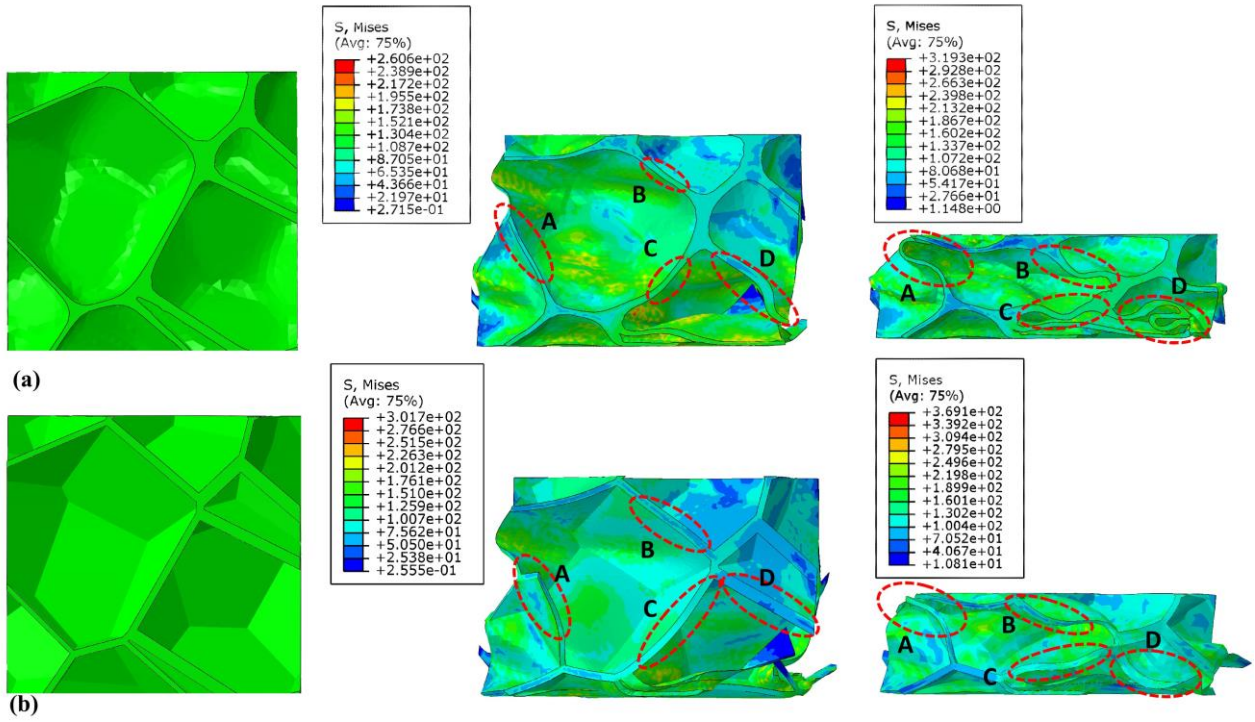

Figure IV.14: Effective von misses stress distribution and observed cell wall deformation mode under uniaxial compression for constructed foam with (a) non-uniform cell-wall thickness and (b) identical cell-wall thickness.

From Figure IV.14, it can be observed that the absence of plastic buckling in the foam sample with uniform cell wall thickness causes a higher stress value and delayed cell walls collapse compared to the model with a non-uniform thickness, which is characterized by a large number of buckled cell walls during the compression.

Figure IV.15 shows the quasi-static compression stress-strain curves of foam samples with uniform and non-uniform cell wall thickness distribution.

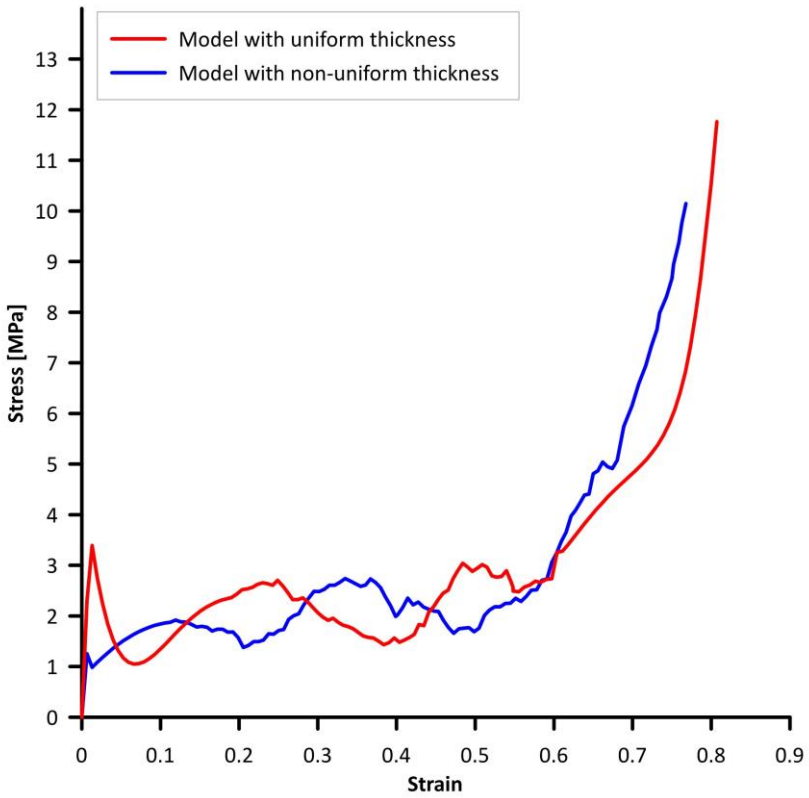

Figure IV.15: Quasi-static compression stress-strain curves of foam samples with uniform and non- uniform cell wall thickness distribution.

The main mechanical properties of the compared foams are calculated from the stress-strain curves (Figure IV.15) according to ISO 13314 standard [158] and listed in table IV.3.

Table IV.3: Summary of calculated mechanical parameters for compared foams under compression.

Foam type	**First maximum compressive strength (MPa)**	**Plateau Stress (σ_{pl}) (MPa)**	**Densification Strain (ε_D)**
Foam with uniform cell walls thickness	3.39	2.14	0.57
Foam with non-uniform cell walls thickness	1.25	1.84	0.55

From the obtained results, the considerable difference observed in the stress-strain curves demonstrated that the Voronoi foam model with identical thickness was characterized by an overestimation of the peak stress value and a delayed start of the densification stage, as discussed in [164].

To show the capability of the developed closed-cell foam model, the deformation morphology during compression of a constructed solid closed-cell foam model was compared

with that of a real aluminum foam sample presented in Movahedi et a1. [165]. As it can be seen in Figure IV.16 the initiation of cell collapse at the thinnest cell wall is well captured.

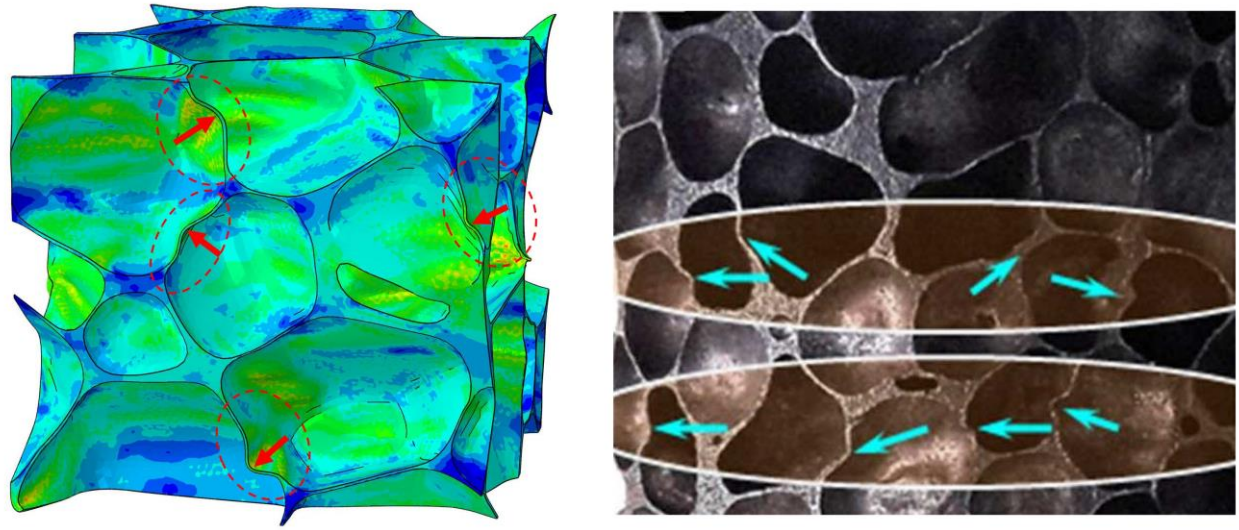

(a) (b)

Figure IV.16: Comparison of deformation morphology of an aluminum closed-cell foam during compression: Initiation of cell collapse at the thinnest cell wall (weakest position) of a cell: a) Constructed model; b) Movahedi et al. [66].

IV.4. Conclusion

In this chapter, the mechanical performances and collapse mechanisms of the designed irregular closed-cell foams with relative density control, were investigated through finite element (FE) simulations under quasi-static loading up to densification, which is the range of deformation usually utilized in engineering applications.

The evolution of spherical particles during the inflation process changes the size, cell-wall irregularity, and thickness variation of foam geometry. This allows the possibility to study the foam at different stages of spherical particle inflation.

The evaluation under the quasi-static compression test of extracted foam samples at different inflation times was carried out. The main compressive mechanical properties of closed-cell aluminum foam have been determined from the stress-strain curves according to ISO 13314 and related to only one parameter, which is the relative density of the foam.

From the obtained results, the following conclusions can be drawn:

- The relative density which is recognized as the most important parameter affect the mechanical behavior of foams was controlled by the gradual decrease in the gap between the inflated particles.
- The quasi-static compression curves of the proposed 3D irregular closed-cell foam models

exhibit the three deformation stages of real closed-cell aluminum foam under compression loading.

- The plateau region which ensures the smooth energy absorption of the foam material can be characterized by a level and a length.
- It was confirmed that the relative density has a major influence on the plateau region level (yield point), and on the plateau region length: increasing the relative density will increase the plateau level and decrease the plateau length of the aluminum foam.
- It was further confirmed that the relation between the plateau stress and relative density of closed-cell aluminum foam could be fitted with a power function, the power of the relative density term is confirmed to be approximately 1.5.
- The effect of loading direction on the compressive behavior of designed models, showed that the proposed foam models exhibit isotropic mechanical properties.
- It was demonstrated that the cell collapse initiates at the thinnest cell wall.
- The proposed numerical models can be readily used to reduce expensive experiment tests of closed-cell foams, and it can be used as an input for several types of FE analysis (thermal, structural, acoustic).

GENERAL CONCLUSION

Due to its interesting combinations of physical and mechanical properties, such as a high stiffness-to-weight ratio, metal foam is one of the most studied topics today.

Based on the type of structure, the metal foam may be divided into two categories: open-cell and closed-cell. Closed-cell metal foam structures are made of a thin layer of a metallic wall that entirely encloses the pores. While open-cell structures have unified pores.

Metallic foams have a variety of applications in several industries. While open porosity is employed in functional fields where load bearing is not the primary aim, closed-cell metal foam is well suited for structural load-bearing applications.

Therefore, the development of new technologies or attachments to reduce the manufacturing costs of metal foams gained more attention and widespread application.

Due to the high degree of randomness in the microstructure of real closed-cell foams, many numerical models reported in the literature are not able to capture precisely the local morphological features found in solid foams geometry. This is still the main impediment that restricts the investigation of this novel material and motivates the development of a sophisticated 3D solid model, which describes properly the complex geometry of real closed-cell foams.

In this regard, this thesis presents an efficient method to generate three-dimensional (3D) realistic models of closed-cell foams. The constructed RVEs solid models resemble to the real foams, in terms of local features such as, cell walls irregularities and thickness variation. The RVE generation is based on the natural foam formation process, which is the efficient technique to rise quickly the porosity and to control the foam geometry. The air phase which is reached up to 96% of foam porosity was created by applying a fluid cavity pressure to inflate a packed random spherical particles in a dynamic FEA using the Abaqus software. The modeling approach was successfully verified by comparing cell-morphological details of the generated models with those produced experimentally. The performance of the proposal in finite element analysis has been investigated by subjecting a designed 3D RVE solid model of closed-cell aluminum foam to a quasi-static loading up to the densification stage, which is the range of deformation usually utilized in engineering applications.

From the obtained results, the following conclusions can be drawn:

- The relative density which is recognized as the most important parameter affecting the mechanical behavior of foams was controlled by the gradual decrease in the gap between the inflated particles.

- The quasi-static compression curves of the proposed 3D irregular closed-cell foam models exhibit the three deformation stages of real closed-cell aluminum foam under compression loading.
- The plateau region which ensures the smooth energy absorption of the foam material can be characterized by a level and a length.
- It was confirmed that the relative density has a major influence on the plateau region level (yield point), and on the plateau region length: increasing the relative density will increase the plateau level and decrease the plateau length of the aluminum foam.
- It was further confirmed that the relation between the plateau stress and relative density of closed-cell aluminum foam could be fitted with a power function, the power of the relative density term is confirmed to be approximately 1.5.
- The effect of loading direction on the compressive behavior of designed models, showed that the proposed foam models exhibit isotropic mechanical properties.
- It was demonstrated that the cell collapse initiates at the thinnest cell wall.
- The proposed numerical models can be readily used to reduce expensive experiment tests of closed-cell foams, and it can be used as an input for several types of FE analysis (thermal, structural, acoustic).

Bibliography

[1] Opiela KC, Zieliński TG, Dvorák T, Kúdela S. Perforated closed-cell aluminium foam for acoustic absorption. Appl Acoust 2021; 174.

[2] Wang Y, Liew JYR, Lee SC, Zhai X, Wang W. Crushing of a novel energy absorption connector with curved plate and aluminum foam as energy absorber. Thin-Walled Struct 2017; 111:145–54.

[3] LI Z bin, LI X Yan, ZHENG Y xuan. Biaxial mechanical behavior of closed-cell aluminum foam under combined shear—compression loading. Trans Nonferrous Met Soc China (English Ed 2020; 30:41–50.

[4] Yang X, An T, Wu Z, Zou T, Song H, Sha J, et al. The effect of outer tube on quasistatic compression behavior of aluminum foam-filled tubes. Compos Struct 2020; 245:112357.

[5] Chen Y, Das R, Battley M, Xu Z. Compressive and shear strengths of the ductile closedcell Kelvin and Weaire-Phelan foams along the lattice direction [100]. Thin-Walled Struct 2018; 132:237–49.

[6] Shi X, Liu S, Nie H, Lu G, Li Y. Study of cell irregularity effects on the compression of closed-cell foams. Int J Mech Sci 2018; 135:215–25.

[7] Burteau A, N'Guyen F, Bartout JD, Forest S, Bienvenu Y, Saberi S, et al. Impact of material processing and deformation on cell morphology and mechanical behavior of polyurethane and nickel foams. Int J Solids Struct 2012; 49:2714–32.

[8] Vengatachalam B, Huang R, Poh LH, Liu Z, Qin Q, Swaddiwudhipong S. Initial yield behaviour of closed-cell aluminium foams in biaxial loading. Int J Mech Sci 2021; 191:106063.

[9] Islam MA, Brown AD, Hazell PJ, Kader MA, Escobedo JP, Saadatfar M, et al. Mechanical response and dynamic deformation mechanisms of closed-cell aluminium alloy foams under dynamic loading. Int J Impact Eng 2018; 114:111–22.

[10] Fahlbusch NC, Grenestedt JL, Becker W. Effective failure behavior of an analytical and a numerical model for closed-cell foams. Int J Solids Struct 2016; 97_98:417–30. 28

[11] Wang E, Sun G, Zheng G, Li Q. Characterization of initial and subsequent yield behaviors of closed-cell aluminum foams under multiaxial loadings. Compos Part B Eng 2020; 202:108247.

[12] Carneiro VH, Lopes D, Puga H, Meireles J. Numerical inverse engineering as a route to determine the dynamic mechanical properties of metallic cellular solids. Mater Sci Eng A 2021; 800:140428.

[13] Luo G, Xue P, Sun S. Investigations on the yield behavior of metal foam under multiaxial loadings by an imaged-based mesoscopic model. Int J Mech Sci 2018; 142–143:153–62.

[14] Ghazi A, Tiago C, Sonon B, Berke P, Massart TJ. Efficient computational modelling of closed cell metallic foams using a morphologically controlled shell geometry. Int J Mech Sci 2020; 168:105298.

[15] Wang Y, Zhai X, Wang W. Numerical studies of aluminum foam filled energy absorption connectors under quasi-static compression loading. Thin-Walled Struct 2017; 116:225–33.

[16] Ha NS, Lu G. A review of recent research on bio-inspired structures and materials for energy absorption applications. vol. 181. Elsevier Ltd; 2020.

[17] Wang Y, Zhai X, Yan J, Ying W, Wang W. Experimental, numerical and analytical studies on the aluminum foam filled energy absorption connectors under impact loading. Thin-Walled Struct 2018; 131:566–76.

[18] He Y, Wu J, Qiu D, Yu Z. Construction of 3-D realistic representative volume element failure prediction model of high density rigid polyurethane foam treated under complex thermal-vibration conditions. Int J Mech Sci 2021; 193:106164.

[19] Ye W, Barbier C, Zhu W, Combescure A, Baillis D. Macroscopic multiaxial yield and failure surfaces for light closed-cell foams. Int J Solids Struct 2015; 69–70:60–70.

[20] Sun Y, Li QM. Dynamic compressive behaviour of cellular materials: A review of phenomenon, mechanism and modelling. Int J Impact Eng 2018; 112:74–115.

[21] Güden M, Kavi H. Quasi-static axial compression behavior of constraint hexagonal and square-packed empty and aluminum foam-filled aluminum multi-tubes. Thin-Walled Struct 2006; 44:739–50.

[22] Wang L, Zhang B, Zhang J, Jiang Y, Wang W, Wu G. Deformation and energy absorption properties of cenosphere-aluminum syntactic foam-filled tubes under axial compression. Thin-Walled Struct 2021;160:107364.

[23] Chen J, Zhang P, Cheng Y, Liu J. On the crushing response of the functionally graded metallic foams based on 3D Voronoi model. Thin-Walled Struct 2020; 157:107085.

[24] Mu Y, Yao G, Liang L, Luo H, Zu G. Deformation mechanisms of closed-cell aluminum foam in compression. Scr Mater 2010; 63:629–32.

[25] Ge C, Gao Q, Wang L, Hong Z. Theoretical prediction and numerical analysis for axial crushing behaviour of elliptical aluminium foam-filled tube. Thin-Walled Struct 2020; 149:106523.

[26] M. Hummel, C. Böhm, W. Verestek, S. Schmauder, Introducing a method of constructing realistic closed-cell nano-porous iron crystals and MD simulations to investigate the influence of the system size on the stability and the mechanical properties, Comput. Mater. Sci. 166

[27] Islam MA, Kader MA, Hazell PJ, Escobedo JP, Brown AD, Saadatfar M. Effects of impactor shape on the deformation and energy absorption of closed cell aluminium foams under low velocity impact. Mater Des 2020; 191:108599.

[28] Talebi S, Sadighi M, Aghdam MM. Numerical and experimental analysis of the closedcell aluminium foam under low velocity impact using computerized tomography technique. Acta Mech Sin Xuebao 2019; 35:144–55. 29

[29] Kabir K, Vodenitcharova T, Hoffman M. Response of aluminium foam-cored sandwich panels to bending load. Compos Part B Eng 2014;64:24–32.

[30] Zu GY, Lu RH, Li XB, Zhong ZY, Ma XJ, Han MB, et al. Three-point bending behavior of aluminum foam sandwich with steel panel. Trans Nonferrous Met Soc China (English Ed 2013; 23:2491–5.

[31] Vesenjak M, Duarte I, Baumeister J, Göhler H, Krstulović-Opara L, Ren Z. Bending performance evaluation of aluminium alloy tubes filled with different cellular metal cores. Compos Struct 2020; 234:111748.

[32] Xiang C, Ningzhen W, Jianyu Y, Yanxiang L, Huawei Z, Yuan L. Modeling of Macrodeformation Behavior of Thin-Walled Aluminum Foam by Gas Injection Method. J Mater Eng Perform 2017; 26:3307–18.

[33] Movahedi, Nima and S. M. H. Mirbagheri. “Comparison of the Energy Absorption of Closed-Cell Aluminum Foam Produced by Various Foaming Agents.” Strength of Materials 48 (2016): 444-449.

[34] Movahedi, Nima, Seyed Mohammad Hossein Mirbagheri and S. R. Hoseini. “Effect of foaming temperature on the mechanical properties of produced closed-cell A356Aluminum foams with melting method.” Metals and Materials International 20 (2014): 757-763.

[35] Linul, Emanoil, Liviu Marşavina and Jaroslav Kováčik. “Compressive Behavior and Energy Absorption Capability of Reinforced Closed-Cell Aluminum Alloy Foams.” IOP Conference Series: Materials Science and Engineering (2018).

[36] Linul E, Movahedi N, Marsavina L. The temperature and anisotropy effect on compressive behavior of cylindrical closed-cell aluminum-alloy foams. J Alloys Compd 2018; 740:1172–9.

[37] Ghazi A, Berke P, Ehab Moustafa Kamel K, Sonon B, Tiago C, Massart TJ. Multiscale computational modelling of closed cell metallic foams with detailed microstructural morphological control. Int J Eng Sci 2019; 143:92–114.

[38] Kader MA, Hazell PJ, Brown AD, Tahtali M, Ahmed S, Escobedo JP, et al. Novel design of closed-cell foam structures for property enhancement. Addit Manuf 2020; 31:100976.

[39] Kumar A, Collini L, Daurel A, Jeng JY. Design and additive manufacturing of closed cells from supportless lattice structure. Addit Manuf 2020;33:101168.

[40] Carneiro VH, Rawson SD, Puga H, Meireles J, Withers PJ. Additive manufacturing assisted investment casting: A low-cost method to fabricate periodic metallic cellular lattices. Addit Manuf 2020; 33:101085.

[41] Babamiri BB, Barnes B, Soltani-Tehrani A, Shamsaei N, Hazeli K. Designing additively manufactured lattice structures based on deformation mechanisms. Addit Manuf 2021; 46:102143.

[42] Wang S, Zheng Z, Zhu C, Ding Y, Yu J. Crushing and densification of rapid prototyping polylactide foam: Meso-structural effect and a statistical constitutive model. Mech Mater 2018; 127:65–76.

[43] Redenbach C. Fitting three-dimensional Laguerre tessellations to foam structures. Journal of Applied Statistics 35 (2008): 985 - 995.

[44] Nie Z., Lin Y., Tong Q. Numerical investigation of pressure drop and heat transfer through open cell foams with 3D Laguerre-Voronoi model. Int J Heat Mass Transf 2017; 113:819–39.

[45] Chai HW, Xie ZL, Xiao XH, Xie HL, Huang JY, Luo SN. Microstructural characterization and constitutive modeling of deformation of closed-cell foams based on in situ x-ray tomography. Int J Plast 2020; 131:102730.

[46] Zhang X, Tang L, Liu Z, Jiang Z, Liu Y, Wu Y. Yield properties of closed-cell aluminum foam under triaxial loadings by a 3D Voronoi model. Mech Mater 2017;104:73–84.

[47] Youssef S, Maire E, Gaertner R. Finite element modelling of the actual structure of cellular materials determined by X-ray tomography. Acta Mater 2005; 53:719–30. 30

[48] Chen Y, Das R, Battley M. Finite element analysis of the compressive and shear responses of structural foams using computed tomography. Compos Struct 2017; 159:784–99.

[49] Chen Y, Das R, Battley M. Effects of cell size and cell wall thickness variations on the stiffness of closed-cell foams. Int J Solids Struct 2015; 52:150–64.

[50] Zhu C, Zheng Z, Wang S, Zhao K, Yu J. Modification and verification of the Deshpande– Fleck foam model: A variable ellipticity. Int J Mech Sci 2019; 151:331–42.

[51] Banhart, J., & Weaire, D. (2002). On the road again: metal foams find favor. *Physics Today*, *55*(7), 37-42.

[52] Davies, G. J., & Zhen, S. (1983). Metallic foams: their production, properties and applications. *Journal of Materials science*, *18*(7), 1899-1911.

[53] Banhart, J. (2000). Manufacturing routes for metallic foams. *Jom*, *52*(12), 22-27.

[54] Davis, J. R. (Ed.). (1999). *Corrosion of aluminum and aluminum alloys*. Asm International.

[55] Banhart, J. (2001). Manufacture, characterisation and application of cellular metals and metal foams. *Progress in materials science*, *46*(6), 559-632.

[56] Miyoshi, T., Itoh, M., Akiyama, S., & Kitahara, A. (2000). ALPORAS aluminum foam: production process, properties, and applications. *Advanced engineering materials*, *2*(4), 179-183.

[57] Zhou, J., 2006. Advanced structural materials. Porous Metallic Materials, ed. e. Winston O. Soboyejo., CRC Press , Taylor & Francis Group. USA, 22.

[58] Bashirzadeh, R., & Gharehbaghi, A. (2010). An investigation on reactivity, mechanical and fire properties of PU flexible foam. *Journal of Cellular Plastics*, *46*(2), 129-158.

[59] Parveez, B., Jamal, N. A., Maleque, A., Yusof, F., Jamadon, N. H., & Adzila, S. (2021). Review on advances in porous Al composites and the possible way forward. *Journal of Materials Research and Technology*, *14*, 2017-2038.

[60] Dairon, J. (2008). *Développement d'une nouvelle technique d'élaboration de mousses d'acier par fonderie et caractérisation mécanique* (Doctoral dissertation, Ecole Centrale de Lille).

[61] Dairon, J., Gaillard, Y., Tissier, J. C., Balloy, D., Degallaix, G., & CORSON, B. (2009). Mousses métalliques: CTIF innove dans les matériaux cellulaires. *Fonderie, Fondeur d'aujourd'hui*, (285), 12-21.

[62] Malekjafarian, M., Sadrnezhaad, S. K., Abravi, M. S., Golestanipour, M., & Mashhadi, H. A. (2011). Manufacturing aluminum foams by melt gas injection process. In *7th International Conference on Porous Metals and Metallic Foams (MetFoam2011)* (p. 195).

[63] García-Moreno, F., Kamm, P. H., Neu, T. R., Bülk, F., Mokso, R., Schlepütz, C. M., ... & Banhart, J. (2019). Using X-ray tomoscopy to explore the dynamics of foaming metal. *Nature communications*, *10*(1), 1-9.

[64] Chen, S. (2015). *A Study on properties of novel metallic foam for nuclear applications*. North Carolina State University.

[65] Yang, D., Hu, Z., Chen, W., Lu, J., Chen, J., Wang, H., ... & Ma, A. (2016). Fabrication of Mg-Al alloy foam with close-cell structure by powder metallurgy approach and its mechanical properties. *Journal of Manufacturing Processes*, *22*, 290-296.

[66] Ashby, M. F., Evans, T., Fleck, N. A., Hutchinson, J. W., Wadley, H. N. G., & Gibson, L. J. (2000). *Metal foams: a design guide*. Elsevier.

[67] De Schampheleire, S., De Jaeger, P., De Kerpel, K., Ameel, B., Huisseune, H., & De Paepe, M. (2016). How to study thermal applications of open-cell metal foam: Experiments and computational fluid dynamics. *Materials*, *9*(2), 94.

[68] Yang, X., Wang, W., Yang, C., Jin, L., Lu, T.J., Solidification of fluid saturated in open-cell metallic foams with graded morphologies, Int. J. Heat Mass Transfer, vol. 98, pp. 60-69, 2016b.

[69] Liu, P. S., & Ma, X. M. (2020). Property relations based on the octahedral structure model with body-centered cubic mode for porous metal foams. *Materials & Design*, *188*, 108413.

[70] Contuzzi, N., Campanelli, S. L., Caiazzo, F., & Alfieri, V. (2019). Design and fabrication of random metal foam structures for laser powder bed fusion. *Materials*, *12*(8), 1301.

[71] Banhart J. Functional Applications. In: Degischer HP, Kriszt B, editors. Handbook of cellular metals-Production, Processing, Applications, Weinheim, Germany: Wiley-VCH Verlag GmbH, 2002.

[72] Haberling, C. (2002). The Range of Applications of Structural Foams Based on Cellular Metals and Alternative Polymer Solutions. *Handbook of Cellular Metals*.

[73] García-Moreno, F. (2016). Commercial applications of metal foams: Their properties and production. *Materials*, *9*(2), 85.

[74] Kretz R. Prototypes of Powder Compact Foaming. Service Properties and Expolitability. In: Degischer HP, Kriszt B, editors. Handbook of cellular metals-Production, Processing, Applications, Weinheim, Germany: Wiley-VCH Verlag GmbH, 2002.

[75] Hangai, Y., Saito, M., Utsunomiya, T., Kitahara, S., Kuwazuru, O., & Yoshikawa, N. (2014). Fabrication of aluminum foam-filled thin-wall steel tube by friction welding and its compression properties. *Materials*, *7*(9), 6796-6810.

[76] Onstad, A. J. (2009). *Additions to compact heat exchanger technology: Jet impingement cooling & flow & heat transfer in metal foam-fins.* Stanford University.

[77] Zhang, C. (2017). *Aluminum foams composite: elaboration and thermal properties for energy storage* (Doctoral dissertation, Université de Technologie de Troyes).

[78] Crupi, V., Epasto, G., & Guglielmino, E. (2011). Impact response of aluminum foam sandwiches for light-weight ship structures. *Metals*, *1*(1), 98-112.

[79] Feng Y, Tan N, Zhu Z, Hu S, Pan Y. Effect of aging treatment on the quasi-static and dynamic compressive properties of aluminum alloy foams. Materials Letters 2003; 57(24- 25): 4058-4063.

[80] Tarlochan, F. (2021). Sandwich structures for energy absorption applications: A review. *Materials*, *14*(16), 4731.

[81] Li, S.; Wang, Z.; Wu, G.; Zhao, L.; Li, X. Dynamic response of sandwich spherical shell with graded metallic foam cores subjected to blast loading. Compos. A Appl. Sci. Manuf. 2014, 56, 262–271.

[82] Jing, L.; Yang, F.; Zhao, L. Perforation resistance of sandwich panels with layered gradient metallic foam cores. Compos. Struct. 2017, 171, 217–226.

[83] Santosa, S.P.; ArifurRahman, F.; Izzudin, M.H.; Widagdo, D.; Gunawan, L. Response Analysis of Blast Impact Loading of Metal-foam Sandwich Panels. Procedia Eng. 2017, 173, 495–502.

[84] Matassi, F., Botti, A., Sirleo, L., Carulli, C., & Innocenti, M. (2013). Porous metal for orthopedics implants. *Clinical Cases in Mineral and Bone Metabolism*, *10*(2), 111.

[85] Mutlu, I., & Oktay, E. (2011). Biocompatibility of 17-4 PH stainless steel foam for implant applications. *Bio-medical materials and engineering*, *21*(4), 223-233.

[86] Nouri, A. (2017). Titanium foam scaffolds for dental applications. In *Metallic Foam Bone* (pp. 131-160). Woodhead Publishing.

[87] George, N., & Nair, A. B. (2018). Porous tantalum: A new biomaterial in orthopedic surgery. In *Fundamental Biomaterials: Metals* (pp. 243-268). Woodhead Publishing.

[88] Tucker, D. J. (2010). Lateral column lengthening in adult flatfoot surgery using a titanium metal foam wedge implant. *Techniques in Foot & Ankle Surgery*, *9*(4), 205-210.

[89] Matsushita, T., Fujibayashi, S., & Kokubo, T. (2017). Titanium foam for bone tissue engineering. In *Metallic Foam Bone* (pp. 111-130). Woodhead Publishing.

[90] Goodall, R., & Mortensen, A. (2014). Porous metals. In *Physical metallurgy* (pp. 2399-2595). Elsevier.

[91] Güner, A., Arıkan, M. M., & Nebioglu, M. (2015). New approaches to aluminum integral foam production with casting methods. *Metals*, *5*(3), 1553-1565.

[92] Ashby MF, Evans AG, Fleck NA, Gibson LJ, Hutchinson JW, Wadley HNG., USA: Butterworth-Heinemenn, 2000.

[93] Smith, B. H., Szyniszewski, S., Hajjar, J. F., Schafer, B. W., & Arwade, S. R. (2012). Steel foam for structures: A review of applications, manufacturing and material properties. *Journal of Constructional Steel Research*, *71*, 1-10.

[94] Bastawros, A. F., Bart-Smith, H., & Evans, A. G. (2000). Experimental analysis of deformation mechanisms in a closed-cell aluminum alloy foam. *Journal of the Mechanics and Physics of Solids*, *48*(2), 301-322.

[95]Motz, C., & Pippan, R. (2001). Deformation behaviour of closed-cell aluminium foams in tension. *Acta Materialia*, *49*(13), 2463-2470.

[96] Andrews, E. W., Gioux, G., Onck, P., & Gibson, L. J. (2001). Size effects in ductile cellular solids. Part II: experimental results. *International Journal of Mechanical Sciences*, *43*(3), 701-713.

[97] STRĘK, A. (2012). Methodology for experimental investigations of metal foams and their mechanical properties. *Mechanics and Control*, *31*(2), 90-90.

[98] Cheng, Y., Li, Y., Chen, X., Zhou, X., & Wang, N. (2018). Compressive properties and energy absorption of aluminum foams with a wide range of relative densities. *Journal of Materials Engineering and Performance*, *27*(8), 4016-4024.

[99] Vengatachalam, B., Poh, L. H., Liu, Z. S., Qin, Q. H., & Swaddiwudhipong, S. (2019). Three dimensional modelling of closed-cell aluminium foams with predictive macroscopic behaviour. *Mechanics of Materials*, *136*, 103067.

[100] Davis, C., & Wilcock, E. (2004). Case studies in engineering. *Effective learning and teaching in engineering*, 51-71.

[101] Amsterdam, E., De Hosson, J. T. M., & Onck, P. R. (2006). Failure mechanisms of closed-cell aluminum foam under monotonic and cyclic loading. *Acta materialia*, *54*(17), 4465-4472.

[102] Peroni, L., Avalle, M., & Peroni, M. (2008). The mechanical behaviour of aluminium foam structures in different loading conditions. *International journal of impact engineering*, *35*(7), 644-658.

[103] Wang, X. Z., Wu, L. Z., & Wang, S. X. (2009). Tensile and shear properties of aluminium foam. *Materials Technology*, *24*(3), 161-165.

[104] Foroughi, B., Degischer, H. P., & Kottar, A. (2013). Characterization and Simulation of Tensile Deformation of Non-Uniform Cellular Aluminium Until Damage. *Advanced Engineering Materials*, *15*(4), 276-286.

[105] Marx, J., & Rabiei, A. (2020). Study on the microstructure and compression of composite metal foam core sandwich panels. *Metallurgical and Materials Transactions A*, *51*(10), 5187-5197.

[106] Blazy, J. S., Marie-Louise, A., Forest, S., Chastel, Y., Pineau, A., Awade, A., ... & Moussy, F. (2004). Deformation and fracture of aluminium foams under proportional and non proportional multi-

axial loading: statistical analysis and size effect. *International journal of mechanical sciences*, *46*(2), 217-244.

[107] Gioux, G., McCormack, T. M., & Gibson, L. J. (2000). Failure of aluminum foams under multiaxial loads. *International Journal of Mechanical Sciences*, *42*(6), 1097-1117.

[108] Lu, T. J., & Ong, J. M. (2001). Characterization of close-celled cellular aluminum alloys. *Journal of materials Science*, *36*(11), 2773-2786.

[109] Styles, M., Compston, P., & Kalyanasundaram, S. (2007). The effect of core thickness on the flexural behaviour of aluminium foam sandwich structures. *Composite Structures*, *80*(4), 532-538.

[110] Triawan, F., Nakagawa, R., Inaba, K., Budiman, B. A., & Kishimoto, K. (2020). Experimental investigation of shear stress effect on the flexural behavior of aluminum foam beam. *Journal of Mechanical Science and Technology*, *34*(5), 1831-1836.

[111] Latour, M., D'Aniello, M., Landolfo, R., & Rizzano, G. (2021). Experimental and numerical study of double-skin aluminium foam sandwich panels in bending. *Thin-Walled Structures*, *164*, 107894.

[112] Triantafillou, T. C., Zhang, J., Shercliff, T. L., Gibson, L. J., & Ashby, M. F. (1989). Failure surfaces for cellular materials under multiaxial loads—II. Comparison of models with experiment. *International Journal of Mechanical Sciences*, *31*(9), 665-678.

[113] Ruan, D., Lu, G., Ong, L. S., & Wang, B. (2007). Triaxial compression of aluminium foams. *Composites Science and Technology*, *67*(6), 1218-1234.

[114] American Society of Testing and Materials Standard C393-62. Test Method for Flexural Properties of Sandwich Constructions. Annual Book of ASTM Standards, (2000).

[115] Jiang, B., Wang, Z., & Zhao, N. (2007). Effect of pore size and relative density on the mechanical properties of open cell aluminum foams. *Scripta materialia*, *56*(2), 169-172.

[116] Jing, L., Su, X., Yang, F., Ma, H., & Zhao, L. (2018). Compressive strain rate dependence and constitutive modeling of closed-cell aluminum foams with various relative densities. *Journal of Materials Science*, *53*(20), 14739-14757.

[117] Jang, W. Y., Hsieh, W. Y., Miao, C. C., & Yen, Y. C. (2015). Microstructure and mechanical properties of ALPORAS closed-cell aluminium foam. *Materials Characterization*, *107*, 228-238.

[118] Fang, Q., Zhang, J., Zhang, Y., Liu, J., & Gong, Z. (2015). Mesoscopic investigation of closed-cell aluminum foams on energy absorption capability under impact. *Composite Structures*, *124*, 409-420.

[119] Abdullahi, H. S., Liang, Y., & Gao, S. (2019). Predicting the elastic properties of closed-cell aluminum foams: a mesoscopic geometric modeling approach. *SN Applied Sciences*, *1*(4), 1-13.

[120] Yang, C., Chen, Z., Yao, S., Xu, P., Li, S., & Alqahtani, M. S. (2022). Quasi-static and low-velocity axial crushing of polyurethane foam-filled aluminium/CFRP composite tubes: An experimental study. *Composite Structures*, *299*, 116083.

[121] Mane, J. V., Chandra, S., Sharma, S., Ali, H., Chavan, V. M., Manjunath, B. S., & Patel, R. J. (2017). Mechanical property evaluation of polyurethane foam under quasi-static and dynamic strain rates-an experimental study. *Procedia engineering*, *173*, 726-731.

[122] A. C. Kak and M. Slaney, *Principles of Computerized Tomographic Imaging*. New York: IEEE Press, 1987.

[123] L. A. Feldkamp, L. C. Daves and J. W. Kress, *Practical cone-beam algorithm*, Journal of the Optical Society of America A , **1** (6), 612-619, 1984.

[124] M. Ding, A. Odgaard and I. Hvid, *Accuracy of cancellous bone volume fraction measured by micro- CT scanning*, Bone, **32**, 323-326, 1999.

[125] D. M. L. Cooper, J. R. Matyas, M. A. Katzenberg and B. Hallgrimsson, *Comparison of Microcomputed Tomographic and Microradiographic Measurements of Cortical Bone Porosity*, Calcified Tissue International, **74**, 437-447, 2002.

[126] C. R. Appoloni, C. P. Fernandes and C. R. Rodrigues. *X-ray microtomography study of a sandstone reservoir rock*, Nuclear Instruments and Methods in Physics Research A , **580**, 629-623, 2007.

[127] K. Remeysen, R. Swennen. *Application of microfocus computed tomography in carbonate reservoir characterization: Possibilities and limitations*, Marine and Petroleum Geology, **25**, 486–499, 2008.

[128] O.B. Olurin, M. Arnold, C. Körner, R.F. Singer. *The investigation of morphometric parameters of aluminium foams using micro-computed tomography,* Materials Science and Engineering A , **328**, 334-343, 2002.

[129] C.R. Appoloni, C.P. Fernandes, M.D. Innocentini, A. Macedo. *Ceramic Foams Porous Microstructure Characterization By X-ray Microtomography*. Materials Research , **7**, 557-564. 2004

[130] Nagata, R., Appoloni, C. R., & Marques, L. C. (2011, June). Analysis of the cell walls of ceramic foams by X-ray microtomography. In *Brazilian Workshop on Nuclear Physics (XXXIV BWNP)* (p. 69).

[131] Barma, P., Rhodes, M. B., & Salovey, R. (1978). Mechanical properties of particulate-filled polyurethane foams. *Journal of Applied Physics*, *49*(10), 4985-4991.

[132] Fazekas, A., Dendievel, R., Salvo, L., & Bréchet, Y. (2002). Effect of microstructural topology upon the stiffness and strength of 2D cellular structures. *International Journal of Mechanical Sciences*, *44*(10), 2047-2066.

[133] Lorensen, W. E., & Cline, H. E. (1987). Marching cubes: A high resolution 3D surface construction algorithm. *ACM siggraph computer graphics*, *21*(4), 163-169.

[134] Dillard, T., N'guyen, F., Maire, E., Salvo, L., Forest*, S., Bienvenu, Y., ... & Cloetens, P. (2005). 3D quantitative image analysis of open-cell nickel foams under tension and compression loading using X-ray microtomography. *Philosophical Magazine*, *85*(19), 2147-2175.

[135] Jeon, I., Katou, K., Sonoda, T., Asahina, T., & Kang, K. J. (2009). Cell wall mechanical properties of closed-cell Al foam. *Mechanics of Materials*, *41*(1), 60-73.

[136] Sone, T., Tamada, T., Jo, Y., Miyoshi, H., & Fukunaga, M. (2004). Analysis of three-dimensional microarchitecture and degree of mineralization in bone metastases from prostate cancer using synchrotron microcomputed tomography. *Bone*, *35*(2), 432-438.

[137] Ghazi, A., Berke, P., Tiago, C., & Massart, T. J. (2020). Computed tomography based modelling of the behaviour of closed cell metallic foams using a shell approximation. *Materials & Design*, *194*, 108866.

[138] Sharma, V., Zivic, F., Grujovic, N., Babcsan, N., & Babcsan, J. (2019). Numerical modeling and experimental behavior of closed-cell aluminum foam fabricated by the gas blowing method under compressive loading. *Materials*, *12*(10), 1582.

[139] Szymczyk, W., & Miedzińska, D. (2009). Numerical analysis of an open cell foam structure with the use of models based on 2D finite elements. *Journal of KONES*, *16*, 441-448.

[140]Talebi, S., Sadighi, M., & Aghdam, M. M. (2018). The effect of impact energy parameters on the closed-cell aluminum foam crushing behavior using x-ray tomography method. *AUT Journal of Mechanical Engineering*, *2*(1), 107-116.

[141] Talebi, S., Sadighi, M., & Aghdam, M. M. (2019). Numerical and experimental analysis of the closed-cell aluminium foam under low velocity impact using computerized tomography technique. *Acta Mechanica Sinica*, *35*(1), 144-155.

[142] Wejrzanowski, T., Skibinski, J., Szumbarski, J., & Kurzydlowski, K. J. (2013). Structure of foams modeled by Laguerre–Voronoi tessellations. *Computational Materials Science*, *67*, 216-221.

[143] Li, K., Gao, X. L., & Subhash, G. (2005). Effects of cell shape and cell wall thickness variations on the elastic properties of two-dimensional cellular solids. *International Journal of Solids and Structures*, *42*(5-6), 1777-1795.

[144] Li, K., Gao, X. L., & Subhash, G. (2006). Effects of cell shape and strut cross-sectional area variations on the elastic properties of three-dimensional open-cell foams. *Journal of the Mechanics and Physics of Solids*, *54*(4), 783-806.

[145] Zhu, W., Blal, N., Cunsolo, S., Baillis, D., & Michaud, P. M. (2018). Effective elastic behavior of irregular closed-cell foams. *Materials*, *11*(11), 2100.

[146] Zhang, X., Chen, Q., Gao, J., Wang, M., Zhang, Y., & Cai, Z. (2021). Numerical Study on the Plastic Forming of Doubly Curved Surfaces of Aluminum Foam Sandwich Panel Using 3D Voronoi Model. *Metals*, *11*(5), 675.

[147] Luo, G., & Xue, P. (2018). Investigations on the mechanism and behavior of dynamic energy absorption of metal foam. *Latin american journal of solids and structures*, *15*.

[148] Chen, Y., Das, R., & Battley, M. (2014, July). Modelling of closed-cell foams incorporating cell size and cell wall thickness variations. In *Proceedings of the 11th World Congress on Computational Mechanics* (pp. 20-25).

[149] Zhang, X., Cai, Z. Y., Liang, X. B., & Gao, J. X. (2020). Numerical investigation on the plastic forming of aluminum foam sandwich panel based on three-dimensional mesoscopic and macroscopic models. *The International Journal of Advanced Manufacturing Technology*, *109*(5), 1431-1445.

[150] Benhizia A, Outtas T, Kanit T, Imad A. Optimal design and non–linear computation of mechanical behavior of sphere reinforced composites. Compos Part B Eng 2017; 126:38–48.

[151] Zhou Z, Su B, Wang Z, Shu X, Zhao L. Impact response of aluminium alloy foams under complex stress states. Lat Am J Solids Struct 2016; 13:665–89.

[152] Hu Y, Fang QZ, Yu H, Hu Q. Numerical simulation on thermal properties of closed-cell metal foams with different cell size distributions and cell shapes. Mater Today Commun 2020; 24:100968.

[153] Lhuissier P. Structural properties of solid foams. Comptes Rendus Phys 2014;15:696– 704.

[154] Su BY, Huang CM, Sheng H, Jang WY. The effect of cell-size dispersity on the mechanical properties of closed-cell aluminum foam. Mater Charact 2018; 135:203–13.

[155] Sadjad P, Mohammad-Hossein E, Sobhan EM. Crashworthiness of double-cell conical tubes with different cross sections subjected to dynamic axial and oblique loads. J Cent South Univ 2018; 25:632–45.

[156] Taherkhani B, Kadkhodapour J, Anaraki AP, Saeed M, Tu H. Drop Impact of ClosedCell Aluminum Foam: Experiment and Simulation. J Fail Anal Prev 2020; 20:464–9.

[157] Sun Y, Amirrasouli B, Razavi SB, Li QM, Lowe T, Withers PJ. The variation in elastic modulus throughout the compression of foam materials. Acta Mater 2016; 110:161–74.

[158] ISO13314:2011, Mechanical testing of metals – Ductility testing – Compression Test for porous and cellular metals.

[159] L.J. Gibson, M.F. Ashby, J. Zhang, T.C. Triantafillou, Failure surfaces for cellular materials under multiaxial loads—I.Modelling. Int J Mech Sci 1989; 31: 635–663.

[160] Shen J, Lu G, Ruan D. Compressive behaviour of closed-cell aluminium foams at high strain rates. Compos Part B Eng 2010; 41:678–85.

[161] Wang E, Sun G, Zheng G, Li Q. On multiaxial failure behavior of closed-cell aluminum foams under medium strain rates. Thin-Walled Struct 2021; 160.

[162] Santosa S, Wierzbicki T. On the modeling of crush behavior of a closed-cell aluminum foam structure. J Mech Phys Solids 1998; 46:645–69.

[163] McCullough KYG, Fleck NA, Ashby MF. Uniaxial stress-strain behaviour of aluminum alloy foams. Acta Mater 1999; 47:2323–30.

[164] Vengatachalam B, Poh L.H., Liu Z.S, Qin Q.H, Swaddiwudhipong S. Three dimensional modelling of closed-cell aluminium foams with predictive macroscopic behaviour. Mech. Mater. 2019, 136, 103067.

[165] Movahedi, Nima, Emanoil Linul and Liviu Marșavina. “The Temperature Effect on the Compressive Behavior of Closed-Cell Aluminum-Alloy Foams.” Journal of Materials Engineering and Performance 27 (2017): 99-108

ملخص

يقدم هذا البحث طريقة جديدة لتصميم نموذج حسابي ثلاثي الأبعاد واقعي ودقيق لرغاوي الخلايا المغلقة غير المنتظمة مع التحكم في الكثافة النسبية وتحليل مفصل باستخدام العناصر المحدودة المفصلة لأدائها الميكانيكي تحت التحميل شبه الثابت حتى التكثيف. تم التحقق من فعالية النمذجة بنجاح من خلال مقارنة التفاصيل المورفولوجية للخلية للنماذج التي تم إنشاؤها مع تلك المنتجة تجريبياً في المراجع والجودة العالية للنماذج المطبوعة ثلاثية الأبعاد التي تم الحصول عليها والتي تحتوي على أشكال معقدة وتوزيع غير منتظم لسمك جدار الخلية. تم التحقيق ايضا في أداء النماذج في تحليل العناصر المحدودة عن طريق إخضاع نموذج صلب ثلاثي الأبعاد مصمم لرغوة الألومنيوم ذات الخلية المغلقة لتحميل شبه ثابت حتى مرحلة التكثيف ، وهو نطاق التشوه المستخدم عادة في التطبيقات الهندسية. تقدم طريقة التصميم الجديدة نماذج رقمية مناسبة لتقنية. التصنيع الإظافي ، ويمكن تقليل الكثير من الأعمال التجريبية على رغوة الخلية المغلقة للتطبيقات الهندسية

كلمات مفتاحية: رغوة خلية مغلقة ؛ اختلاف جدران الخلايا ؛ اختلاف السماكة ؛الكثافة النسبية؛ تحميل شبه ثابت؛ الأداء الميكانيكي.

Abstract

This research work presents an original approach to generate a realistic and accurate 3D computational model of irregular closed-cell foams with relative density control and detailed finite element analysis of their mechanical performance under quasi-static loading up to densification. The modeling approach was successfully verified by comparing cell-morphological details of the generated models with those produced experimentally available in the literature and by the high-quality of obtained 3D printed models containing complex shapes and irregular cell wall thickness distribution. The performance of the proposal in finite element analysis has been investigated by subjecting a designed 3D RVE solid model of closed-cell aluminum foam to a quasi-static loading up to the densification stage, which is the range of deformation usually utilized in engineering applications. The new design method offers suitable numerical models for AM technology, and plenty of experimental works on closed-cell foam can be reduced for engineering applications.

Keywords: Closed-cell foam; Cell walls irregularities; Thickness variation; Relative density; Quasi-static loading; Mechanical performances;

Résumé

Ce travail de recherche présente une approche originale pour générer un modèle numerique 3D réaliste et précis de mousses à cellules fermées irrégulières avec contrôle de densité relative et analyse détaillée par éléments finis de leurs performances mécaniques sous chargement quasi-statique jusqu'à la densification. L'approche de modélisation a été vérifiée avec succès en comparant les détails morphologiques cellulaires des modèles générés avec ceux produits expérimentalement disponibles dans la littérature et par la haute qualité des modèles imprimés en 3D obtenus contenant des formes complexes et une distribution irrégulière de l'épaisseur de la paroi cellulaire. La performance des modèles générés dans l'analyse par éléments finis a été étudiée en soumettant des modèles 3D conçu de mousse d'aluminium à cellules fermées à un chargement quasi-statique jusqu'à l'étape de densification, qui est la plage de déformation habituellement utilisée dans les applications d'ingénierie. La nouvelle méthode de conception proposée offre des modèles numériques adaptés à la technologie AM, et de nombreux travaux expérimentaux sur la mousse à cellules fermées peuvent être réduits pour des applications d'ingénierie.

Mots clés : Mousse à cellules fermées ; Irrégularités des parois cellulaires ; variation d'épaisseur ; Densité relative; Chargement quasi-statique ; Performances mécaniques ;